Anthracite Fillers for Specialty Graphite – Feedstock Selection and Product Improvement

FINAL REPORT

Report Period:
January 1, 2001 – May 30, 2002

Prepared By:

Harold Schobert and Peter Pappano

The Penn State University
The Energy Institute
C211 Coal Utilization Laboratory
University Park, PA 16802

May 2002

DOE Award # DE-FC26-98FT40350

Disclaimer

Abstract

This report presents the findings of a study on the possible use of Pennsylvania anthracite as a replacement for petroleum coke in the production of isostatically molded graphite. The study had two main components: an investigation of the mechanisms of graphitization of anthracites, and the production of isomolded graphite articles in industrial tests. In the first part of the study, it was discovered that some of the mineral constituents in anthracites can act as *in situ* graphitization catalysts. The mechanism of graphitization catalysis involves the transformation of minerals, such as quartz and rutile, to the corresponding carbides. At higher temperatures, these carbides decompose, presumably releasing highly reactive carbon atoms. The highly reactive forms of carbon can eliminate crosslinks between the graphene layers or improve structural order in existing graphene layers, or possibly both. X-ray diffraction evidence shows the formation and disappearance of these carbides as heat-treatment temperature is increased. The disappearance of the carbides appears to coincide with the onset of the so-called graphitization jump, marked by sharpening of the (*002*) peak and the appearance of the (*hkl*) peak (the indicator of true three-dimensional ordering) in the X-ray diffractograms. Differences in the graphitization behavior of the four anthracites studied can be attributed to differences in *in situ* graphitization catalysis. LCNN anthracite was selected for scale-up studies. This anthracite was used as the filler material for the production of test pieces of isomolded graphite, being carried through an industrial processing scheme. Petroleum sponge coke was used to produce control artifacts in the same production cycle. The various properties of the anthracite-derived graphite fall into the low end of the range of acceptable specifications for isomolded graphites. Additional testing in future years could likely lead to commercialization of this premium carbon material made from anthracitic coals.

Table of Contents

List of Graphical Materials

List of Tables

List of Figures

Executive Summary

Anthracites are high-carbon-content coals that behave as both a graphitizing and non-graphitizing carbon, depending on the heat-treatment temperature (HTT) to which they are exposed. The reason for this dual behavior must lie in the nature of the physical, organic, or inorganic properties of these coals. Previous studies have focused on one of these traits, and have not looked at any interaction between them. Thus, the theories developed to this time concerning the mechanism of anthracite graphitization are incomplete. This present study focuses on the interaction between the organic and inorganic portions of anthracites to show that graphitization is influenced by both properties, and that differences in degree of graphitization—how close in structure to graphite anthracite can become—can be explained by carbide formation and decomposition.

Carbides are able to form because the minerals in anthracites contain elements capable of reacting with carbon to form carbides. These carbides form at 2200°C after heating for one hour, and decompose by 2600°C. The carbon reacting with the metallic elements from the minerals is, we hypothesize, the least stable carbon present, or those carbon atoms not contained within a polynuclear aromatic ring system. The removal of these less-stable or disordered carbons allows the already planar ring systems to condense into graphite crystallites. Also, when the carbides decompose they leave behind a reactive dicarbene atom that will attack any imperfections in the adolescent graphite crystallites.

A suite of anthracites was tested to determine the most graphitizable anthracite. This information was used to select one anthracite for industrial graphitization trials by Carbone of America. The anthracite selected was used as a filler in the production of an isostatically molded graphite. The anthracite-based molded graphite was then tested against a petroleum-coke-based graphite, produced as a control experiment, to determine whether property differences could be detected. In some properties, the petroleum-based graphite was superior, but in others the anthracite- based molded graphite was better. These preliminary data show that, at the least, anthracite can be used as a "low end" specialty molded graphite; work is in progress to produce a normal grade specialty graphite from anthracite.

Introduction

Graphite is formed in nature in large deposits around the world, including Mexico, the United States, Brazil, Canada, and Sri Lanka. Natural graphite is entirely aromatic carbon, lustrous, soft, and is often used as a solid lubricant because it easily shears and flakes apart. Graphite can also be produced by heating some carbon materials to temperatures in the range of 2000-3000°C, or by pressurizing the carbon as it is heated to a lower temperature. The vast majority of artificial graphite is produced from the combination of an aromatic petroleum by-product filler, i.e. petroleum coke, and binders that allow the graphite to be shaped or molded for a specific application. Natural graphite is not used as a filler for manufacture of molded graphites because it is more expensive than petroleum coke, and, because of its lubricity, it forms a viscous, non-shapeable paste, when mixed with a binder. Petroleum coke is an acceptable feedstock for graphite production for three reasons: (1) it undergoes structural changes at graphitization heat-treatment temperatures of ≈3000°C that leave the final structure close to that of natural graphite; (2) when mixed with a binder, it produces a shapeable product that has properties that make it suitable for electrical-conducting or thermal applications; and (3) it is less expensive than other aromatic feedstocks, such as anthracene, naphthalene, or natural graphite.

Anthracite is primarily carbon, having 92-98% fixed carbon on a mineral-matter- and moisture-free basis. Anthracite could also be used as a filler for graphite production if it met the three criteria listed above for petroleum coke. Therefore, it was necessary to determine why some anthracites will do better than others at achieving a structure similar

to that of natural graphite after being exposed to identical graphitization heat treatment temperatures. The reason for the differences in extent of graphitization must lie in differences in physical, organic, or inorganic properties. After this understanding had been developed, a selected anthracite was tested to determine whether it will form a product comparable to petroleum-coke-based graphite when mixed with a binder. The third criterion, cost, has already been met in that anthracite is ≈$200-300 per ton cheaper than petroleum coke.

One component of this project was the determination of which anthracite, selected from a suite of Pennsylvania anthracites, best approaches the structure of graphite when exposed to graphitzation heat treatment temperatures. The hypothesis tested in this component was that the amount and identity of the inorganics in the selected anthracites are the crucial factors for explaining differences in their extent of graphitization, or why some better approach the structure of graphite. The determination of how close in structure a heat-treated anthracite is to graphite was made by a comparison of X-ray diffraction data available on natural graphite, and the X-ray diffraction patterns of the heat-treated anthracite samples. Natural graphite produces characteristic peaks during X-ray diffraction at specific angles that can be used to determine the dimensions and interlayer spacing of the graphitic crystallites comprising its structure. Therefore, the level of similarity to natural graphite in the heat-treated anthracites, or graphitizability, can be measured by analysis of the X-ray diffraction peaks produced by the heat treated anthracites. To determine if differences in graphitizability of anthracites that have been exposed to the same graphitization temperatures is the result of inorganic differences,

four samples, which had different levels of mineral matter content and weight percentages of carbon, were obtained from active Pennsylvania mines .

The second component of this research was the production, using standard industrial procedures, of a synthetic graphite, with properties suitable for industrial applications, using anthracite as the filler instead of petroleum coke. The hypothesis tested in this component was that the anthracite that best approaches the structure of natural graphite as a result of laboratory-scale heat-treatment will produce a graphite most similar to a petroleum-based graphite. The production of the anthracite-based graphite was carried out by Carbone of America, a graphite manufacturer located in St. Marys Pennsylvania. Carbone produces petroleum-based graphites as a standard product line, and thus they have a wealth of information on the properties of their materials, which can be compared to the properties of the anthracite-based graphite.

Experimental Methods

Sampling

Anthracite samples for the study were selected from the field by sampling from four active anthracite mines selected on the bases of mine longevity (with mining of same seam planned for, at minimum, five years) and geological variations, such as amount of mineral matter present. The mines which met these criteria were Jeddo, UAE, Lehigh Coal and Navigation (LCNN), and Summit. Jeddo and LCNN mine the Mammoth vein of the Eastern Middle Seam in Pennsylvania while UAE mines the Lykens Valley #2 vein. Summit mines a conglomeration of veins, but for this research run-of-mine, or unprocessed, anthracite was recovered from the Tracey vein. The Jeddo and LCNN samples were separated in heavy media into pea size and UAE was processed using a Diester table. Three 55-gallon drums of each anthracite (twelve total barrels) were collected from the pea-sized pile of processed coal. This method could be referred to as a "grab" sample from the preparation plant, as opposed to a "channel" sample taken underground.

In order to ensure the homogeneity of the coal for analysis, a rigorous sampling procedure was followed. First, all three barrels of a particular anthracite were dumped onto a clean surface. The coal was shoveled on top of itself until the particles that were originally at the bottom of the pile had cycled from bottom to top and through the pile twice. After this, the pile was coned and quartered, by simply forcing a plus-sign-shaped system of boards through the pile, separating it into quarters. These quarters were each returned to a barrel, with the idea that each barrel would now have the same makeup as

far as particle size and chemical composition. One of these barrels was coned and quartered again, taking opposite quarters (or half the barrel) and crushed down to $-^1/_4$ inch using a hammer mill. This quantity of $-^1/_4$ inch coal was put through a riffler three times. Next, one half of the $-^1/_4$ inch was saved in bags of approximately 10 lbs. each. The other half of $-^1/_4$ inch was put through the hammer mill again, this time with a –20 mesh screen in place. The quantity of –20 mesh was riffled again and broken down into aliquots of approximately 4 lbs. each.

After the above work was completed on all four samples, one bag of –20 mesh was separated into eight aliquots using a rotary splitter. Seven of these aliquots, weighing 250g each, were sealed in foil laminate bags under an argon atmosphere; the remaining aliquot was further crushed to –60 mesh. This 250g quantity of –60 mesh was also separated with a rotary splitter into sections weighing 35g each. These –60 mesh aliquots were then sealed in foil laminate bags under argon. This sampling should ensure a good representation of the entire coal sample that was collected. The argon atmosphere will prevent any further oxidation so consistency of analytical results from one date of testing to another will not be a problem. Also, the small quantities sealed in each bag will further increase accuracy because they eliminate the problem of having to constantly open the bag, select the desired quantity of anthracite, and reseal the bag. This opening and closing will allow oxygen into the system, which can alter the coal structure by oxidation.

Characterization

This suite of anthracites was characterized by proximate and ultimate analysis. The instruments used were a CHN-600, SC-132 sulfur determinator, and MAC-400 proximate analyzer, all made by the Leco Corporation. For the CHN-600 between 0.03 and 0.07 grams of sample were weighed and placed in a tin crucible of cylindrical shape. The crucible was then crimped and folded over twice in order to promote smooth entry into the combustion chamber, where the sample is burned and its CO_2 and H_2O infrared spectrum is reduced to a weight percentage of elemental C and H. The nitrogen is calculated via a thermal conductivity cell against a standard. Oxygen was calculated by difference.

The sulfur analyzer worked much on the same principle, except that instead of the IR spectrum of CO_2 and H_2O, the IR spectrum of SO_2 is measured and related to a weight percentage. In this device approximately 0.5 grams of sample is weighed and placed in a ceramic boat, which is then placed in a hot zone where all of the sample is combusted.

Proximate analysis was determined using the MAC-400. This involved placing approximately 0.5 grams of anthracite in the crucibles provided and following the weight loss percentages as heat is increased to the crucibles. The MAC-400 follows ASTM heating guidelines, which are 105°C for one hour to determine moisture, 950°C (no oxygen present) for seven minutes to determine volatile matter, and 750°C for two hours to determine ash.

The ultimate and proximate analysis results were then converted to a dry, or moisture and ash free basis (maf), and the fixed carbon from proximate analysis was also reported on a mineral matter and moisture free basis (mmmf). The equations used for

these conversions are listed below. The mmmf conversion requires the use of the Parr formula for percentages of mineral matter

$$\text{MAF: } \%X_{maf}=100*\%X_{ar}/[100-(\%M_{ar}-\%A_{ar}])$$

$$\text{Parr formula: } MM=1.08A + 0.55S$$

$$\text{MMMF: } \%X_{(mmmf)}=100*\%X_{ar}/[100-(\%M_{ar}-\%MM])$$

In these equation "X" represents the property of interest, "M" represents moisture, "A" represents ash, "MM" represents mineral matter, and "S" is sulfur.

Graphitization

Following initial characterization, the samples were graphitized in a Centorr Vacuum Industry Series 45 furnace which operates in either a vacuum or argon atmosphere. The samples were weighed to 10 g and placed in graphite crucibles with lids, provided by POCO Graphite. These crucibles were then placed in the hot zone of the furnace (6 in X 9 in) and the top graphite plug and steel plate secured. The environment of the hot zone was purged by pulling a vacuum, and then backfilling with ultra-high purity argon three times. Following this purge, the samples were heated to 2000, 2200 2500, and 2600°C with a heating rate of 20°C/min and hold at the maximum temperature for one hour (in vacuum). Following heat treatment, the anthracites were removed from the furnace for further characterization.

X-ray Diffraction

X-ray diffraction data were acquired using a SCINTAG PAD-V X-ray diffraction unit that uses Cu Kα radiation. The slit widths of this unit are 2° for the primary beam, and 0.1° for the diffracted beam. The PAD-V was set for continuous scanning at a rate of 2.5°/min from 5° to 90° 2θ.

The anthracites were prepared for analysis in several different manners in order to check the effect of sample preparation on the X-ray diffraction pattern. First, the anthracites were taken directly from the graphitization furnace and mounted on a single crystal quartz slide from the Gem Dugout. The particle size of the anthracites was -60 mesh in this case, and the samples were mounted to the slide with petroleum jelly. The jelly was spread thinly over the surface of the slide and the anthracite powder was sprinkled over the top of this jelly layer. The idea behind this mounting process is to produce a random orientation of particles along the surface of the slide, approximately the same width everywhere. This method of sample preparation was repeated for –60 mesh anthracite samples that were heat-treated and then ground to pass a –100 mesh screen. The petroleum jelly must be used because the X-ray diffraction unit used for this research holds the quartz slide in a vertical position.

A second method of mounting the samples was carried out by drilling a 4-mm circular recess into the quartz slide and packing the powder into this constant volume. Again, –60 mesh and –100 mesh anthracites that had been heated to 2600°C were analyzed by this method. The two different mounting techniques produced different intensities, but the values for d-spacing, L_c, and L_a are all within experimental error. The

finer grinding also increased the peak intensity, but slightly reduced Lc, in agreement with grinding experiments in the literature.

The raw data curves were corrected for Cu $K_\alpha 2$ scattering and smoothed by both Pierson VII and Box Car fitting software built into the SCINTAG operating system. Next, the peaks were found by the peak finder program, also built into the SCINTAG software. The peak finder application uses a digital filter that contains two parameters the user must input. The two parameters are the ESD multiplier, and the ripple multiplier, which were set at seven and nine, respectively—the most stringent settings available for what curves will represent an identifiable peak. Once the peak finder application was performed the properties of the identified peaks were exported to a viewable file where d-spacing, relative intensities (as percents), absolute intensities, and full width at half maximum (FWHM) were listed. The d-spacing, an important indicator of graphitic development, was instantaneously calculated from the (*002*) peak by the Bragg equation derived using simple geometry applied to the crystal configuration shown below.

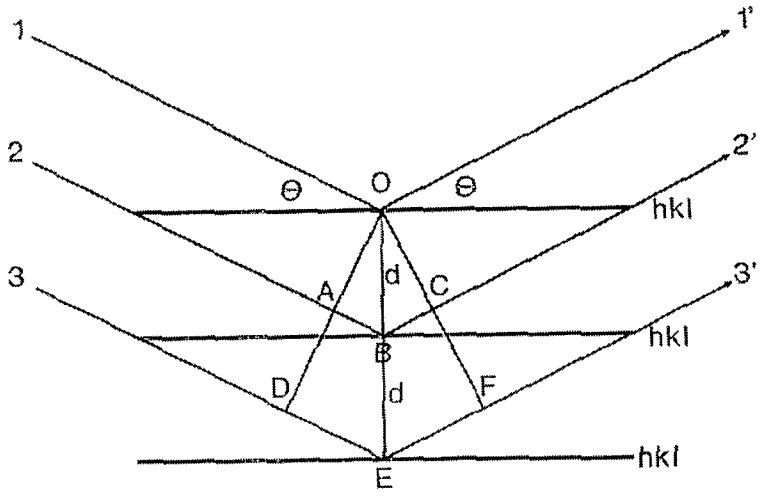

The Bragg equation is:

$$n\lambda = 2d \sin\theta$$

where n=diffraction order, or 1 for the (*002*) peak

λ= wavelength of Cu K_α which is 1.54059 Å

d= interlayer spacing

θ= diffraction angle of (*002*)

The crystallite size, L_c, was also calculated from the (*002*) peak for all the samples using the Scherrer equation:

$$L_c = K\lambda / (\beta \cos\theta)$$

where L_c= crystalline height

K= Scherrer constant, taken as 0.9

β= FWHM in radians and:

$$\beta^2 = B^2 - b^2$$

and B= peak broadening of the (*002*) reflection of the sample

b= peak broadening of crystal standard, quartz was used for this

As seen in the Scherrer equation a standard is used to correct for instrumental broadening. The standard was a highly crystalline material that should have little broadening due to its structure, thus any broadening can be attributed to the instrument. Quartz was used as the standard for this research. In the case of graphitized anthracite, broadening of the (*002*) peak is due more to small crystallite size than instrumental effects. The reason why small crystallite size causes broadening deals with the absence of planes capable of producing diffracted X-rays that will cancel out other rays that are very close to the Bragg angle.

The crystal diameter, L_a, was calculated by the Biscoe and Warren method where

$$L_a = 1.84 \lambda / (\beta \cos \theta)$$

A 95% confidence interval was placed on the X-ray diffraction parameters of d-spacing, L_c, and L_a obtained for the 2600°C samples. The equation used for this confidence interval was:

$$\text{Crystallite parameter} \pm 2.015*(\text{stdev}/\sqrt{(\ \#\ \text{of samples})})$$

where "stdev" is standard deviation.

Transmission Electron Microscopy

The structures of the four raw anthracites were analyzed using transmission electron microscopy (TEM). The goals of this analysis were to view the arrangement of the aromatic sheets of carbon comprising the anthracite, and to view the shapes of the pores present in the raw samples. The sample preparation used to accomplish these goals involved the grinding of the samples to as fine a possible size as possible; all could pass a –325 US mesh screen. The fine powders were then immersed in an alcohol solution and the larger particles sank to the bottom, thus leaving the finest particles in a suspended state. A tweezer was then dipped into the anthracite and alcohol mixture so that the suspended particles were contained in the droplet that adhered to the end of the tweezer. The droplet was then allowed to drip onto a TEM mount. The alcohol then evaporated, leaving behind the finest particles.

The analysis was performed using a Hitachi HF-2000 transmission electron microscope operated at 200 kV, with a point-to-point resolution of approximately 0.24 nm. High-resolution images were taken at magnifications of 100K to 500K on a negative

film on the vicinity of the optimal defocus. The films were than scanned on a flatbed negative scanning device at 400% image enlargement and 300DPI.

Computer Controlled Scanning Electron Microscopy CCSEM

The samples were prepared for analysis by first placing the anthracite or heat treated anthracite in a furnace at 90°C for 24 hours. Two grams of sample were then mixed with three grams of melted carnuba wax and poured in a rubber sample mold. An epoxy was then used to cover the surface of the sample and wax. The epoxy was then polished in six steps with each step a less severe grade of grit used in the polishing. Once the polishing was complete, the samples was inserted into the computer controlled scanning attachment and the analysis begun. The electron beam was rastered over the surface of the sample at three magnification 800, 250, and 50X magnification. The shape of the particle is recorded using the equation:

$$\text{Shape factor}=(\text{perimeter})^2/\text{Area}*4\pi$$

The weightof each element comprising an inorganic was determined by totaling the number of X-ray counts and then dividing an individual elements number of counts by this total to get the percentage of an element's X-ray counts. This percentage was then multiplied by the amount of ash determined from proximate analysis.

Results and Discussion

Part 1. Anthracite graphitization via carbide formation

Introduction:

Anthracite behaves as both a graphitizing (soft) and non-graphitizing (hard) carbon [1-6]. Franklin used a detailed X-ray diffraction study of raw and heat treated anthracites to explain this phenomenon [1]. She found that the anisotropy of the pores in char samples heated to 1000°C were responsible for this dual behavior [1]. The flattened pores were created by the edge-on alignment of the basic, pre-graphitic crystallites in these pore walls. The edge-on alignment allowed for the crystallites to condense into larger crystallites when exposed to temperatures in excess of 2000°C. Franklin states that whole graphene layer movement was responsible for anthracites ability to graphitize, as opposed to individual carbon atoms being added to the end of an aromatic layer [1]. The evidence for this theory was the recognition of a significant increase in degree of graphitization, or graphitization "jump," above 2500°C. A single carbon addition would be a continuous process, she argued, and therefore would not produce a dramatic increase in degree of graphitization over a narrow temperature range.

Franklin's work was the first and most substantial in explaining the difference in behaviors during heat treatment between graphitizing and non-graphitizing carbons, and only minor modifications to her theories have been made. Mering and Mare followed up Franklin's work by basically agreeing with her findings, but point out that the graphene or aromatic layers of carbon are not perfectly planar in the raw carbon source, whether it be a graphitizing or non-graphitizing carbon [4]. In her illustration depicting the graphitization process, Franklin shows perfectly flat graphene layers contained within

small crystallites at temperatures at or below 1000°C. Mering and Mare argue that these small crystallites exist, but the layers comprising them are twisted and non-planar, and that interstitials or cross-links can bind these stacked layers together [4]. Therefore the graphitization process occurs in several stages. First, the layers must be healed or annealed in order to become planar. Next, the interstitials connecting the stacked layers must be removed, which allows ordering in the c-direction and is evidenced by a narrowing of the (*002*) peak. Lastly, the now-planar graphene layers contained within small crystallites that have no cross-links can combine with neighboring layers to form larger crystallites. This last step is achieved by whole-layer movement, as Franklin stated, and leads to growth in the a-direction.

The next breakthrough in understanding of the graphitization process with particular reference to anthracite was made by Oberlin, using high resolution transmission electron microscopy (HRTEM) [2,3]. Oberlin used HRTEM to visualize the microtexture of anthracites heat-treated to various temperatures in order to determine whether the flattened or anisotropic pores described by Franklin could be detected. Indeed Oberlin saw the development of flattened pores and anisotropic microtexture as heat treatment temperature (HTT) was increased. The study included twelve anthracites from various parts of the world [2]. This method, in essence, provided pictorial evidence for Franklin's assumptions that made decades earlier when such powerful techniques as HRTEM were not yet available.

The use of HRTEM to study anthracite graphitization was continued by Rouzaud and co-workers [7]. They published no TEM images, but claimed to be able to predict differences in degree of graphitization of various anthracites by viewing the pore shape in

the raw, or unheated, anthracite samples. Four classes were defined: microtexture 1A consists of spherical pores where the basic structural units (BSU) show no preferential alignment and essentially form a pore wall by being compacted together in no particular order. Microtexture 1B shows a random distribution of BSU and is indicative of immature, or low-rank coals. Microtexture 2A is described as pore flattening and considered the best orientation for enhanced graphitizability. The BSU are aligned end-to-end and therefore are more easily able to experience dehydrogenation and condensation reactions necessary for crystallite growth. Microtexture 2B, or flow anisotropy, also has the end-to-end alignment, but flattened pores are not witnessed. So the anthracites with flattened or anisotropic pores present in the raw sample were the most highly graphitizable.

However, several items contradict this theory that degree of graphitization can be predicted by pore shape of the raw samples. In the original paper by Oberlin describing the novel use of HRTEM for carbon study, she showed two types of microtexture in the same anthracite sample [2]. Oberlin studied an Abernant anthracite char (heated to 1000°C) and showed that both Type A and Type B microtextures, which she described as isotropic or anisotropic microtexture respectively, were present in one sample of the char. Because at least two microtextures can be found in a single anthracite, it would seem difficult to define four classes of pore microtexture and be able to predict degree of graphitization based on these classes, because one anthracite sample has been shown to contain more than one type of microtexture.

Because no actual HRTEM images of the four types of microtexture described by Rouzaud were published, the four anthracites used in this study were analyzed using HRTEM in order to determine if these four types of microtexture could be visualized.

High Resolution Transmission Electron Microscopy for Microtexture Evaluation:

For this evaluation the experimental techniques developed by Oberlin were followed as closely as possible [2]. However, the HF2000 TEM unit located at Penn State's Materials Research Institute was not capable of completely re-creating Oberlin's work, but the images produced are sufficient for microtexture visualization.

Oberlin "gently grinds" her anthracites and used lattice fringe imaging, bright field, and dark field techniques to study the anthracites' microtextures [2]. Oberlin first produced a selected area diffraction (SAD) pattern in order to view what (*hkl*) bands are visible. She then used a beam aperture small enough so that visualizations could be made at various points along the (*hkl*) lines. The investigations were done in dark field, so she is essentially taking a picture of the diffracted image, so carbon layers appear dark and pores bright.

The HF 2000 instrument used in our work did not have dark field availability, nor a beam aperture small enough to view the structure at various points along a given (*hkl*) band. Therefore the investigations were done in bright field, where all (*hkl*) bands are present because the image seen is transmitted, not diffracted as in dark field work. In the case of raw anthracites, though, the only (*hkl*) band of any intensity is the (*002*), so a transmission image (i.e. a bright field image) would essentially be a (*002*) band image

anyway. The results of this bright field investigation are presented on the next page and show that Oberlin's method of visualization was adequately reproduced.

In summary, Oberlin used HRTEM to visualize the microtexture of twelve different anthracites that had been to various temperatures [2]. She found that the microtextures changed with increasing HTT from isotropic to anisotropic, indicating the transition from a non-graphitic carbon to a graphitic carbon. In the 1000°C heat-treated samples she identifies two types of microtexture, Type A and B, representing isotropic versus anisotropic. Oberlin also identified both types of microtexture in one sample, or in different regions of the same anthracite. Her TEM approach to explaining anthracite graphitization was later continued by Rouzaud, who identified, via cartoons, four different pore shapes and microtextures found in anthracite that will lead to different degrees of graphitization.

The TEM studies reviewed here serve two purposes. The first is to present a generic mechanism for anthracite graphitization that is true for all anthracites from all parts of the world. The second is to point out microtextural differences in raw anthracites from various geological regions and show that these differences are responsible for varied degrees of graphitization. Both studies focus on the physical and organic portion of the anthracites, in terms of pore shape and basic structural unit alignment. However, there is evidence from Oberlin's work that elements contained within the minerals of an anthracite react with the carbon present to form carbides [2,3,8]. Oberlin noted the formation of hollow graphitic shells left behind after the metal from the carbide vaporized at highest HTT. She did not go into detail about how these carbides formed and then how they formed hollow graphitic shells, but only said that this carbide

formation is "a parasitic effect that masks the true anthracite graphitization mechanism" [2]. So even in work that was undertaken to show the importance of microtexture as a controlling factor in the anthracite graphitization mechanism, evidence of "catalytic graphitization" or modified graphitization was found [2]. Therefore, the amount and type of mineral matter present may be responsible for observed differences in extent of graphitization of various anthracites, and, in some instances, may be the crucial factor in the graphitization mechanism itself.

X-ray Diffraction Analysis of Raw and Heat Treated Anthracites:

Oberlin used HRTEM to visualize anthracite graphitization, and Rouzaud used the technique to predict differences in degree of graphitization of various anthracites [2,7]. In our research, X-ray diffraction was used to follow the structural changes incurred during heat treatment, and to show any differences in degree of graphitization. The methodology of this research was to select a suite of anthracites from Pennsylvania and expose them to the same HTTs for the same period of time and then determine if any differences in extent of graphitization could be observed. This information would then be used to select an anthracite for use as a filler in graphite production. The four anthracites, LCNN, Jeddo, UAE, and Summit were all heat treated to 2000, 2200, 2500, and 2600°C for one hour in a vacuum. The X-ray diffraction patterns of the raw and heat-treated anthracites are shown in Figures 1 to 20 beginning on the pages that follow.

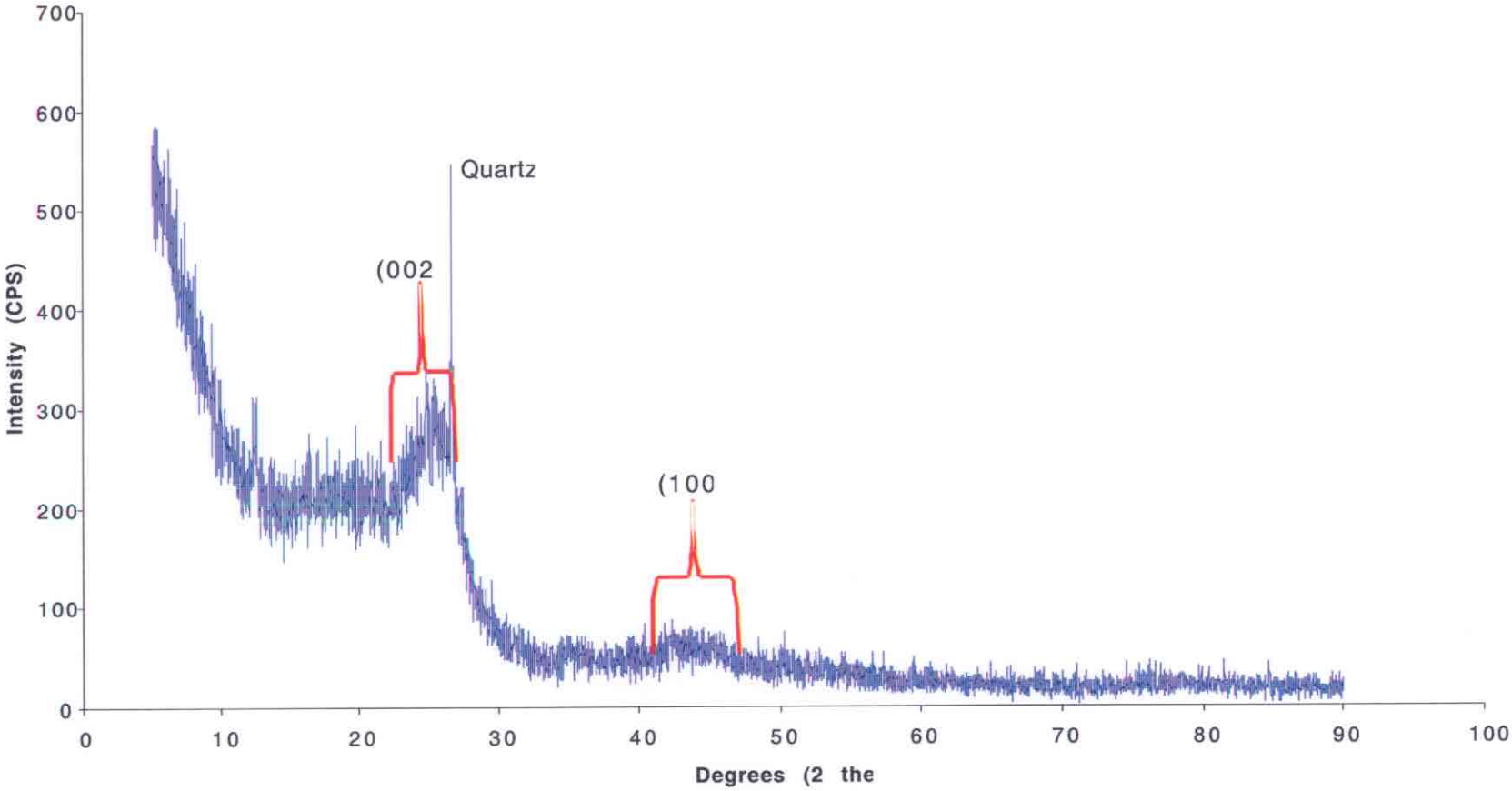

Figure 1 X-ray diffractogram of raw UAE anthracite

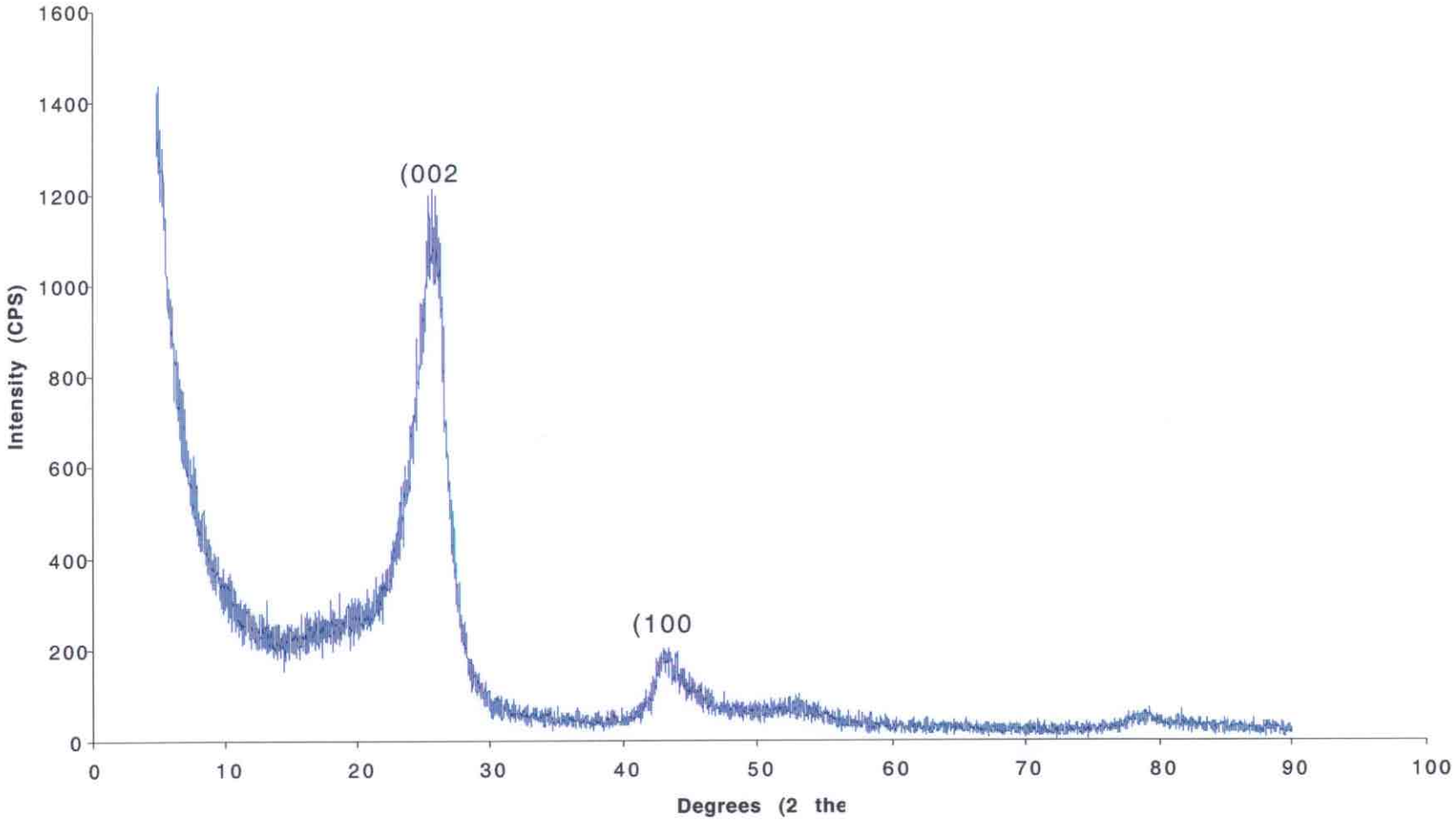

Figure.2 X-ray diffractogram of UAE anthracite heated to 2000°C

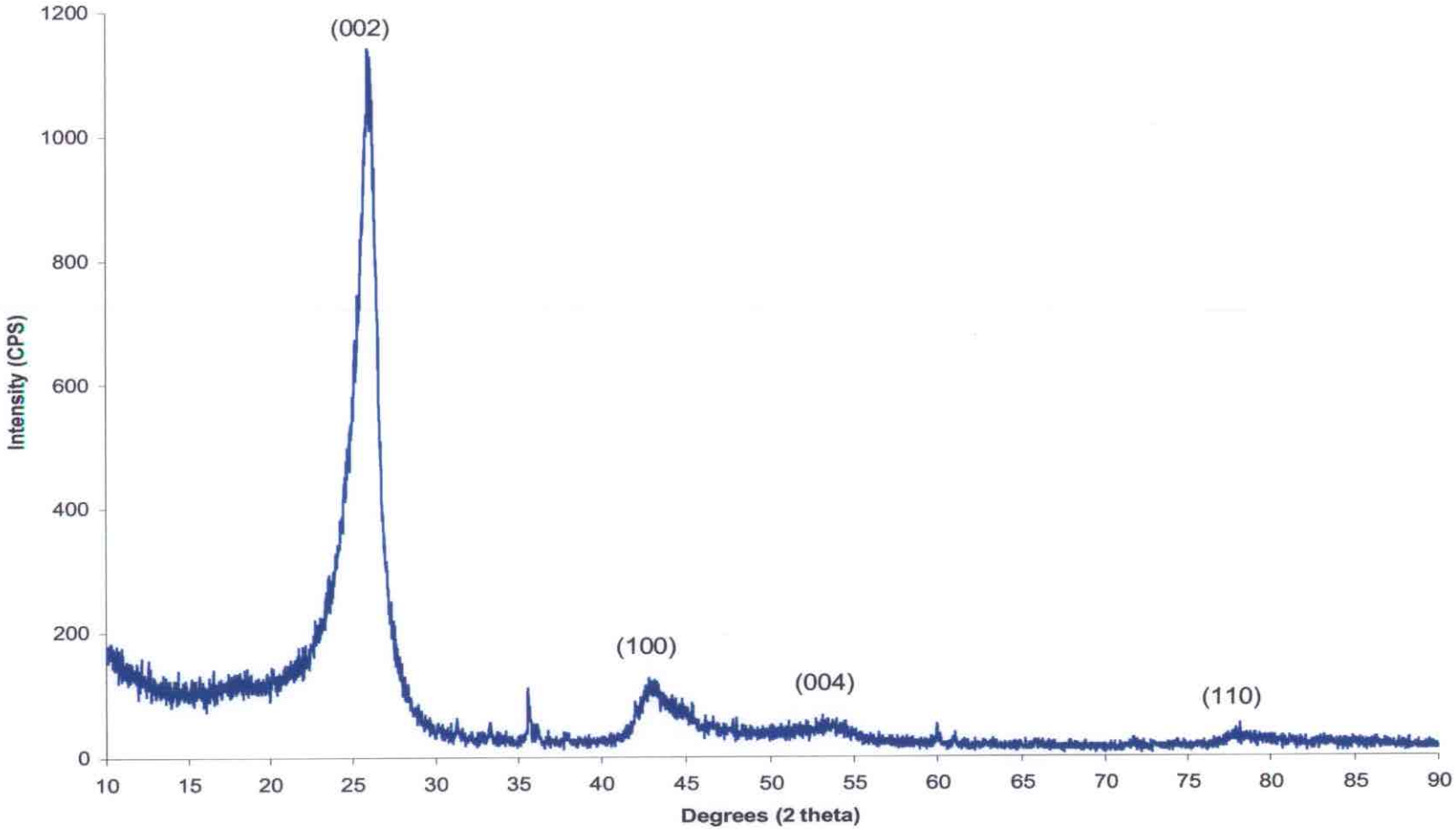

Figure.3 X-ray diffractogram of UAE anthracite heated to 2200°C

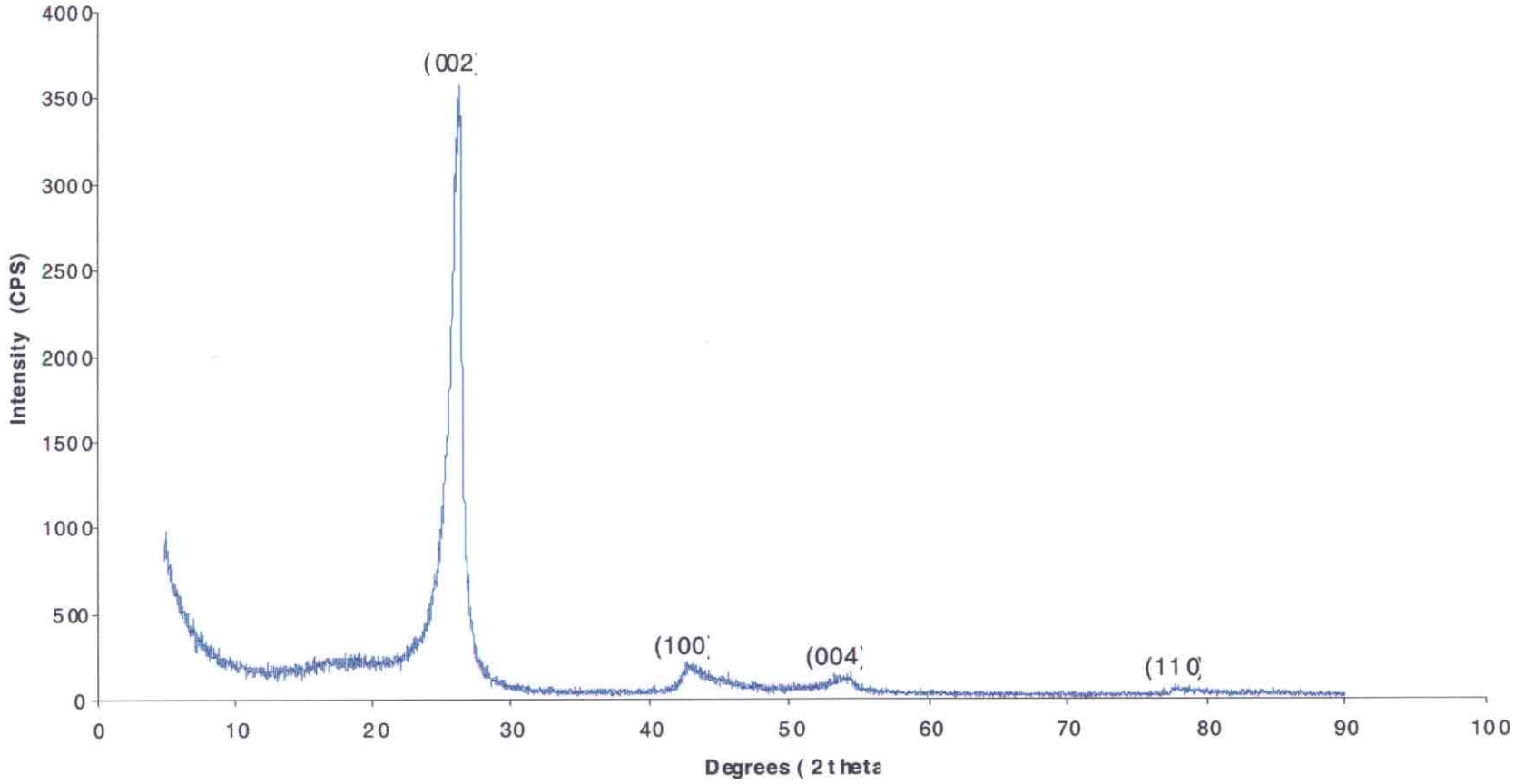

Figure 4 X-ray diffractogram of UAE anthracite heated to 2500°C

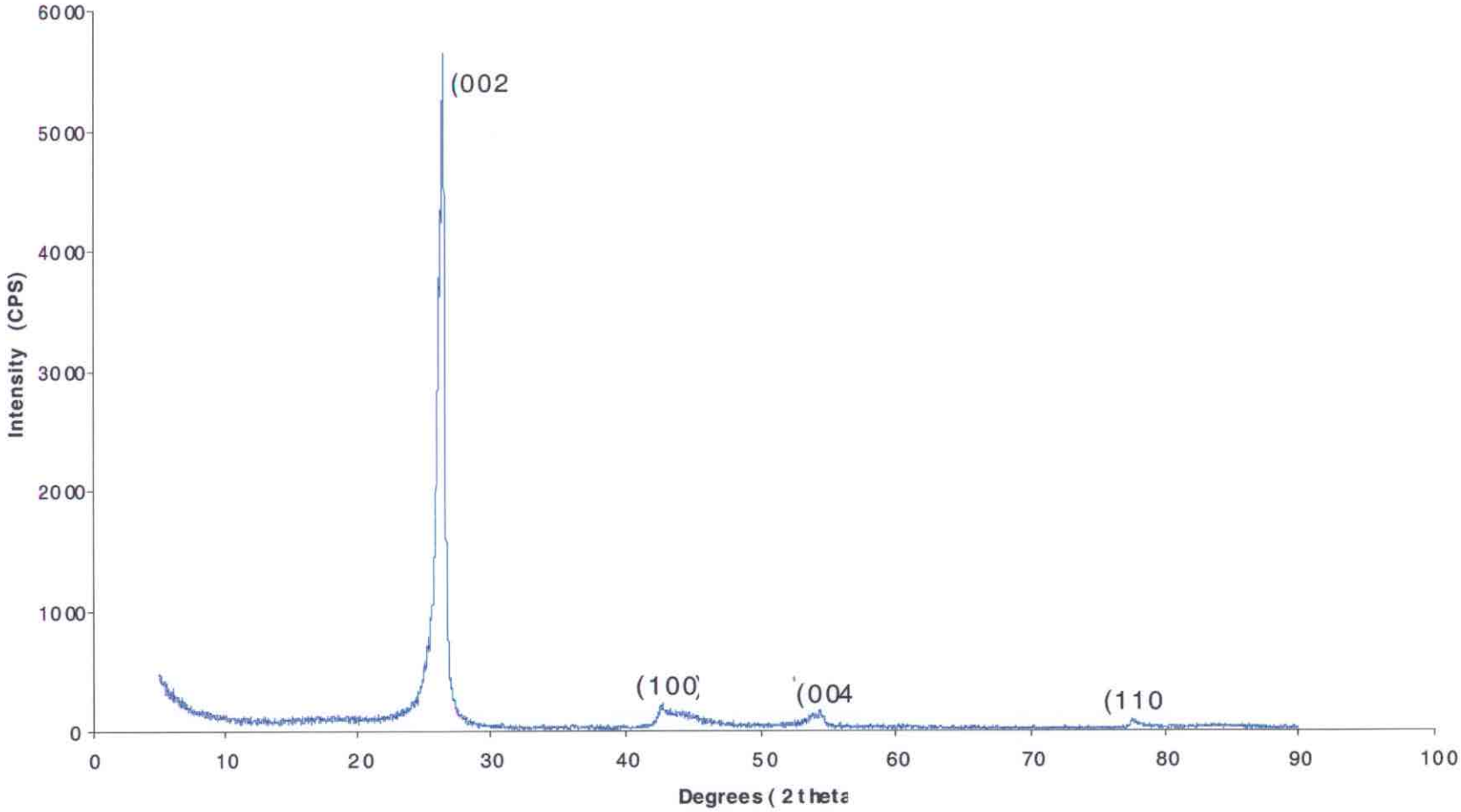

Figure 5 X-ray diffractogram of UAE anthracite heated to 2600°C

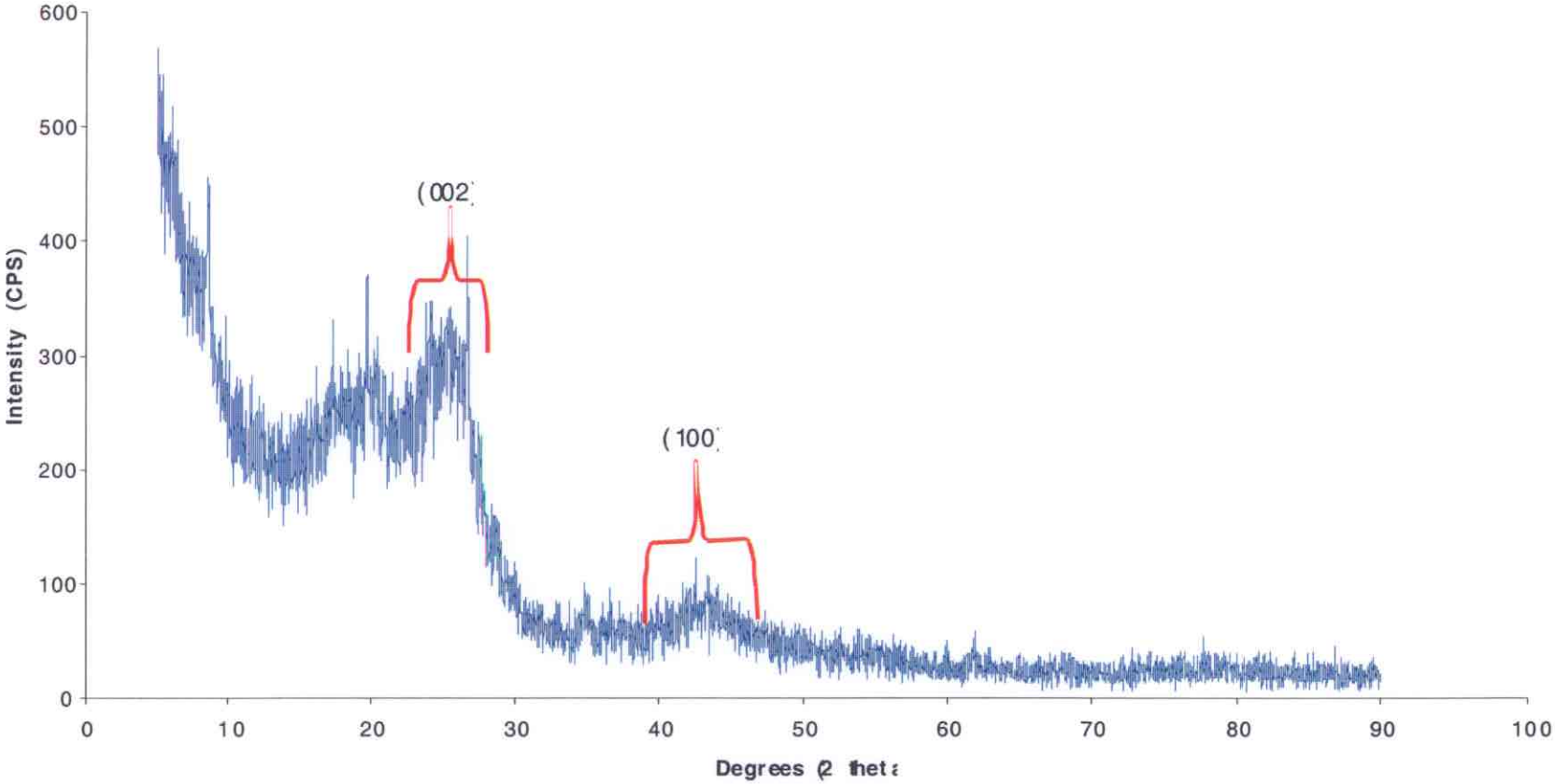

Figure.6 X-ray diffractogram of raw Jeddo anthracite

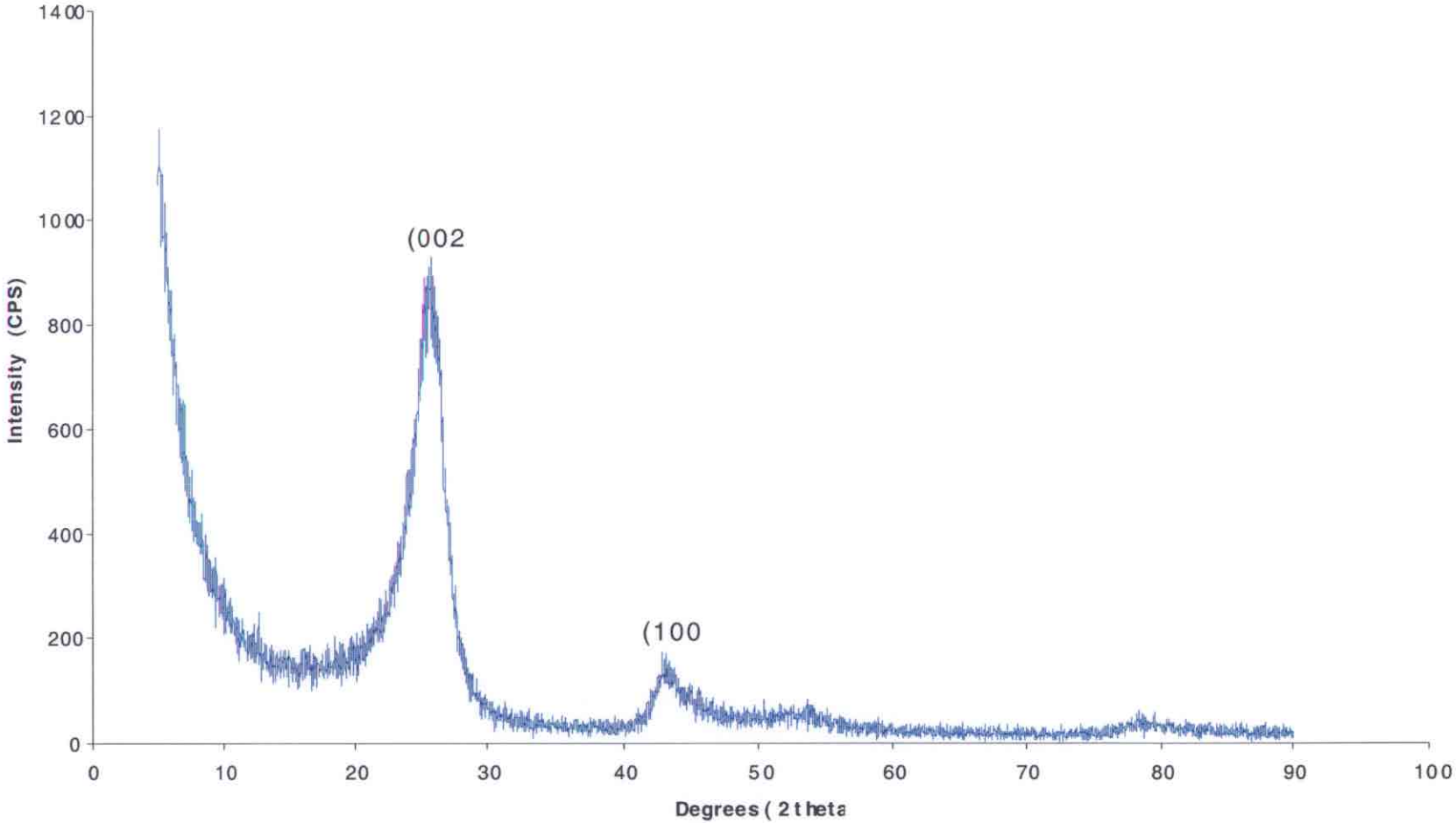

Figure 7 X-ray diffractogram of Jeddo anthracite heated to 2000°C

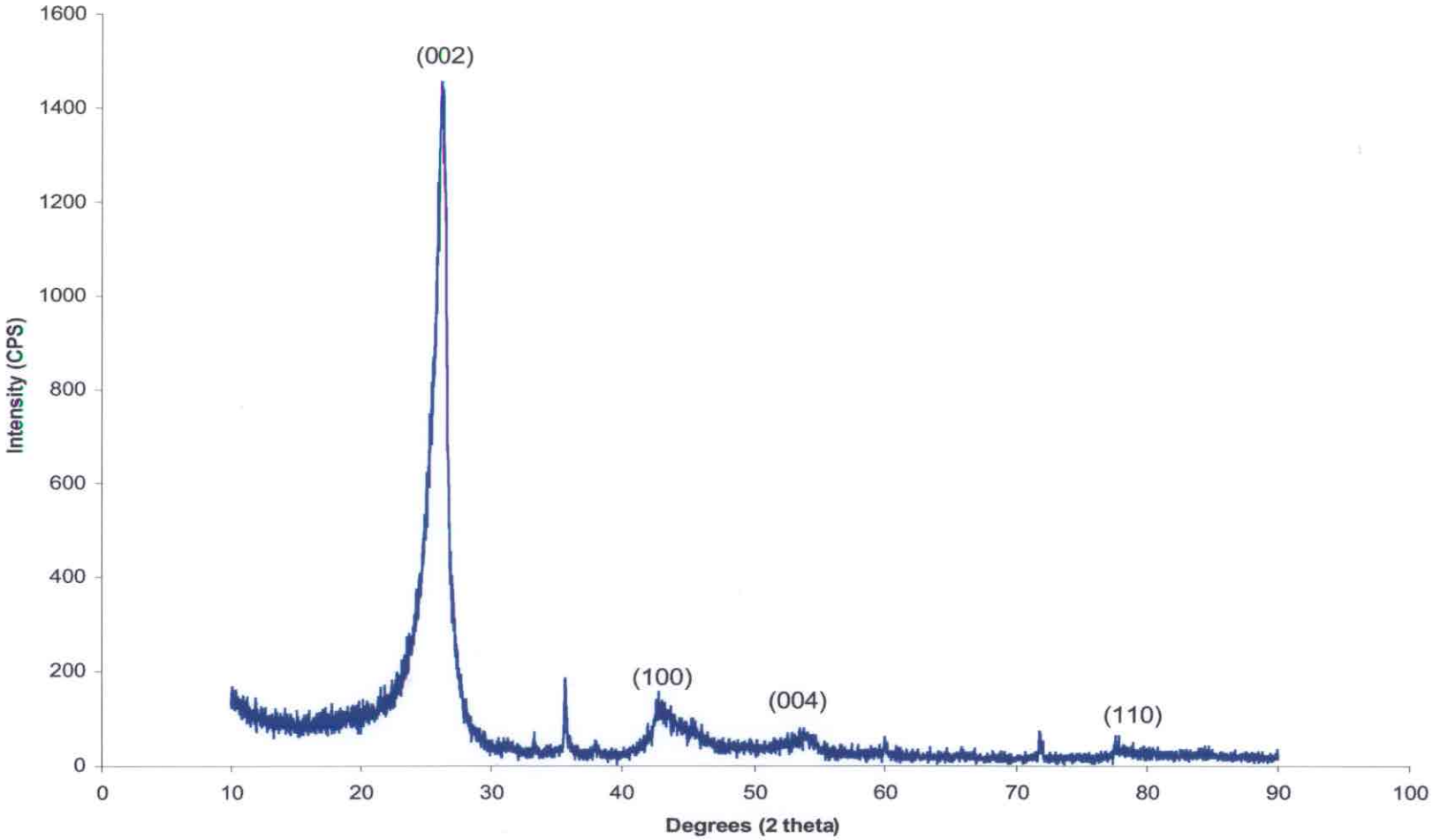

Figure 8 X-ray diffractogram of Jeddo anthracite heated to 2200°C

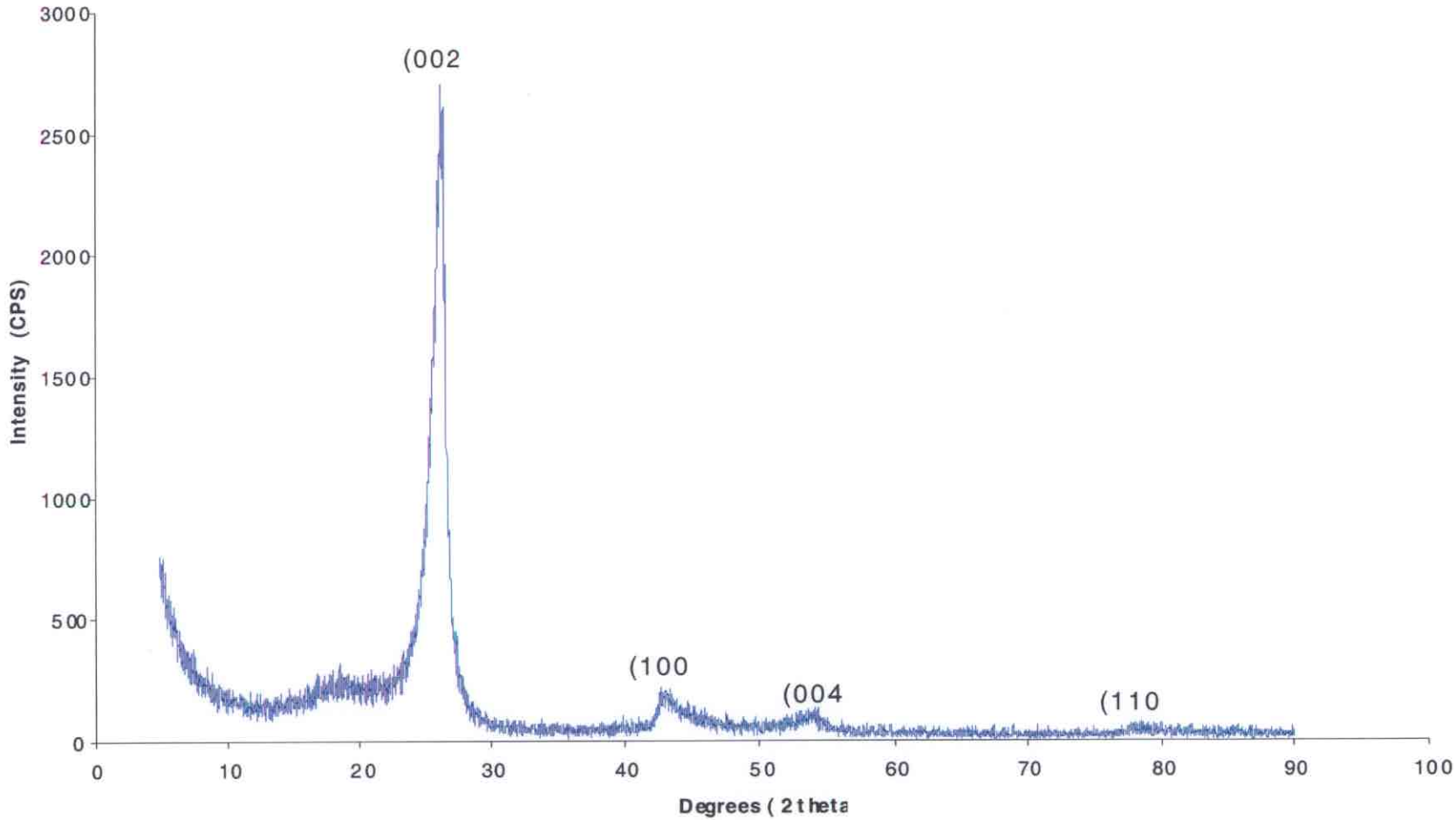

Figure.9 X-ray diffractogram of Jeddo anthracite heated to 2500°C

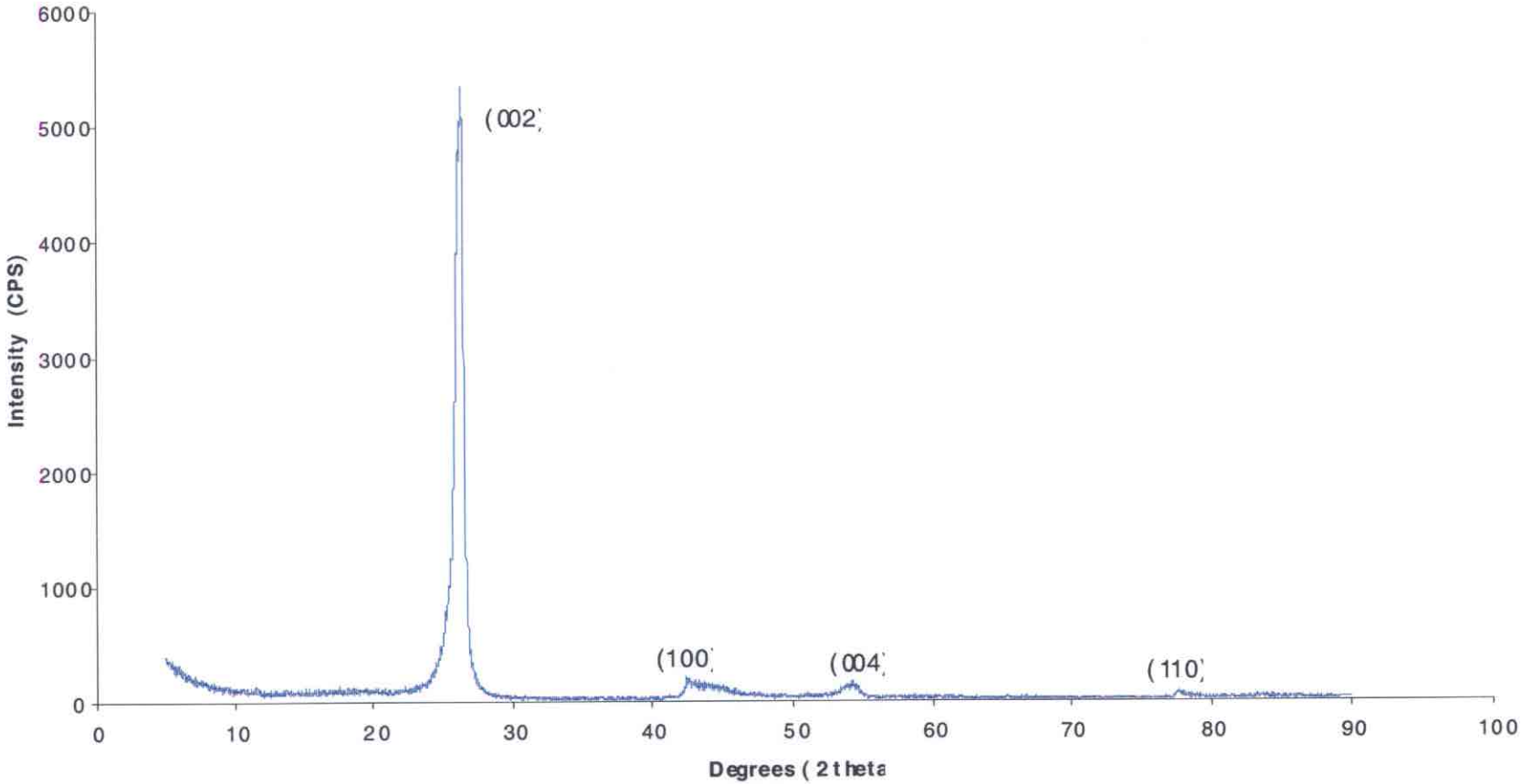

Figure 10 X-ray diffractogram of Jeddo anthracite heated to 2600°C

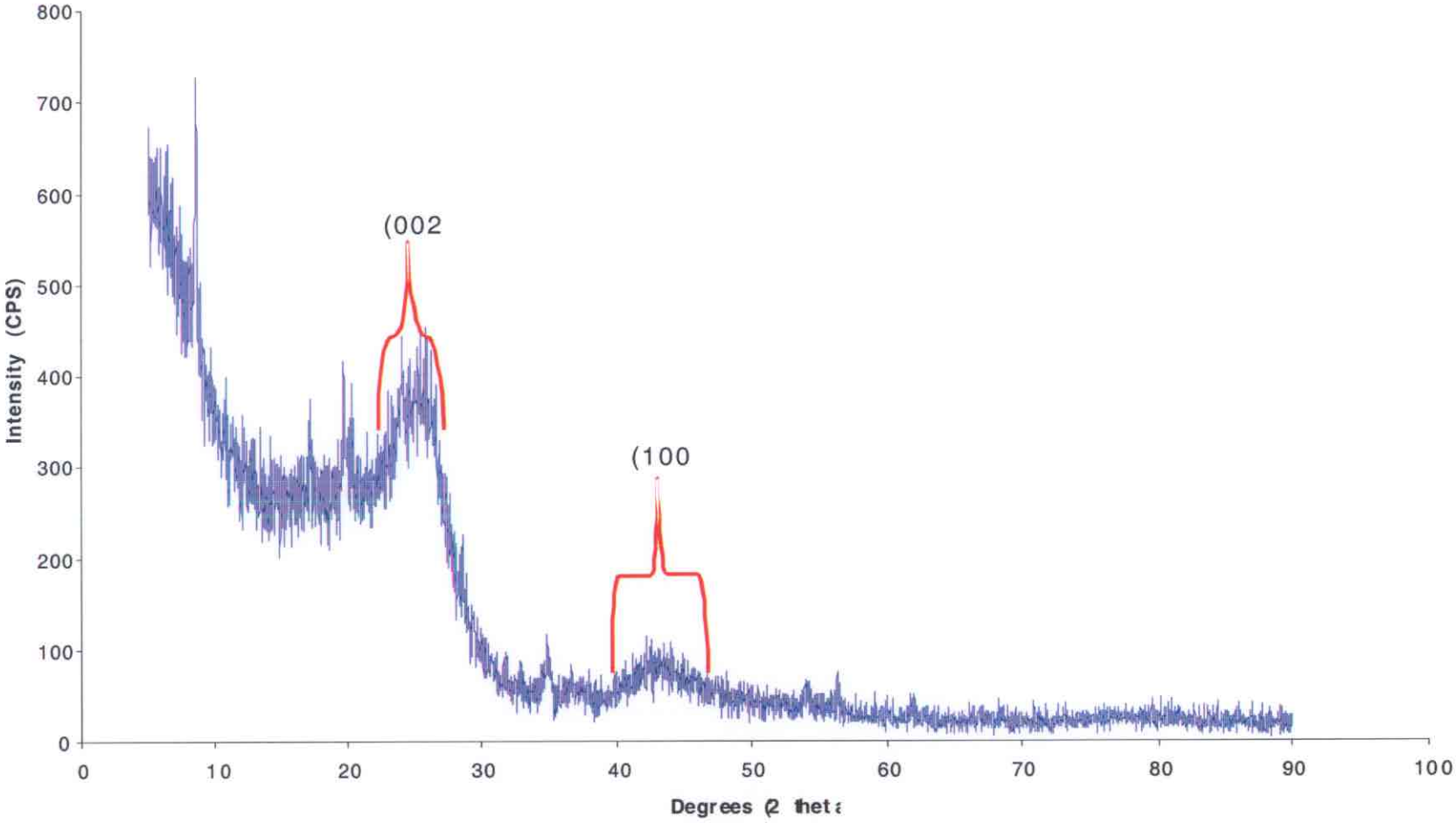

Figure 11 X-ray diffractogram of raw LCNN anthracite

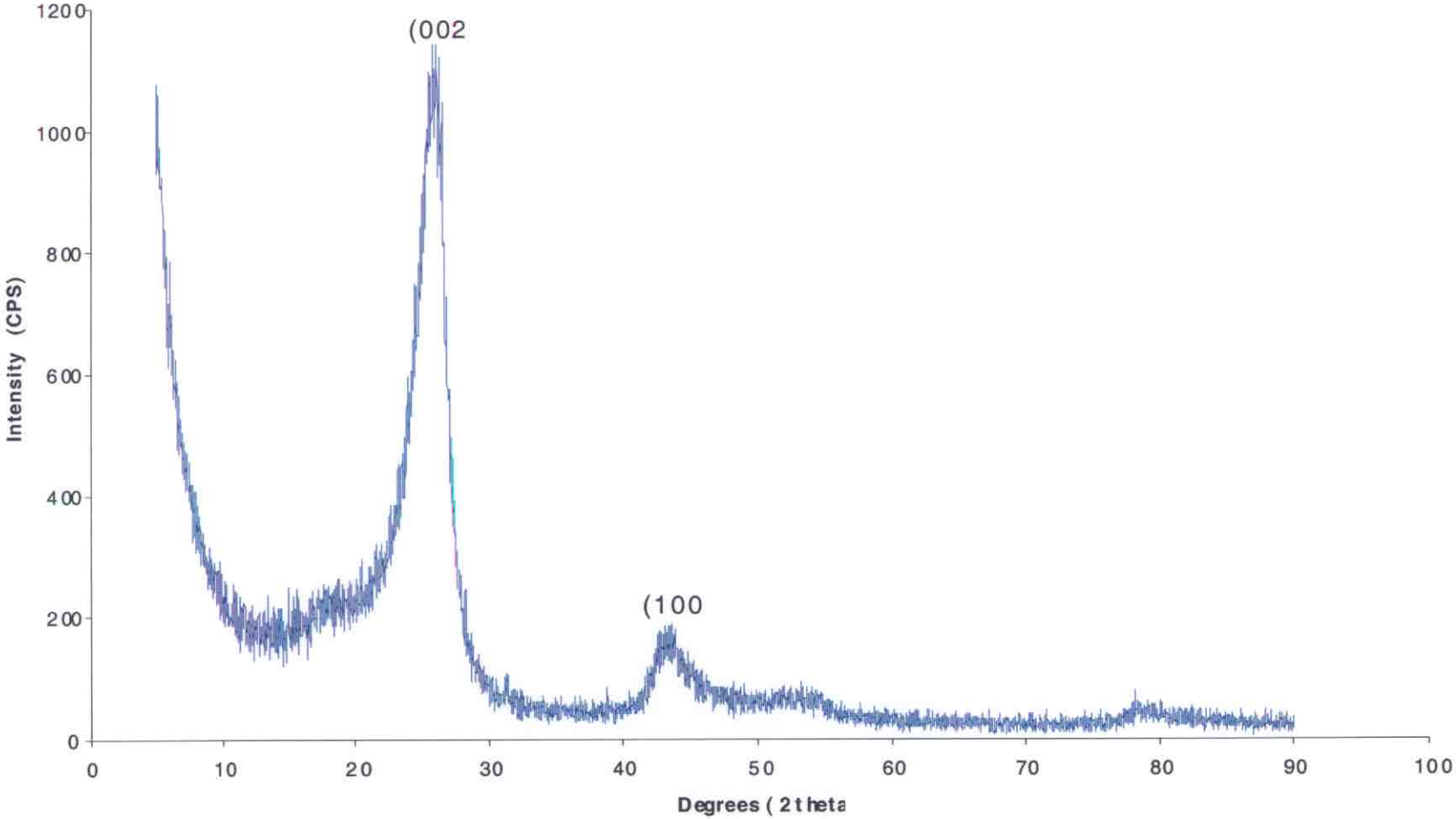

Figure.12 X-ray diffractogram of LCNN anthracite heated to 2000°C

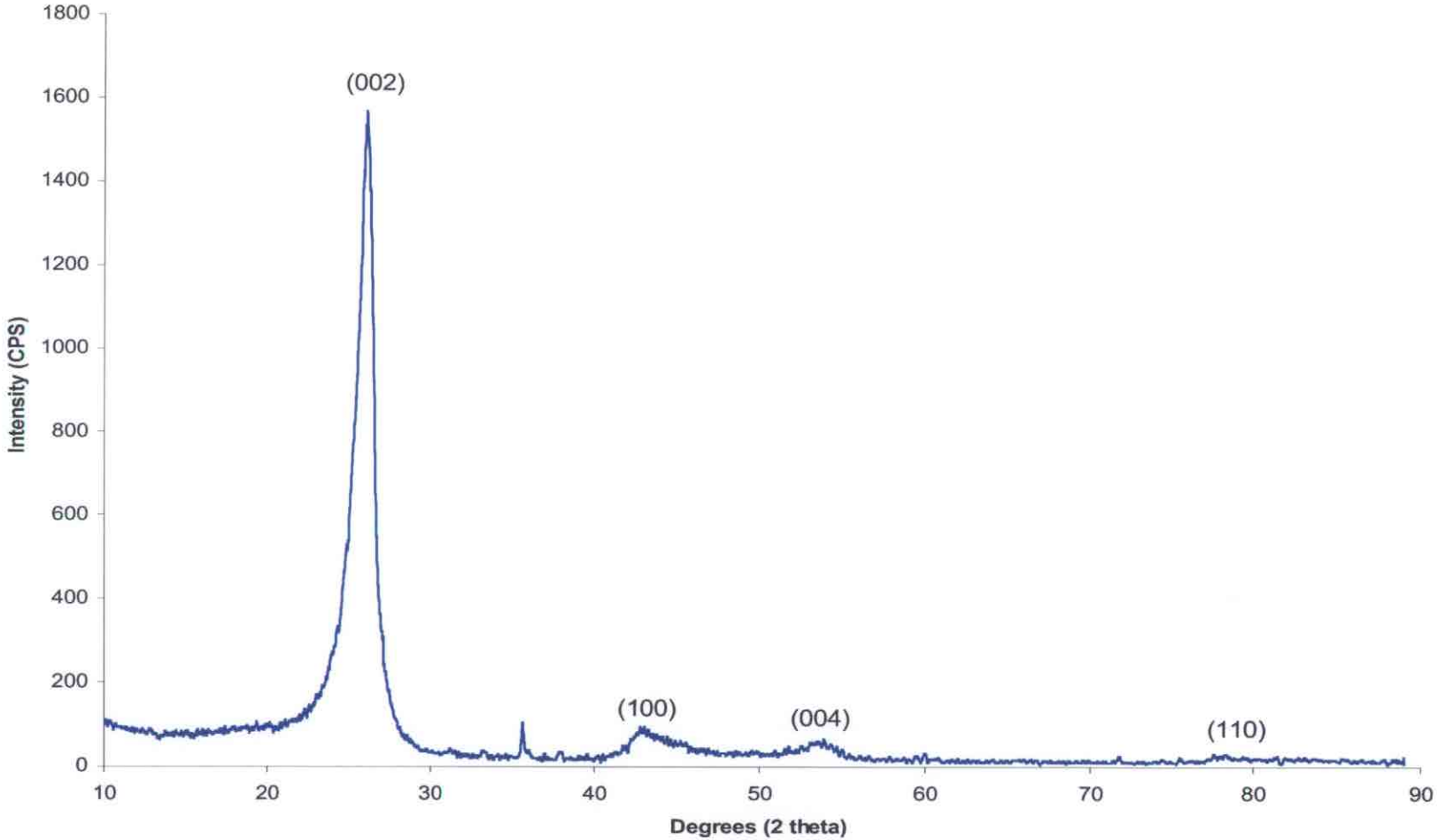

Figure 13 X-ray diffractogram of LCNN anthracite heated to 2200°C

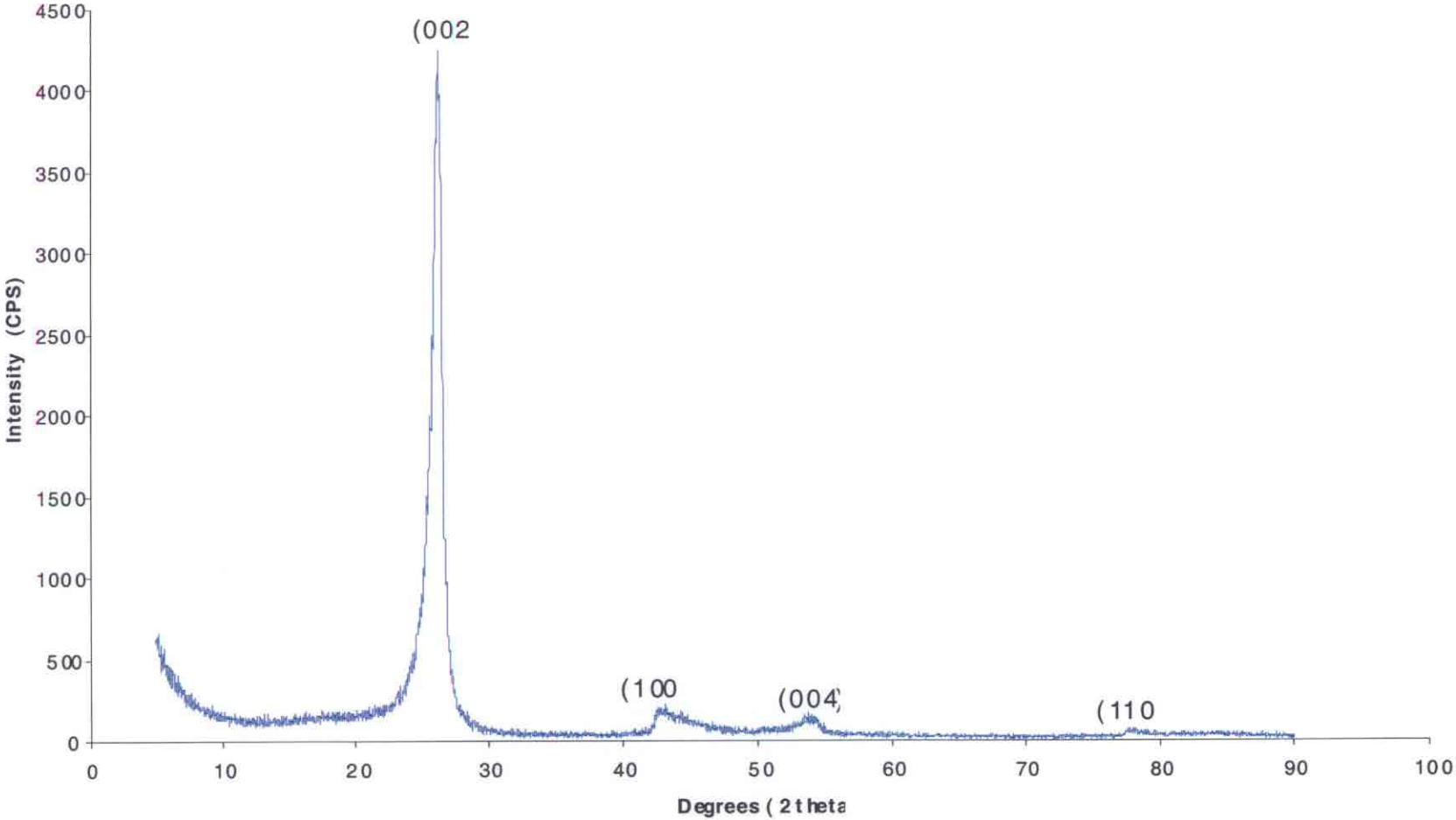

Figure.14 X-ray diffractogram of LCNN anthracite heated to 2500°C

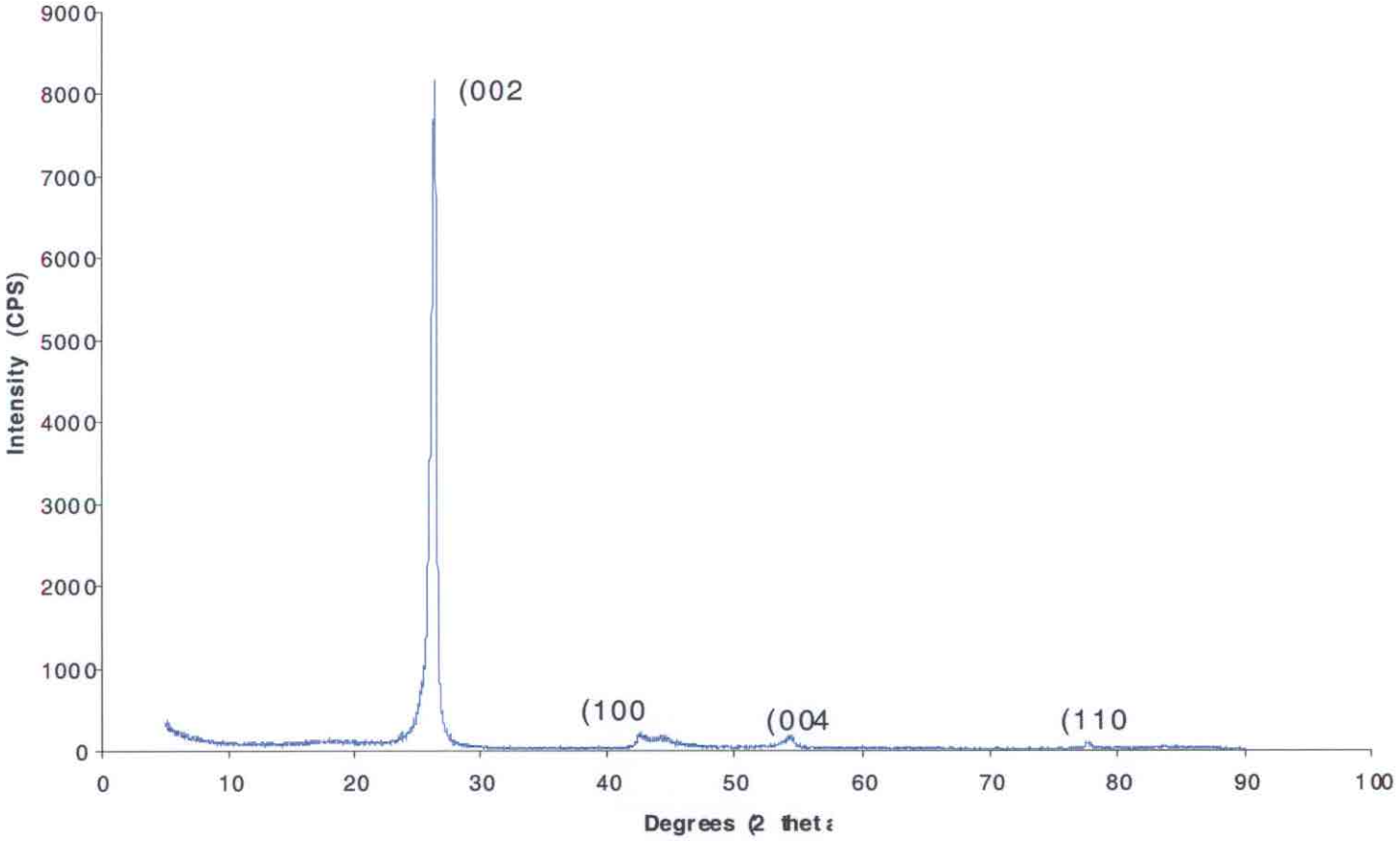

Figure.15 X-ray diffractogram of LCNN anthracite heated to 2600°C

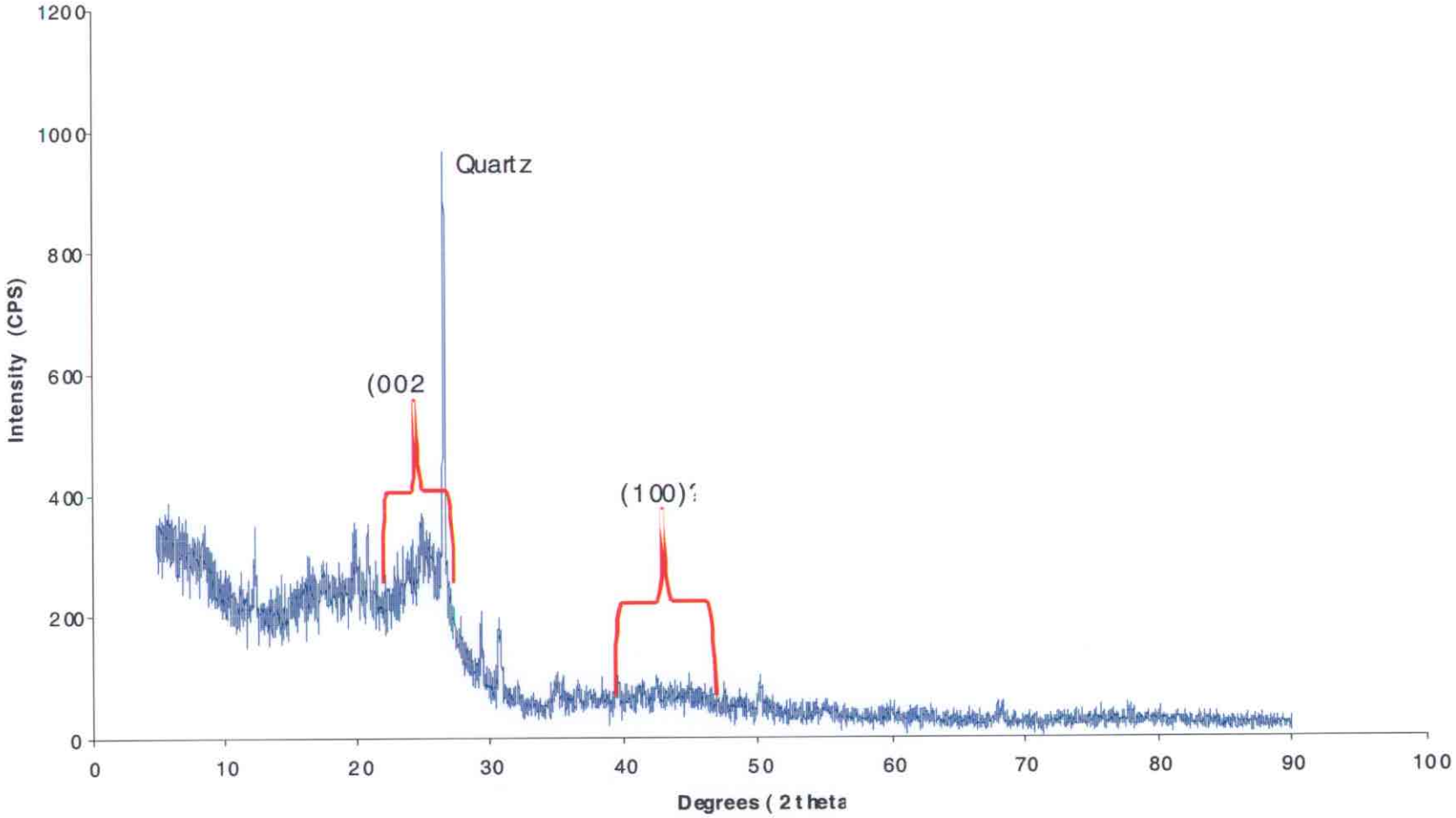

Figure 16 X-ray diffractogram of raw Summit anthracite

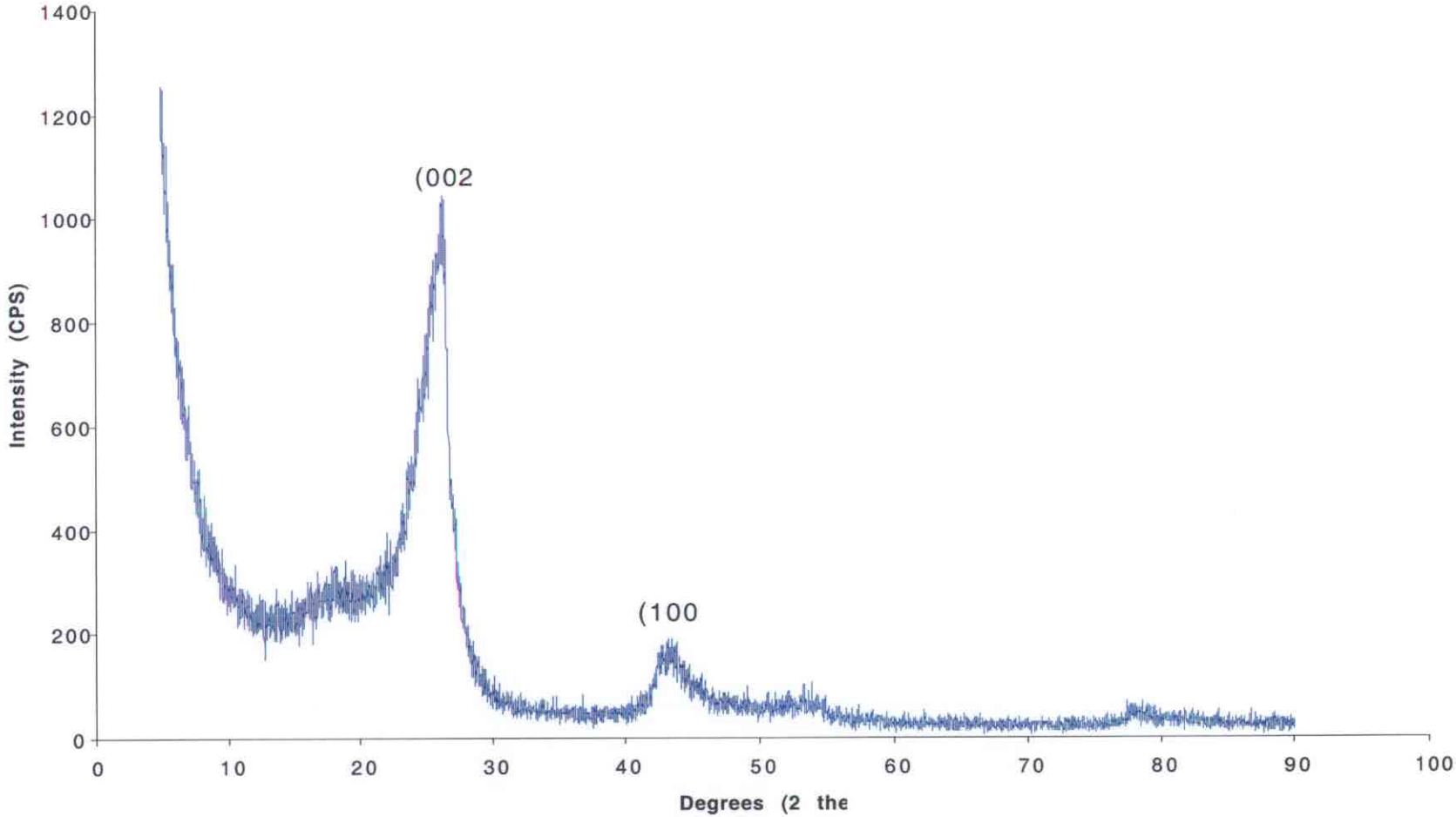

Figure 17 X-ray diffractogram of Summit anthracite heated to 2000°C

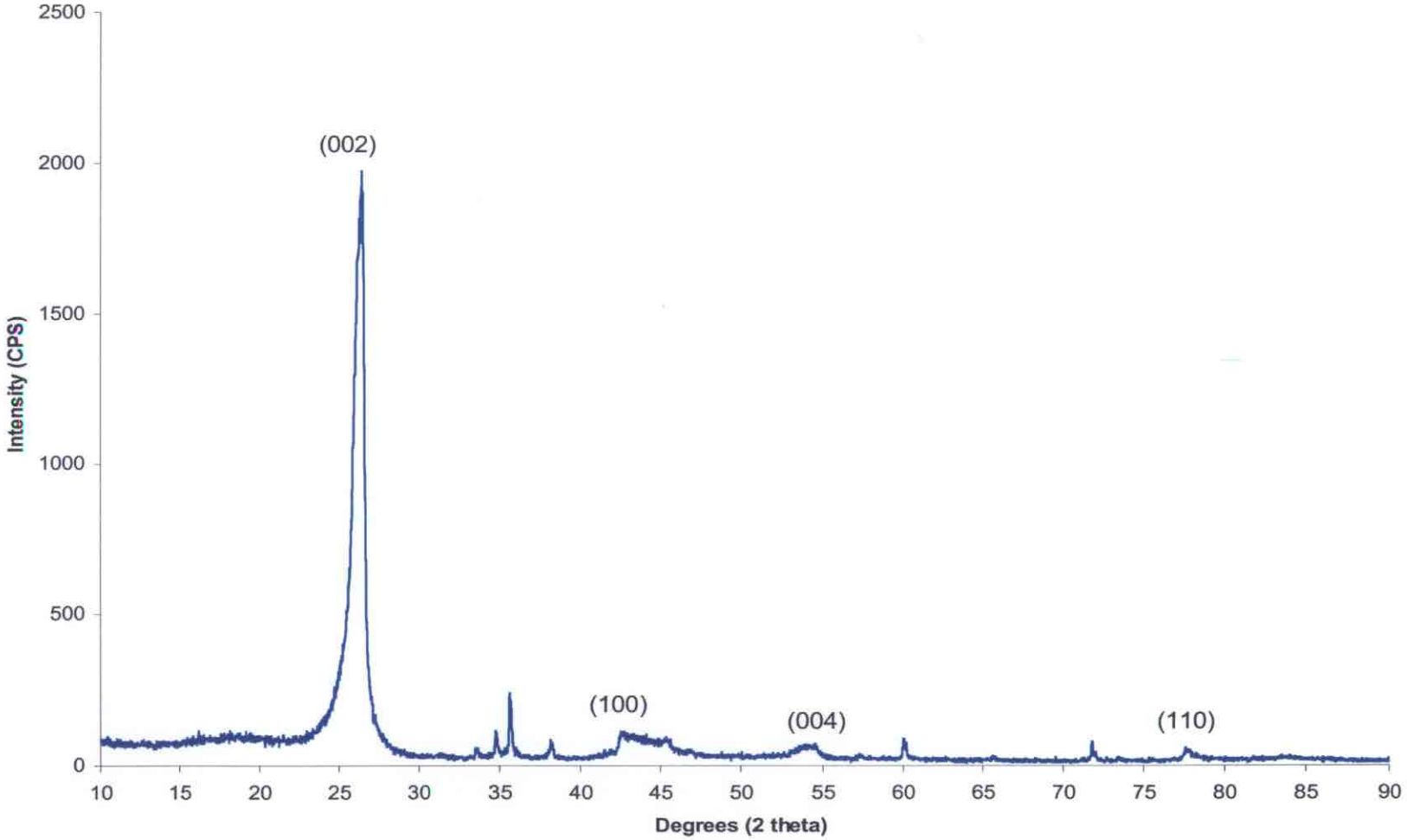

Figure 18 X-ray diffractogram of Summit anthracite heated to 2200°C

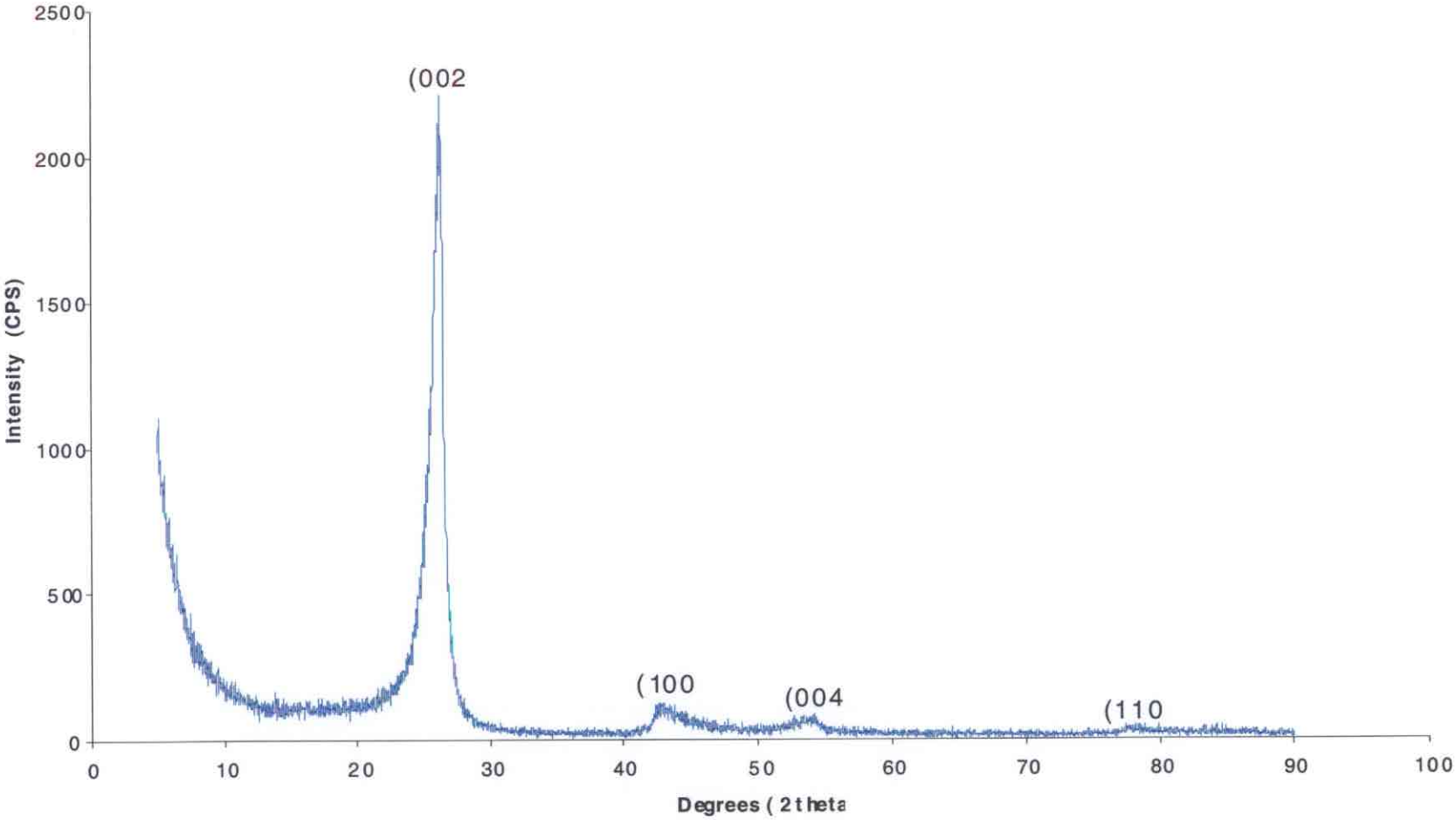

Figure 19 X-ray diffractogram of Summit anthracite heated to 2500°C

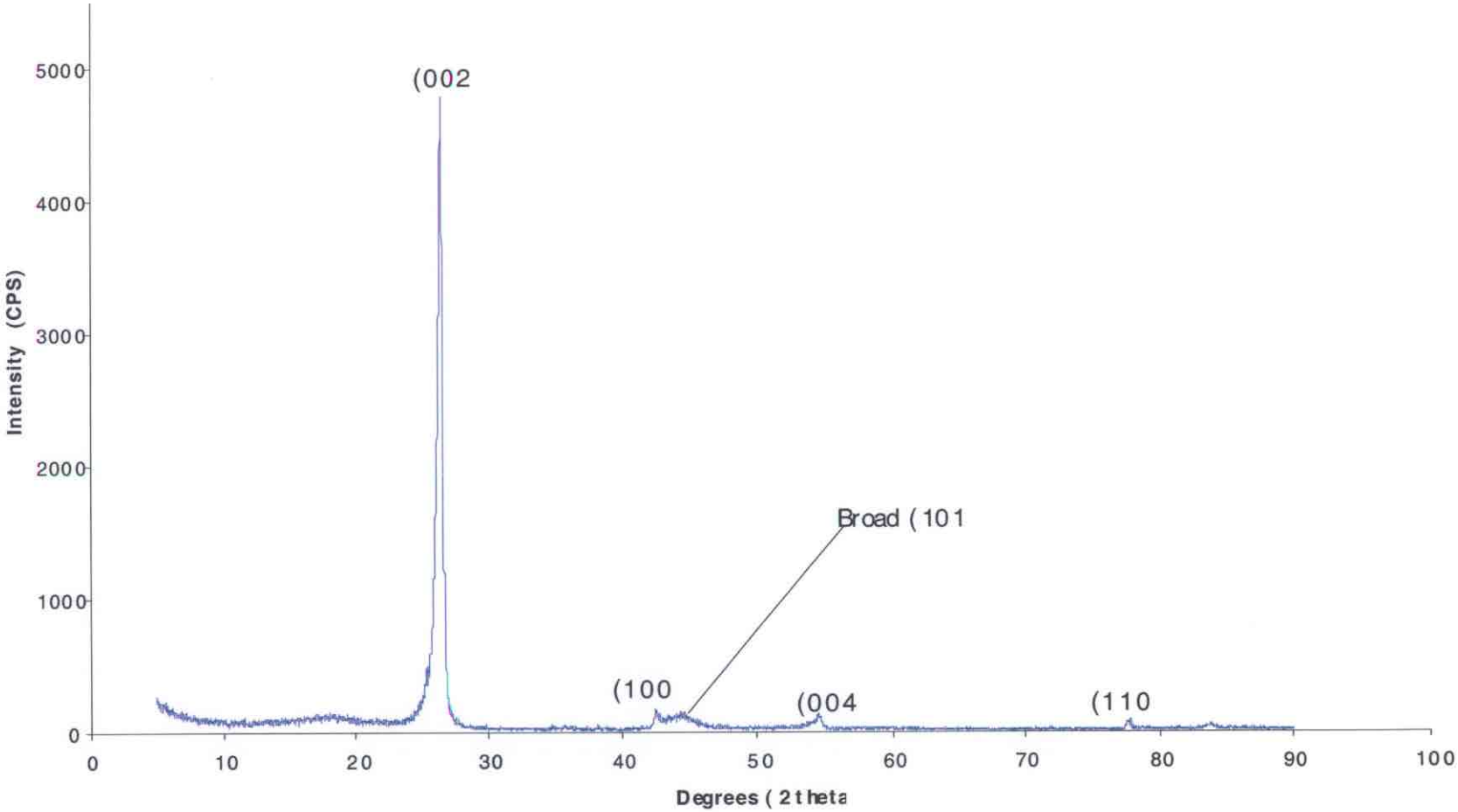

Figure.20 X-ray diffractogram of Summit anthracite heated to 2600°C

A determination of which sample becomes more like graphite is made by comparing the diffraction patterns, and in particular the location and properties of the peaks present, of these heat treated anthracites to the characteristic X-ray diffraction pattern of graphite. Therefore, the (*hkl*) reflections and their locations for a typical graphite are given in Table 1, to act as a reference for discussion of the X-ray diffraction patterns of the heat-treated anthracites.

Table 1 (*hkl*) peak location of characteristic graphite peaks

(*hkl*) peak	Location in 2θ
(*002*)	26.54°
(*100*)	42.39°
(*101*)	44.58°
(*004*)	54.66°
(*103*)	59.91°
(*110*)	77.54°
(*112*)	83.67°
(*006*)	87.06°

All the raw anthracites show weak and broad (*002*) and (*100*) peaks. These broad peaks are shown by the red brackets present in the X-ray diffraction patterns of the raw samples, Figure 1 for example. In some cases, the X-ray diffraction patterns of the raw anthracites show mineral, or inorganic, peaks. Again, an example of this is seen in Figure 1, where an intense, narrow, quartz peak is seen at 26.68°, to the right of the broad (*002*) peak. The presence of a distinct quartz peak can also be seen in Figure 16, the raw Summit anthracite. The fact that all the anthracites exhibit broad (*002*) and (*100*) peaks indicates that they have a turbostratic structure. Stacking is indicated by (*001*) peaks, such as (*002*), and two-dimensionality is observed as (*hk0*) peaks, like the (*100*) peak.

As temperature is increased, the broad (*002*) and (*100*) peaks become more intense and begin to sharpen, or narrow. The 2000°C heat treated samples clearly show an increase in intensity and decrease in full width at half maximum (FWHM) of these peaks. Also, there is a faint indication of the (*004*) and (*110*) reflections in all the 2000°C heat-treated samples that becomes more pronounced in the 2200°C samples. The appearance of the (*004*) peak represents the second order diffraction of the (*002*) peak, or where constructive interference is observed when the term "n" in the Bragg equation is equal to two. The (*110*) reflection is not related to the (*100*) peak in terms of being a whole integer multiple, as the (*004*) reflection is to the (*002*), but is another and separate (*hkl*) plane that indicates two dimensionality.

Analysis of the 2200°C heat-treated samples shows the continued narrowing and intensity increase of the (*002*) and (*100*), plus the definite appearance of the (*004*) and (*110*) peaks, as seen in Figures 3, 8, 13, and 18. However, the presence of reflections unrelated to those characteristic of graphite are also observed. These new peaks must be carbide peaks, because carbide formation is common between carbonaceous materials and metallic elements at these temperatures [10-16]. The specific carbides responsible for these peaks can be determined by recording their peak locations and comparing them with characteristic peaks from a database of carbides. However, this will provide only a partial list of the carbides present because of three reasons: (1) the detection limit of X-ray diffraction for a carbide mixed with graphite is 0.75 weight percent, so a carbide could be present, but in a quantity below the detection limit of the instrument; (2) a carbide could be present in a detectable quantity, but have peaks in the angle range of graphite, so they would be obscured, for example, by the broader (*002*) peak; (3) a

carbide could be amorphous, and not detected by X-ray diffraction at any concentration. Nonetheless, there unquestionably are carbide peaks present in the 2200°C heat treated anthracites that can be identified and assigned a 2θ position. Comparing these positions with characteristic carbide peaks will at least give a partial list of the carbides formed during thermal treatment.

A method for defining the position of carbide peak must now be established. SCINTAG software, the manufacturer of the X-ray diffraction unit used for this research, is available that will take input from the user and analyze the diffraction pattern in order to "find" peaks. The user can vary the stringency of the requirements used by the peak-finder software from SCINTAG to find literally hundreds of peaks, or just one. Because of this variation in the number of peaks found based on the input parameters, the method for "finding" carbide peaks in the 2200°C samples was decided to be a visual inspection of the diffraction pattern. This method does introduce a bias into the number of peaks recorded for each diffraction pattern, but there is also bias involved in the peak-finding software because the number of peaks found depends upon the parameters entered by the user. In order better to define a peak visually, the 2200°C samples are presented again in Figures 21 to 24 but on exactly the same scale in terms of CPS and 2θ range. In these figures, the carbide peaks are labeled, as well as those characteristic of graphite.

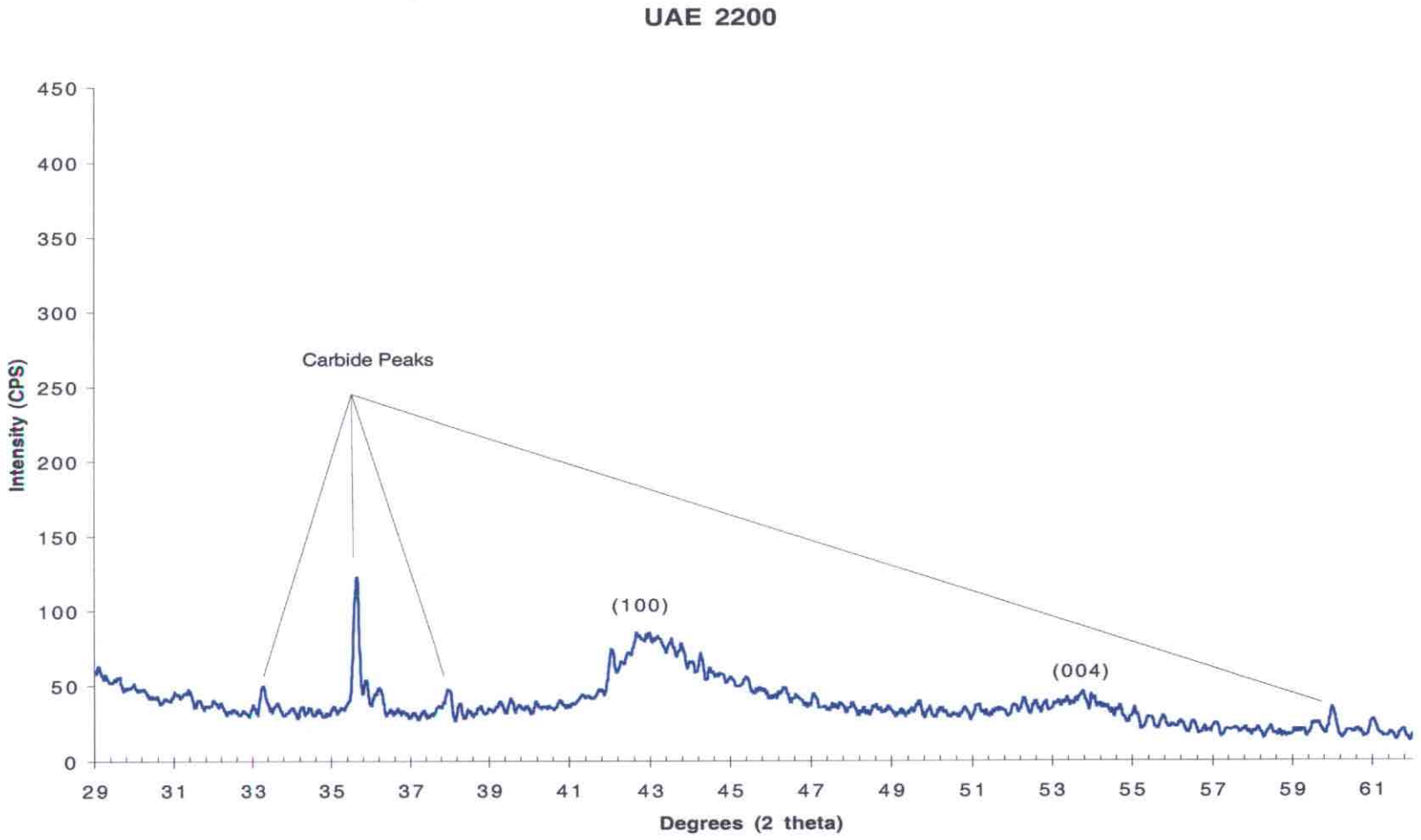

Figure 21 2200°C heat treated UAE anthracite, partial 2θ range

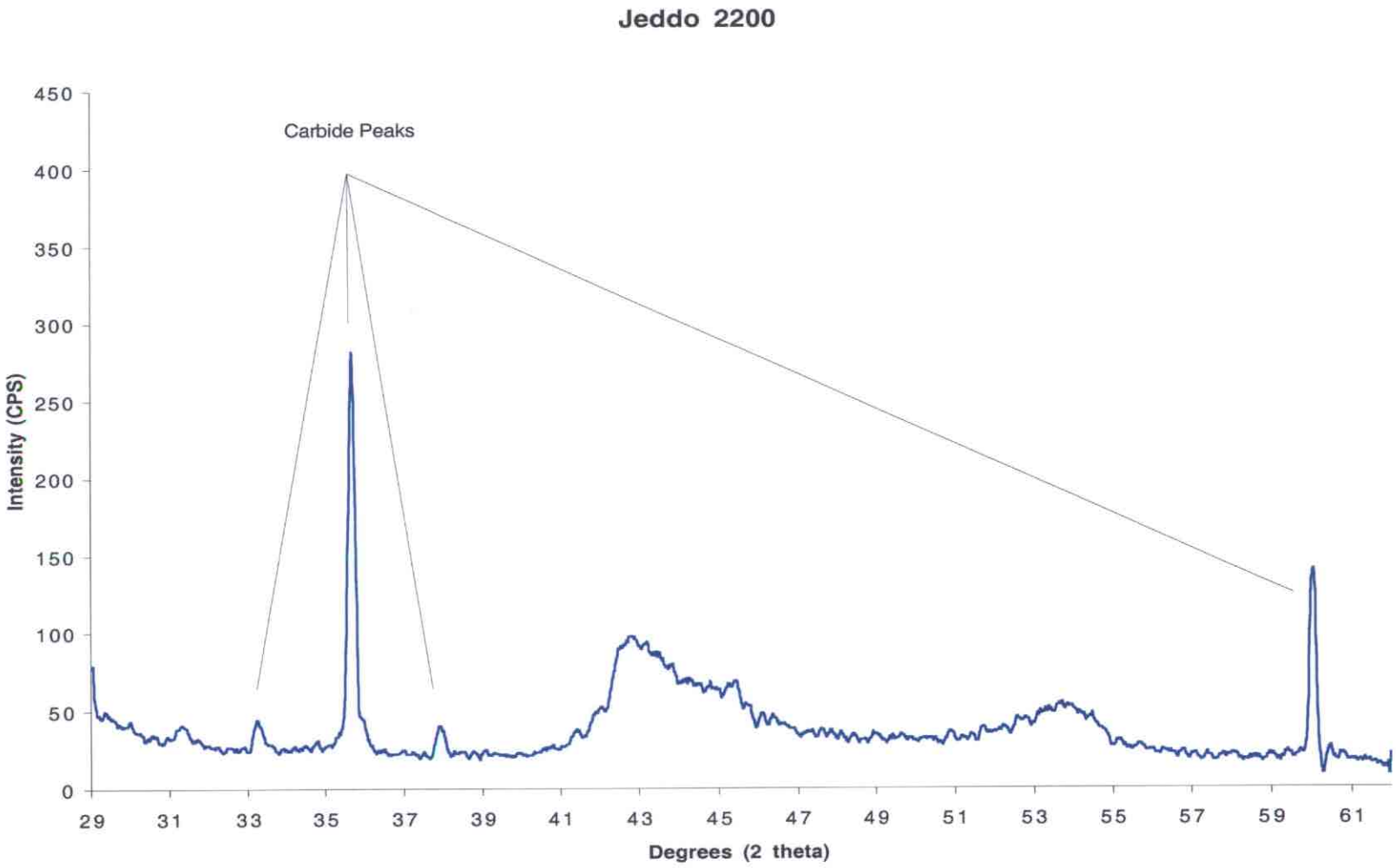

Figure 22 2200°C heat treated Jeddo anthracite, partial 2θ range

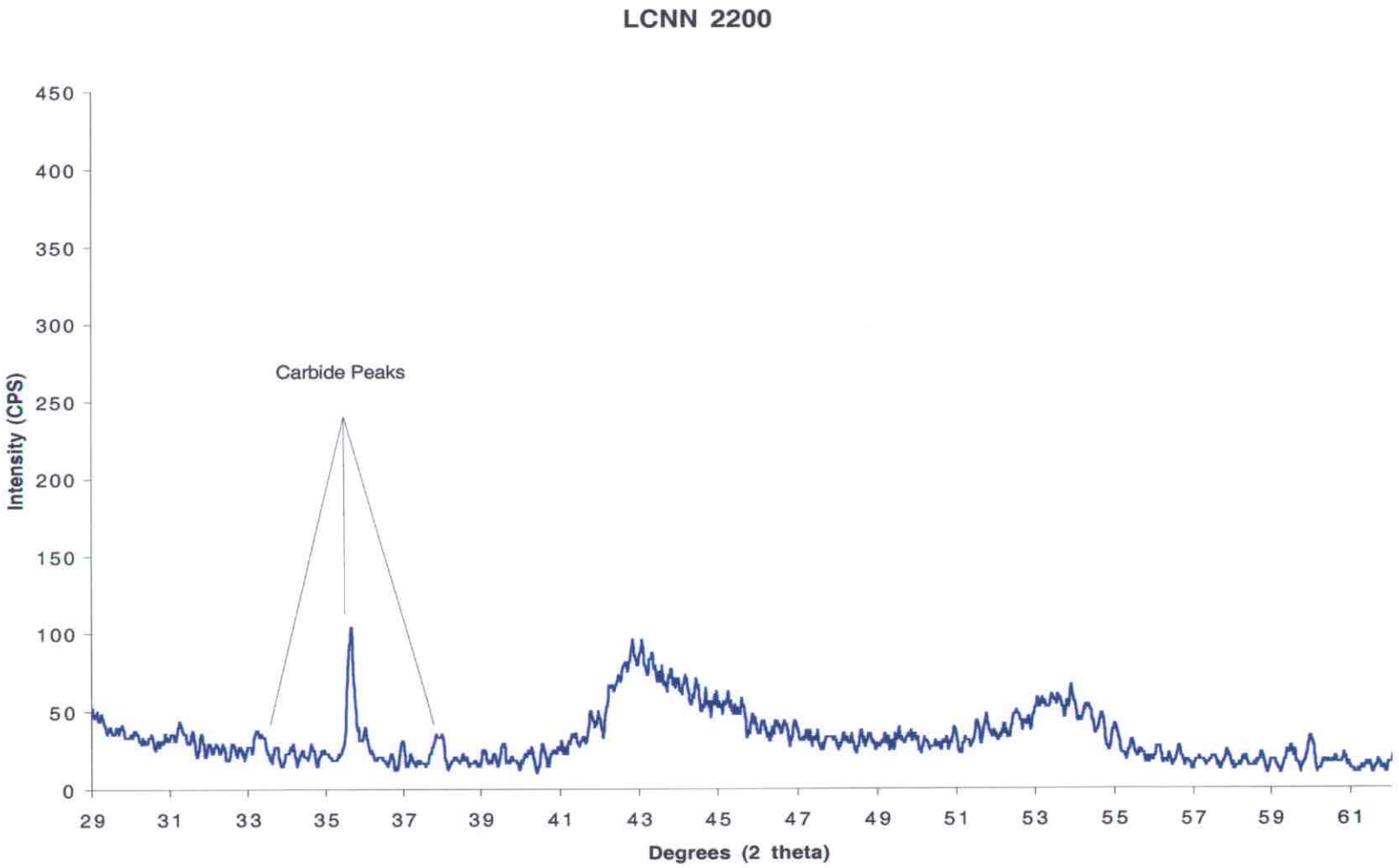

Figure 23 2200°C heat treated LCNN anthracite, partial 2θ range

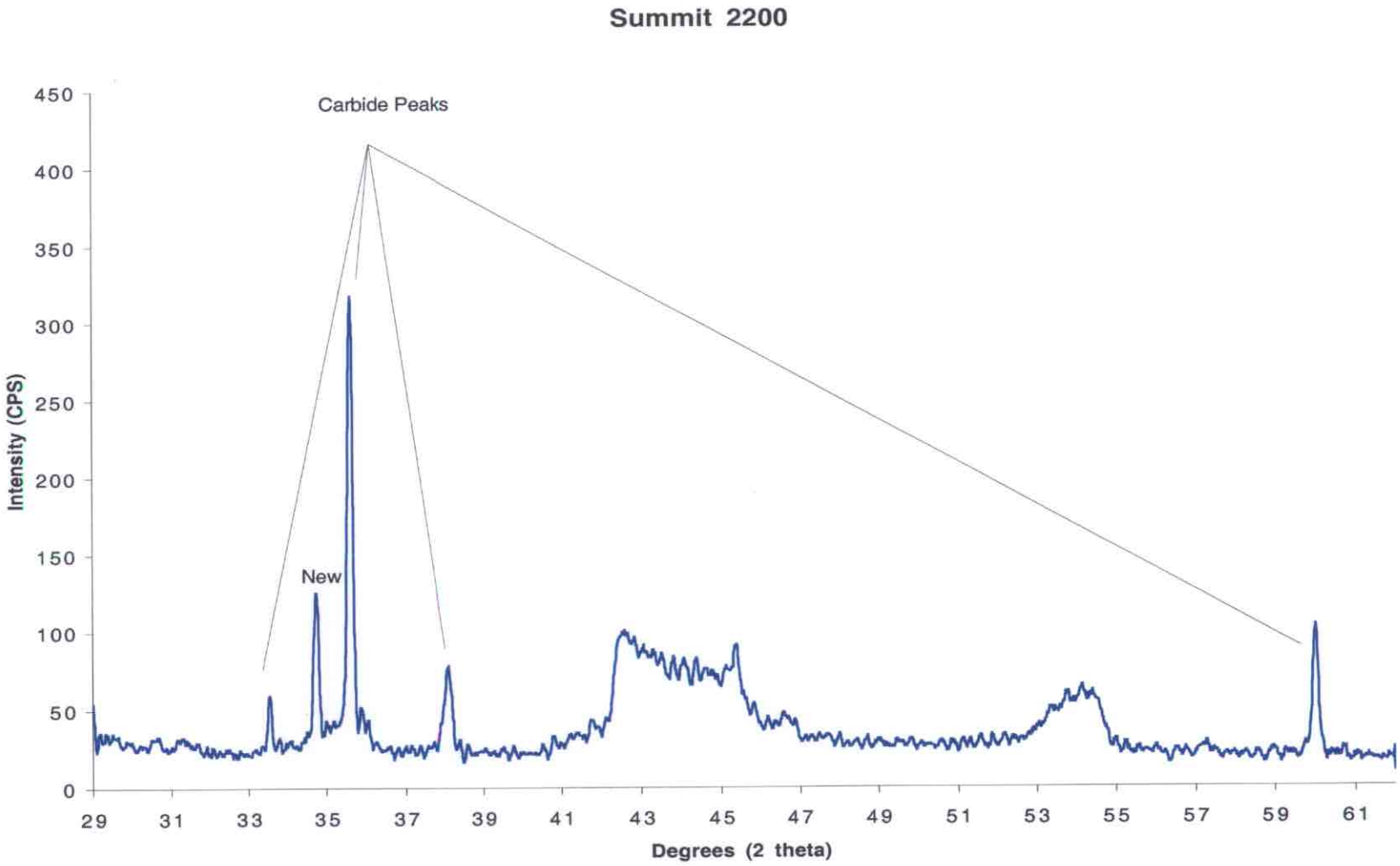

Figure 24 2200°C heat treated Summit anthracite, partial 2θ range

Table 2 Peak location of carbides in 2200°C heat treated anthracite samples

Heat treated anthracite	2Θ Angle of Carbide Peaks
UAE	33.34, 35.64, 38.06, 60.52°
Jeddo	33.34, 35.72, 38.10, 60.06°
LCNN	33.44, 35.64, 38.04°
Summit	33.72, 34.86, 35.68, 38.20, 60.10, 71.80°

The process of identifying the location of non-graphite related peaks and then determining what material has characteristic peaks in that angle range is similar to identifying the peaks present after heat-treating anthracite to various temperatures. In the case of the carbides that will form when an anthracite is exposed to graphitization heat treatment temperatures, though, the question of which peaks to look for becomes more complicated because a number of different carbides could be present. To better predict which carbides could form, the type and amount of minerals in the raw anthracites must be known. This information was obtained by computer controlled scanning electron microscopy (CCSEM), performed by Microbeam Technologies, Inc. Figure 25 shows the weight of a given element in the raw anthracites. The values on the y-axis represent the weight of each element normalized to 100 grams of anthracite. For example, in every 100g of the Summit anthracite there is 8.22g of silicon. The weight of each element was obtained by translating the number of characteristic X-ray counts for a given element into a percentage based on the total number of X-ray counts for every element, then multiplying that percentage by the amount of ash found during proximate analysis.

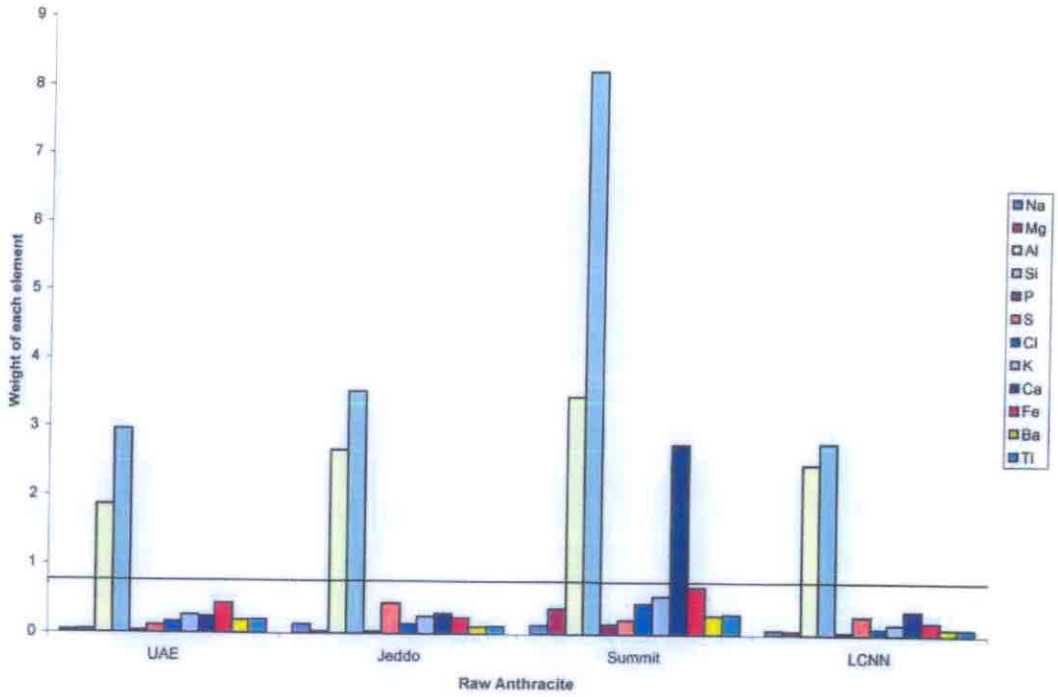

Figure 25 Weight in grams of each element for the raw anthracites

Figure 25 helps in predicting which carbides will form and also be detected by the X-ray diffraction unit. The detection limit for a carbide in graphite is 0.75 weight percent, or 0.75 g in a 100 g sample, so an element must be present in at least this amount in the raw anthracite in order to be detected by the diffractometer. Again, this is not to say that only those elements present in quantities greater than 0.75 grams, or greater than the horizontal line drawn in Figure 25, will form carbides, but they are the only ones that will be "seen." According to this requirement, only aluminum carbide, silicon carbide, and, in the case of Summit, calcium carbide can be detected. Now that these three carbides have been established as distinct possibilities, their characteristic X-ray diffraction patterns can be reviewed in order to see if any match the peak position listed in Table 2.

Figure 26 is the X-ray diffraction card for aluminum carbide that shows the (*hkl*) peak positions, and which are most intense, or would be most likely to be observed during X-ray diffraction. In the upper right corner of the Figure the data are designated as "Quality data." Only quality or "normal" data are used for this research, as "Doubtful quality" is also available, but, logically enough, of doubtful quality. Also, a "Calculated pattern" is not used because it is based on tabulated data for all the (*hkl*) peaks when the crystal system is known, regardless of whether or not all the listed peaks are observed in an X-ray diffraction experiment. Figure 26 shows that the two most intense peaks, and two most likely to be found, for aluminum carbide are at 31.74° and 55.04°. However, comparing these values with Table 2 does not produce a match for any of the 2200°C heat-treated anthracites. The only possible matches for all the heat-treated samples are the (*015*) peak at 35.85°, and the (*0014*) peak at 60.9°. These peaks can be ruled out as

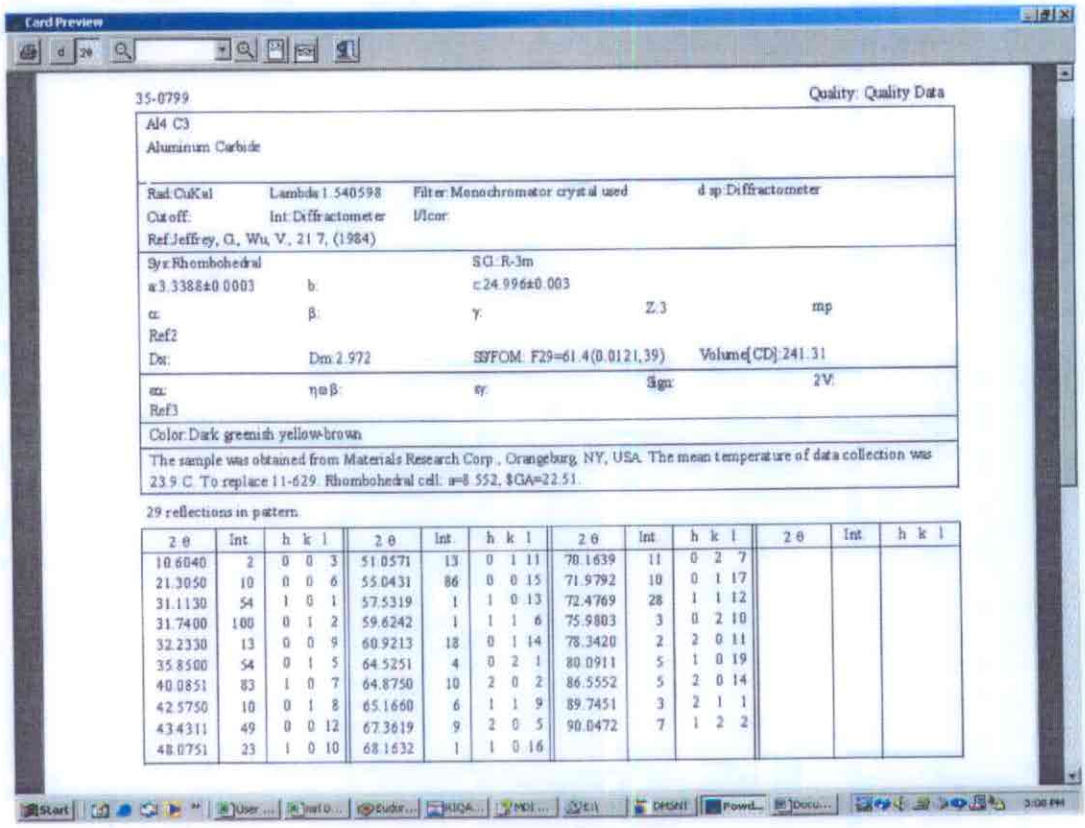

Figure 26 XRD card for aluminum carbide

aluminum carbide peaks, because peaks of roughly half and one-fifth maximum intensity, respectively, would not appear before the two most intense peaks.

A better match is observed between the peak positions listed in Table 2 and the card for silicon carbide. Figure 27 shows that the most intense peak for silicon carbide is found at 35.45°. All the 2200°C heat-treated samples have a peak in the 35° range. Granted, none are exactly 35.45°, but some discrepancy must be expected because these are not pure carbide samples, so their peaks can be influenced by the thermally stressed anthracite present. Another common peak in all the four anthracites, other than the LCNN anthracite, is found at approximately 60°. Silicon carbide's second most intense peak is located at 60.03°, which is in good agreement with peaks from the heat treated anthracites. Basically, should silicon carbide be present in a detectable quantity, its two most prominent peaks would be located at 35.45°, and 60.03°. All the anthracites exhibit peaks in this 2θ range, so silicon carbide must be present in all the 2200°C heat-treated samples. Table 2 confirms that silicon carbide should be present in all the anthracites because silicon is present in all the raw anthracites in a quantity capable of forming a carbide detectable by X-ray diffraction.

Lastly, the card for calcium carbide is presented because the Summit anthracite contained enough calcium to form detectable calcium carbide. Reviewing Figure 28 shows, however, that calcium carbide's two most intense peaks are located at 32.65°, and 43.47°. The peak at 43.47° would be obscured by the broad (*110*) peak, but the peak at 32.65° should be visible, but it is not. The Summit anthracite, after heat-treatment to 2000°C, has an additional peak at 34.86° that none of the other heat-treated samples exhibit. The Summit anthracite is also the only anthracite with enough calcium present to

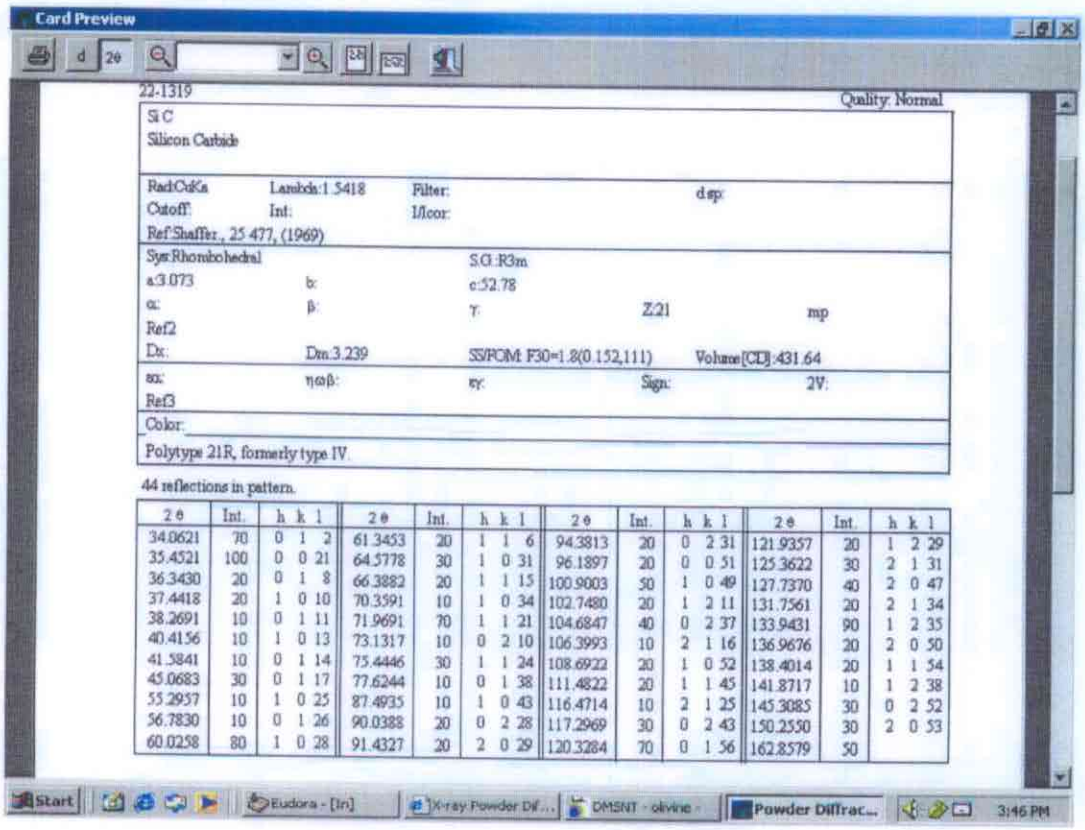

Figure 27 XRD card for silicon carbide

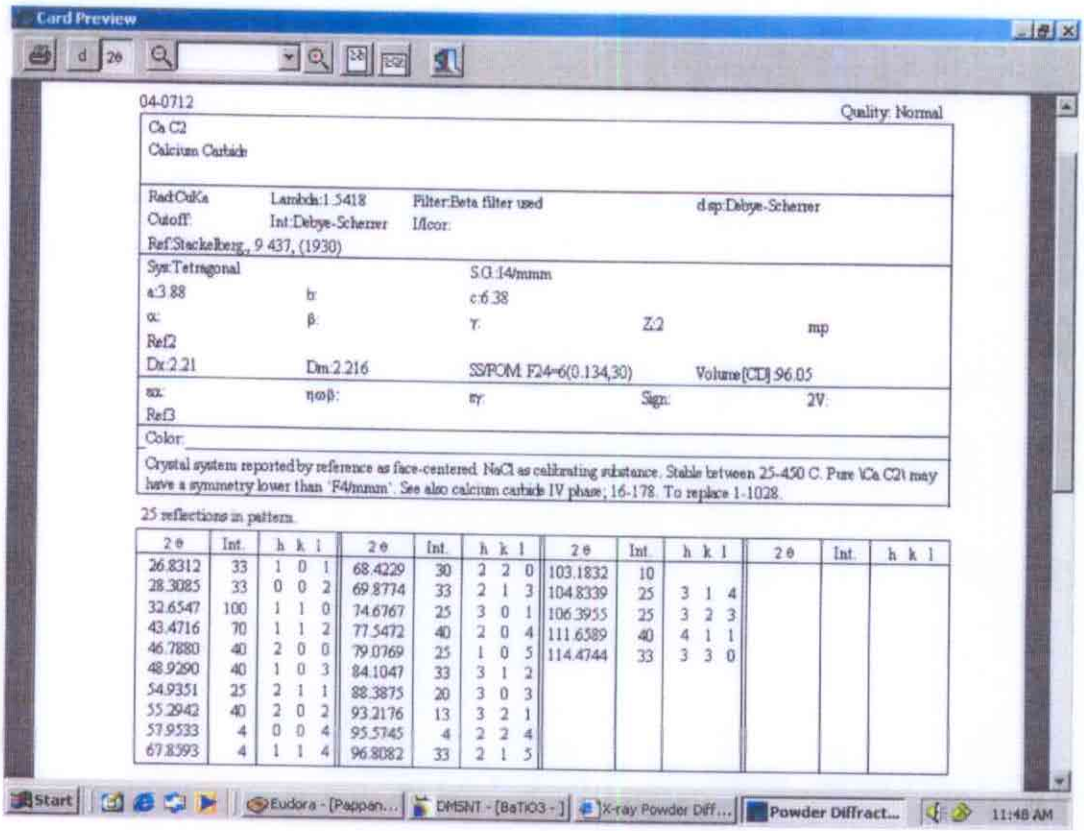

Figure 28 XRD card for calcium carbide

form a detectable calcium carbide, so it was assumed that this additional peak was the result of calcium carbide, but the X-ray diffraction card for calcium carbide does not support this hypothesis. Therefore, another material besides calcium carbide, that none of the other anthracites have, must be responsible for the peak at 34.86°.

Figure 25 shows that the raw Summit anthracite has more iron than any of the other anthracites, but it is still present in a quantity slightly lower than 0.75 grams, so it would be undetectable by X-ray diffraction. However, the mineral content of the raw anthracites was also determined by ashing the anthracites and analyzing the ash with plasma emission. Figure 29 shows the elemental (oxide basis) composition of the ashes of the four anthracites. The values obtained by plasma emission are in good agreement with those presented in Figure 25. A significant difference is that the amount of iron in the Summit anthracite is now slightly over 0.75%, meaning if it were to form iron carbide in the 2200°C sample, the carbide could be detected by X-ray diffraction. Unfortunately, no iron carbide X-ray diffraction cards of normal or quality data exist. Of the cards of doubtful quality, none lists a peak in the angle range of 34°. This means the peak at 34.86° in the 2200°C heat-treated Summit sample is most likely one of three things: (1) a calcium-based species that is not calcium carbide, (2) an iron-based species that is not iron carbide, or (3) the (*012*) reflection of silicon carbide located at 34.06°. The (*012*) peak at 34.06° is certainly not an exact match for 34.86°, but it is the only peak at 34° for any of the possible carbides, including iron and calcium carbide. The (*012*) peak is 70% intensity of the most intense peak for SiC, so it would be one of the first peaks to be witnessed, but none of the other heat treated anthracites show this peak even though they

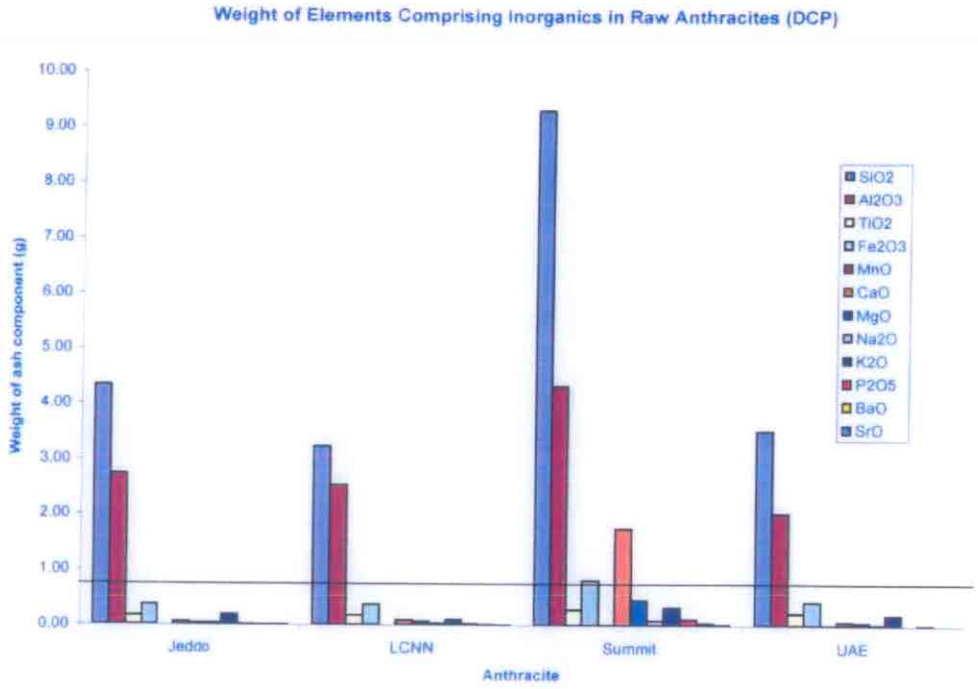

Figure 29. Weight of elemental oxides by plasma emission

definitely contain silicon carbide. The peak at 34.86° must be attributed to silicon carbide, but iron and calcium definitely have and impact on graphitization behavior.

In summary, all the anthracites show clear silicon carbide peaks after heat treatment to 2200°C. Therefore, all that can be said with certainty is: (1) all the heat-treated anthracites contain silicon carbide, (2) none of the heat-treated anthracites contain aluminum carbide, (3) all the heat-treated anthracites could contain more than just silicon carbide, but they are not present in enough mass to be "seen" by the diffraction unit. The role of these carbides in terms of their effect on degree of graphitization is discussed following analysis of the 2500° and 2600° diffraction patterns for the heat-treated anthracites.

The 2500°C heat-treated anthracites show no carbide peaks, which does not mean carbides are not present, only that there is not enough carbide for detection by X-ray diffraction. This does, however, mean that less carbides are present in the 2500°C heat-treated samples then in the 2200°C heat-treated samples. The importance of this is discussed later, in a follow-up discussion to carbide formation and its impact on graphitization. The 2500°C samples show a continued increase in intensity of the (*002*), as well as a broad and weak appearance of the (*110*) reflection.

The final heat treatment temperature was 2600°C, as shown in Figures 5, 10, 15, and 20. Again, the intensity of the (*002*) peak increases and the (*100*), (*004*), and (*110*) become more defined. Also, the broad (*100*) peak begins to split into the (*100*) and (*101*) peak, as evidenced by the "two humped" peaks over the 2θ range of 40° to 45°. Lastly, the appearance of the (*112*) peak is observed, which indicates that all the anthracites can be considered graphitizing carbons, or that they achieved long-range three-dimensional

crystalline order. Figures 30 to 33 show close-ups of the (*110*) and (*112*) peaks for all four heat-treated anthracites. The (*112*) peak is a broad hump, but even a weak presence is indicative of three-dimensional ordering. The (*112*) of a needle coke is also shown in Figure 34 for comparison purposes—needle coke is a well known graphitizing carbon and a main feedstock of the graphite industry.

Although all the anthracites exhibit a broad (*112*) peak following heat treatment, some differences in the degree of graphitization are observed in comparing their crystallite parameters obtained from the (*002*) and (*100*) peaks. The information indicative of graphitic development, assuming an (*hkl*) peak is present, is d-spacing. d-Spacing is obtained from the Bragg equation applied to the (*002*) peak. Figure 35 summarizes how d-spacing changes with increased HTT. None of the heat-treated anthracites achieves a d-spacing of 3.354 Å, the horizontal black line in the figure, but there are definite differences in how closely each comes. The curves in Figure 35 are shown only for visualization purposes and their slope is not indicative of any kinetics. Judging by the final d-spacing, the Summit sample has the highest degree of

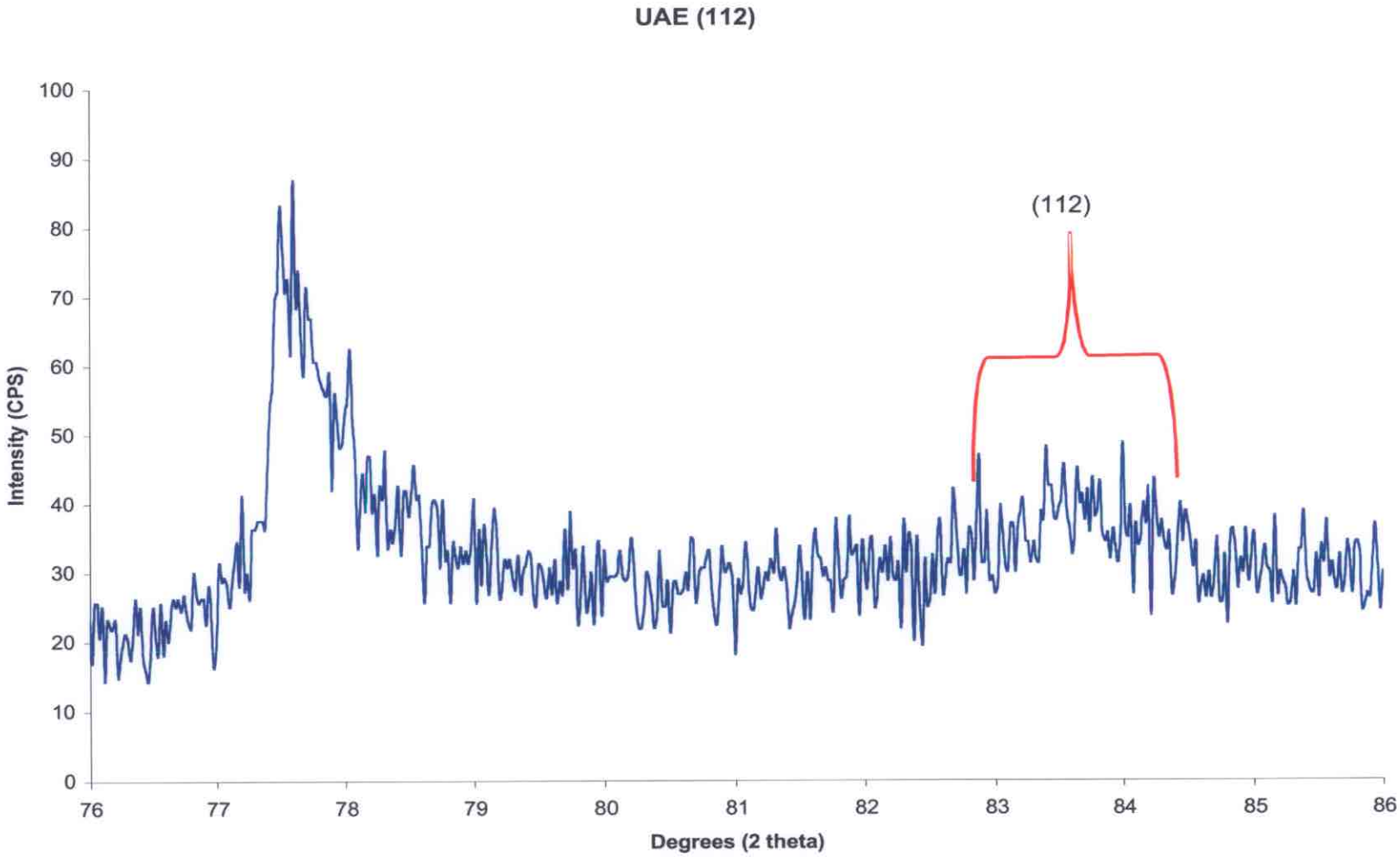

Figure 30 (*112*) peak for heat-treated UAE anthracite

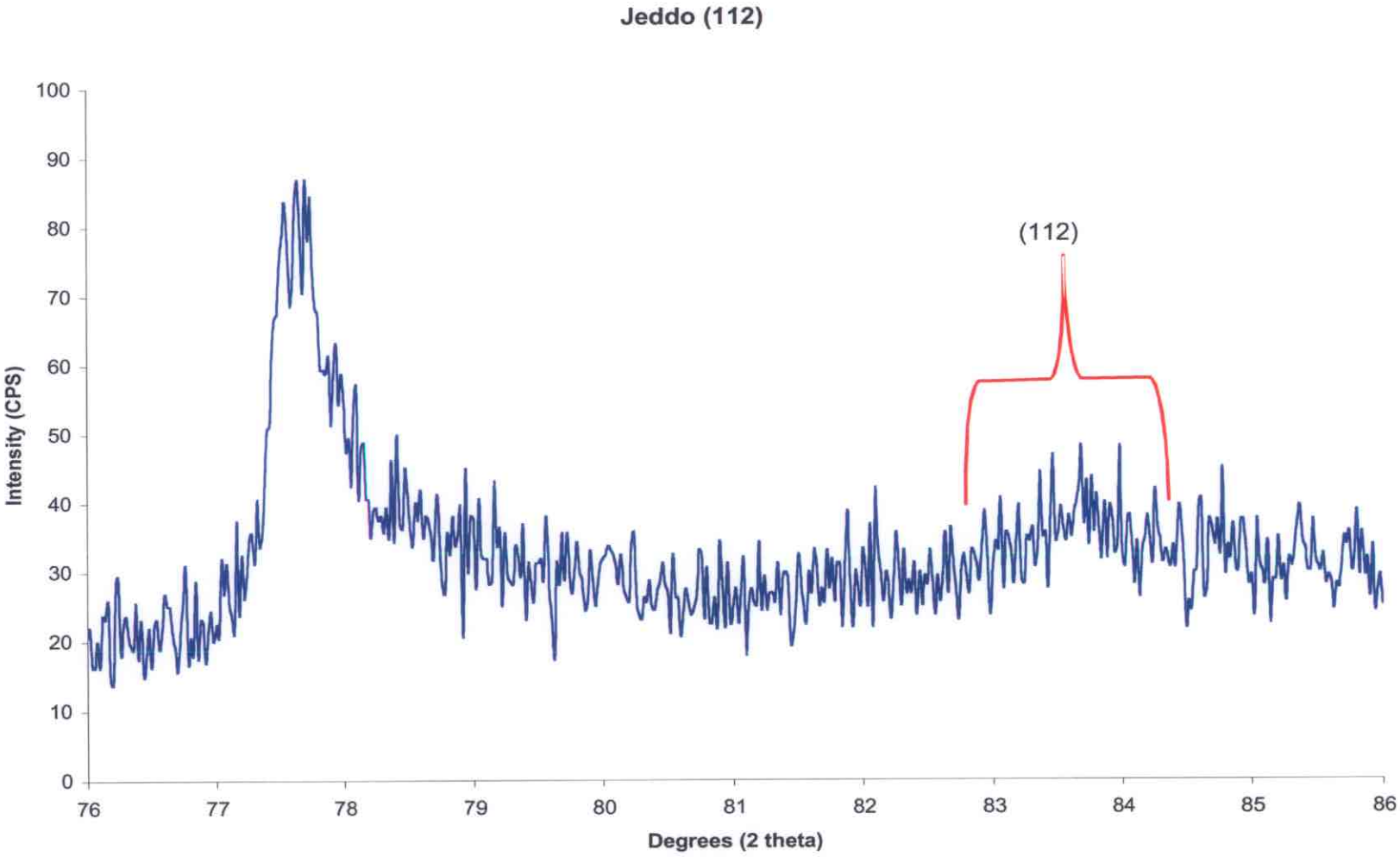

Figure 31 (*112*) peak for heat-treated Jeddo anthracite

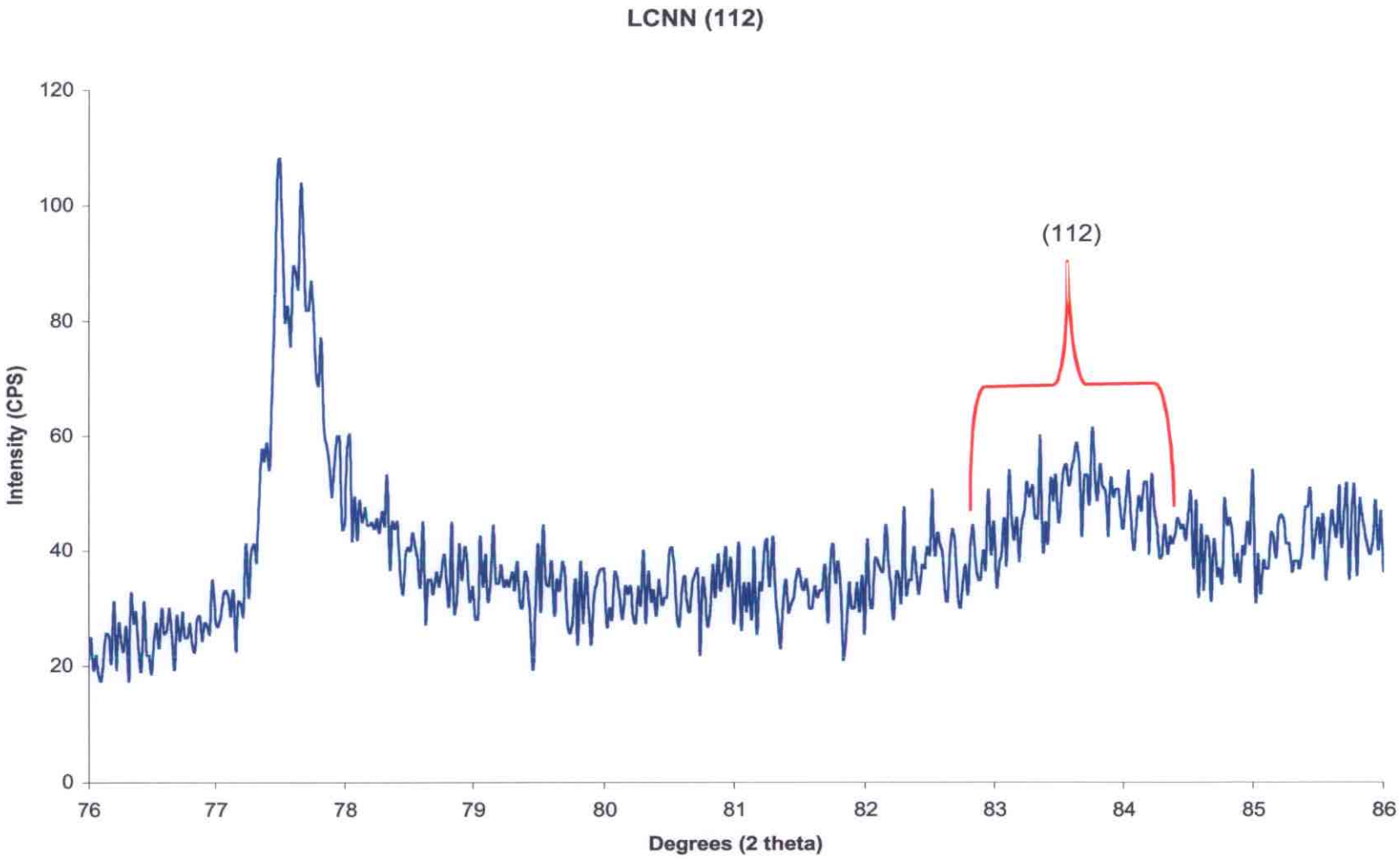

Figure 32 (*112*) peak for heat-treated LCNN anthracite

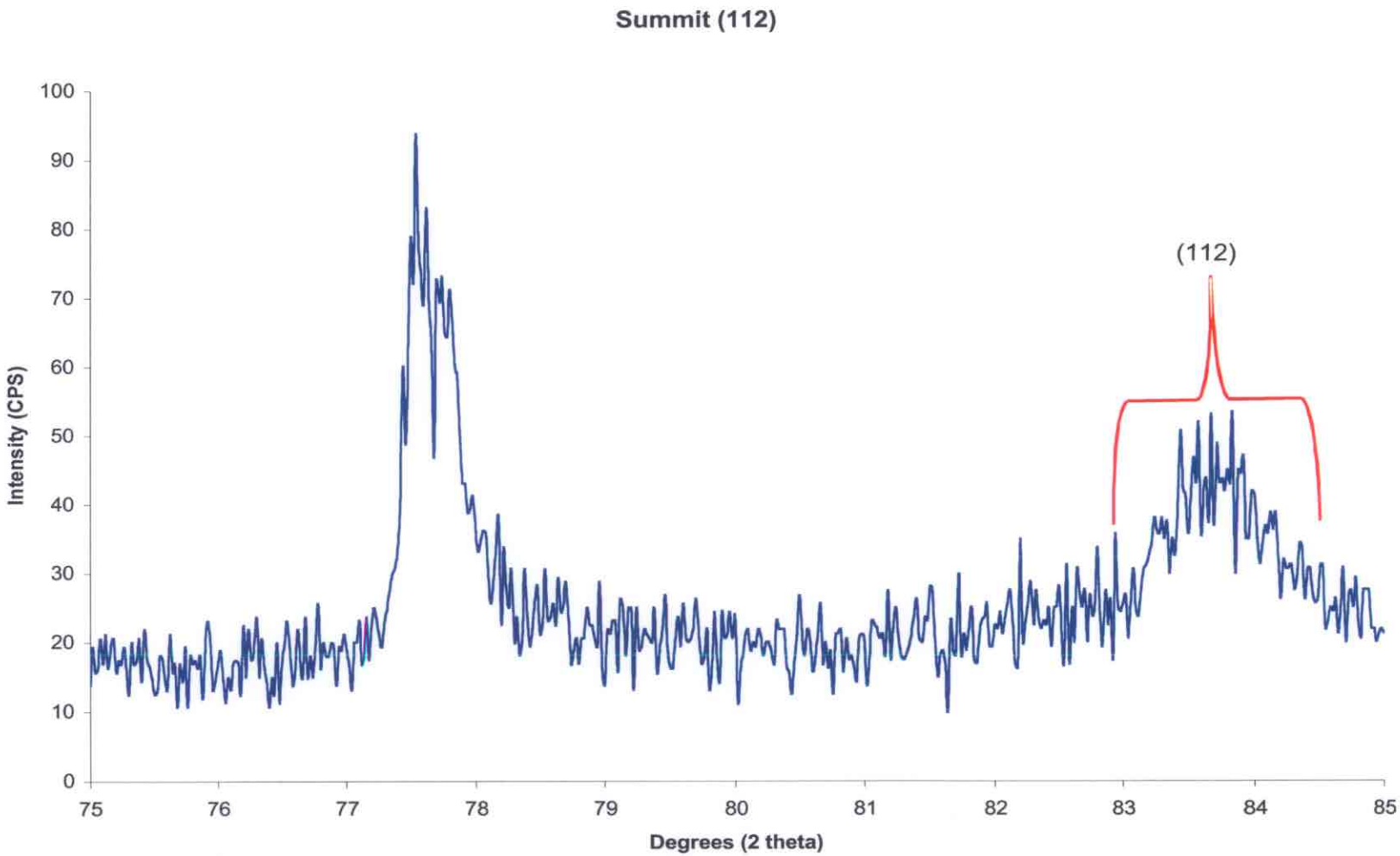

Figure 33 (*112*) peak for heat treated Summit anthracite

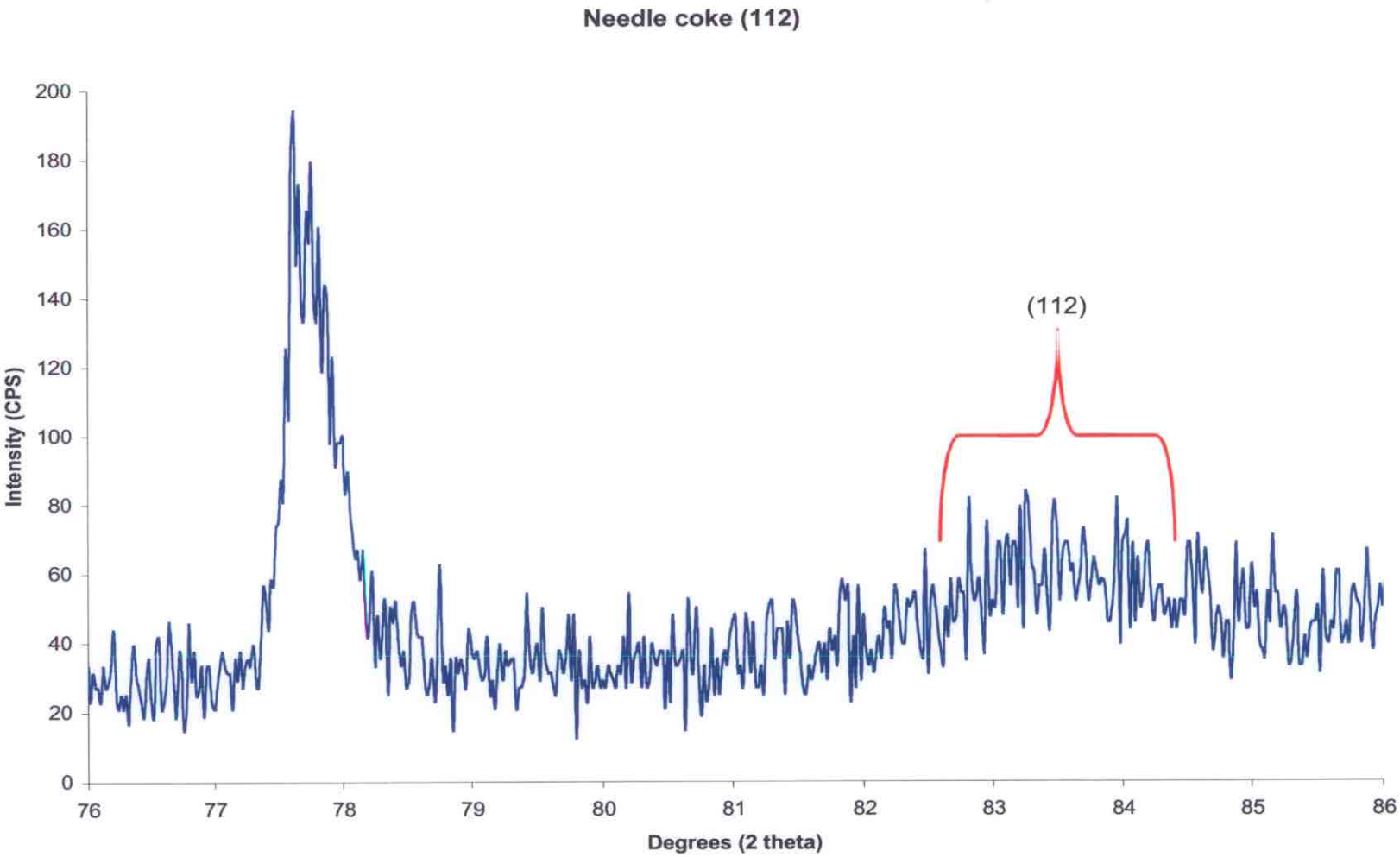

Figure 34 (*112*) peak for heat-treated needle coke

graphitization, the UAE and LCNN are about the same, and Jeddo is the least graphitizing. The error in the d-spacing is ± 0.001 Å, which is the thickness of the points on the line plots, which is why LCNN and the UAE anthracite appear to be the same in terms of final d-spacing.

Other measurements used to show differences in the graphitic development of the four anthracites are crystallite height, L_c, and crystallite diameter, L_a. Figures 36 and 37 show how crystallite height and diameter increase with HTT, respectively. The Summit anthracite, as seen in Figure 36, has the largest graphitic crystallites when compared to the other heat-treated anthracites. In this measurement, the LCNN and UAE samples are not identical; the graphitized LCNN anthracite has a larger L_c than the UAE sample. Again, the graphitized Jeddo anthracite has the least graphitic nature, evidenced this time by the smallest average graphitic crystallites. In terms of crystallite diameter, all the graphitized anthracites are about the same, based on the curves shown in Figure 37.

In summary, all of the anthracites are graphitizing carbons, because after heat treatment to 2600°C they all exhibit a broad (*112*) peak. However, not all the anthracites reach the same level of degree of graphitization in terms of a d-spacing close to that of graphite, 3.354 Å. There must be a reason why differences in extent of graphitization are observed. As stated in the introduction, Rouzaud believes that these differences are the result of differences in pore shape in the raw anthracites, where a flattened pore leads to a higher degree of graphitization, and a spherical pore is less highly graphitized. The X-ray diffraction patterns presented here show that carbides form during heat treatment to 2200°C, and then the carbides decompose, at least to some extent, before reaching 2500°C. We hypothesizethat this decomposition leaves behind a reactive carbon atom

that will add to the edge of a graphene layer, or react with cross-links between neighboring graphene layers, or layers stacked perpendicular to one another. If carbide formation and subsequent decomposition indeed affects the graphitization behavior of an anthracite, the crystallite properties of an anthracite should be altered by the addition or removal of minerals that contain elements that form carbides. This idea was tested by adding minerals to the least graphitizing Jeddo anthracite, and by demineralizing the most highly graphitizing Summit anthracite.

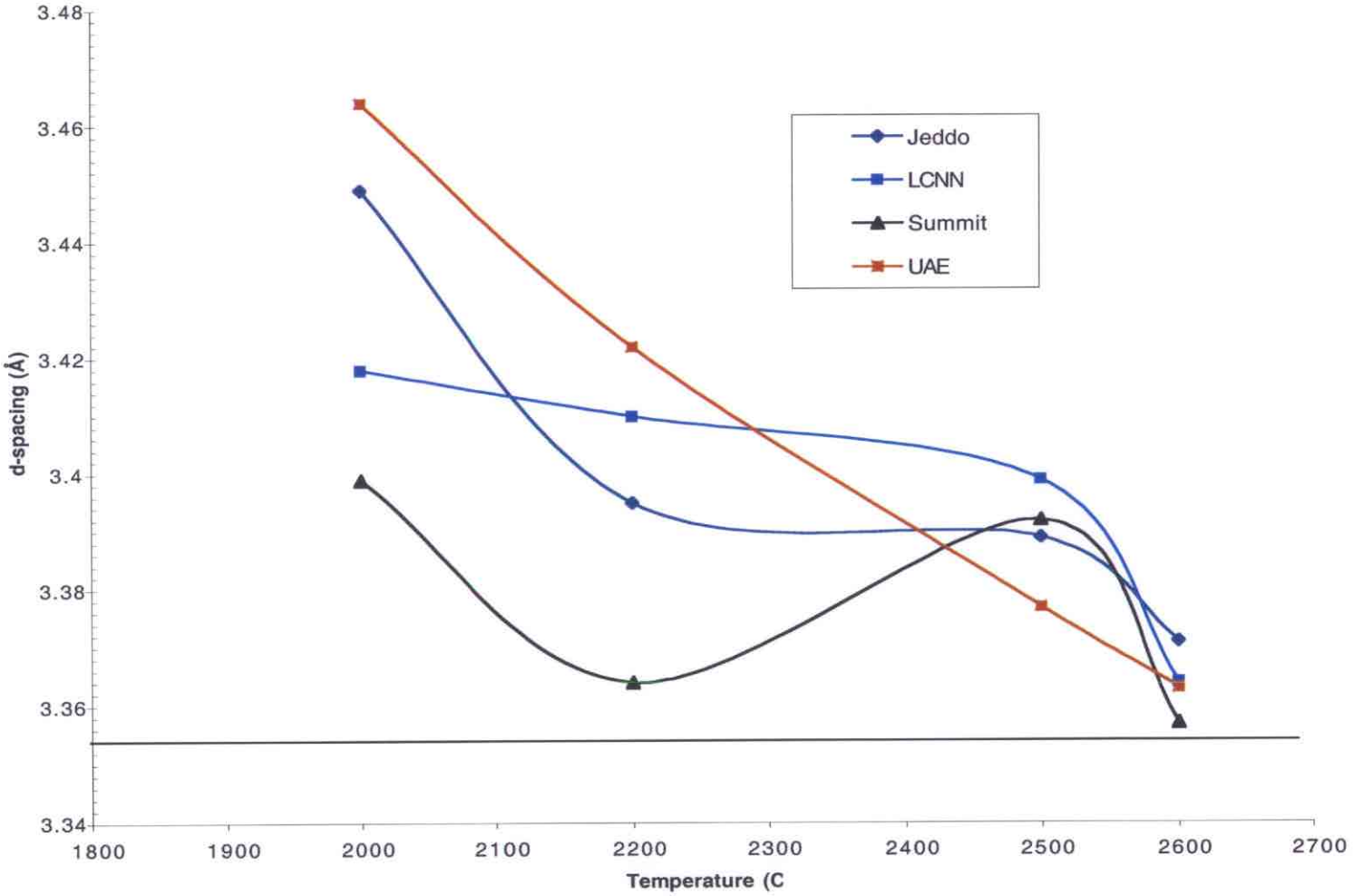

Figure 35 d-spacing decreased with increased HTT

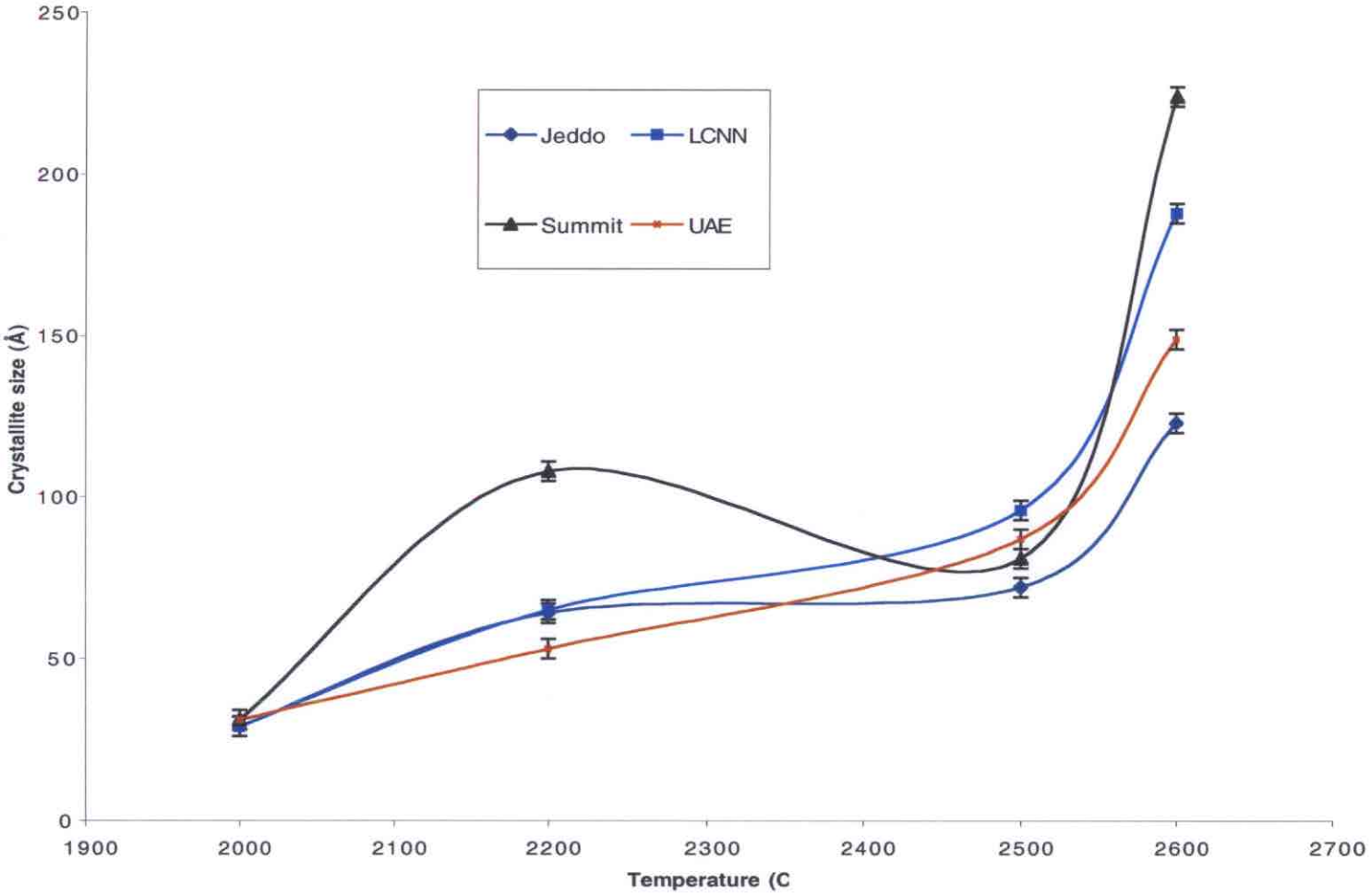

Figure 36 Crystallite height increases with increased HTT

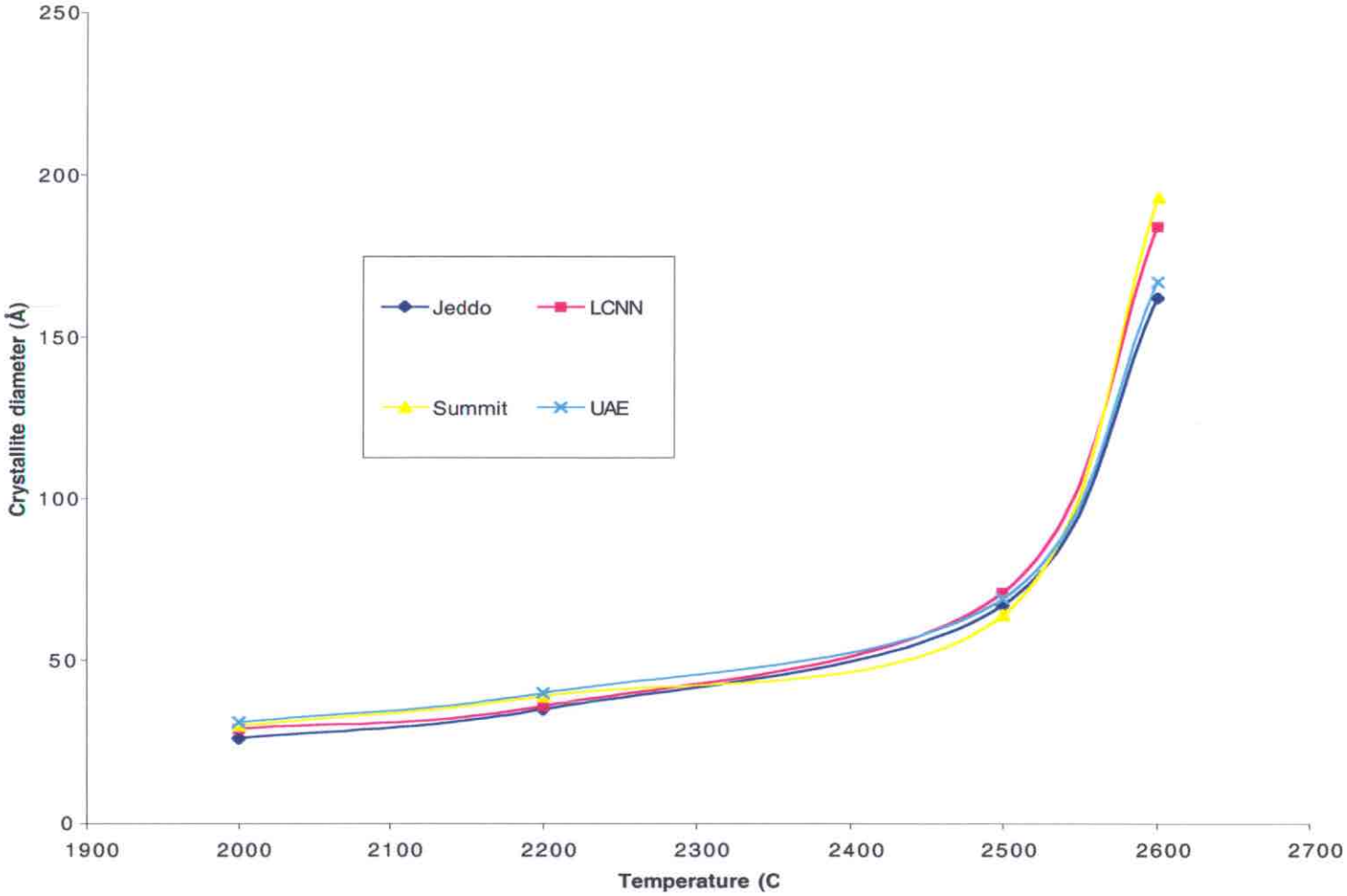

Figure 37 Crystallite diameter increased with increased HTT

Demineralization and Graphitization with Added Minerals:

Figure 35 shows that Summit was the best graphitizing anthracite, while Jeddo was the least graphitizing. It is believed that the amount of carbide-forming mineral matter present is responsible for these observed differences. Therefore, if Jeddo contained more mineral matter, then it might exhibit a higher degree of graphitization due to more carbide formation and decomposition to leave behind reactive carbon atoms. This hypothesis was tested by adding quartz, calcite, rutile, and iron oxide to the Jeddo anthracite in a 3:1 ratio. Quartz (SiO_2) was added because it is the primary contributor of silicon, calcite ($CaCO_3$) because it contributes calcium, rutile (TiO_2) because it contributes titanium, and iron oxide (Fe_2O_3) because it contributes iron. Rutile and iron oxide were added even though they are present in non-detectable quantities (i.e., by X-ray diffraction) because they have been shown in the literature to readily form carbides, and also because iron oxide and titanium oxide are commonly used in the graphite industry as graphitization "catalysts." As stated before, titanium carbide, for example, could form at 2200°C, but be invisible to the X-ray diffraction unit. Addition of rutile and iron oxide provides enough quantity for a carbide formed from them to be seen. Figures 38 to 41 show the X-ray diffraction patterns of the Jeddo anthracite with added mineral and heated to 2600°C.

Before discussing the crystallite parameter changes incurred by adding these minerals, the X-ray diffraction patterns of the Jeddo anthracite plus calcite and iron oxide are analyzed in terms of the number of peaks present. It was discussed earlier in this report that the Summit anthracite heated to 2200°C showed an additional diffraction peak that none of the other heat-treated anthracites produced. It was thought possible this peak

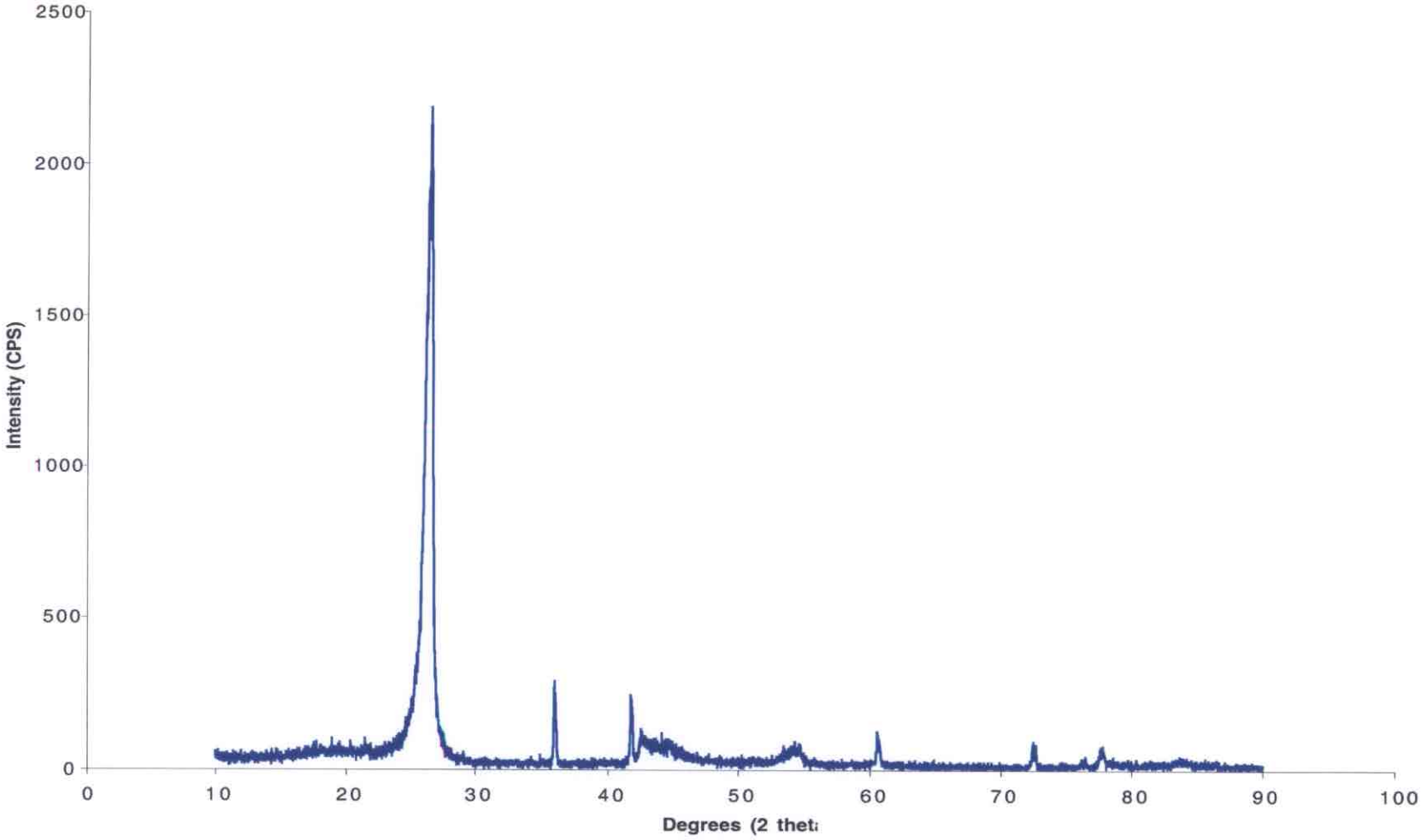

Figure 38 X-ray diffractogram of Jeddo plus rutile heated to 2600°C

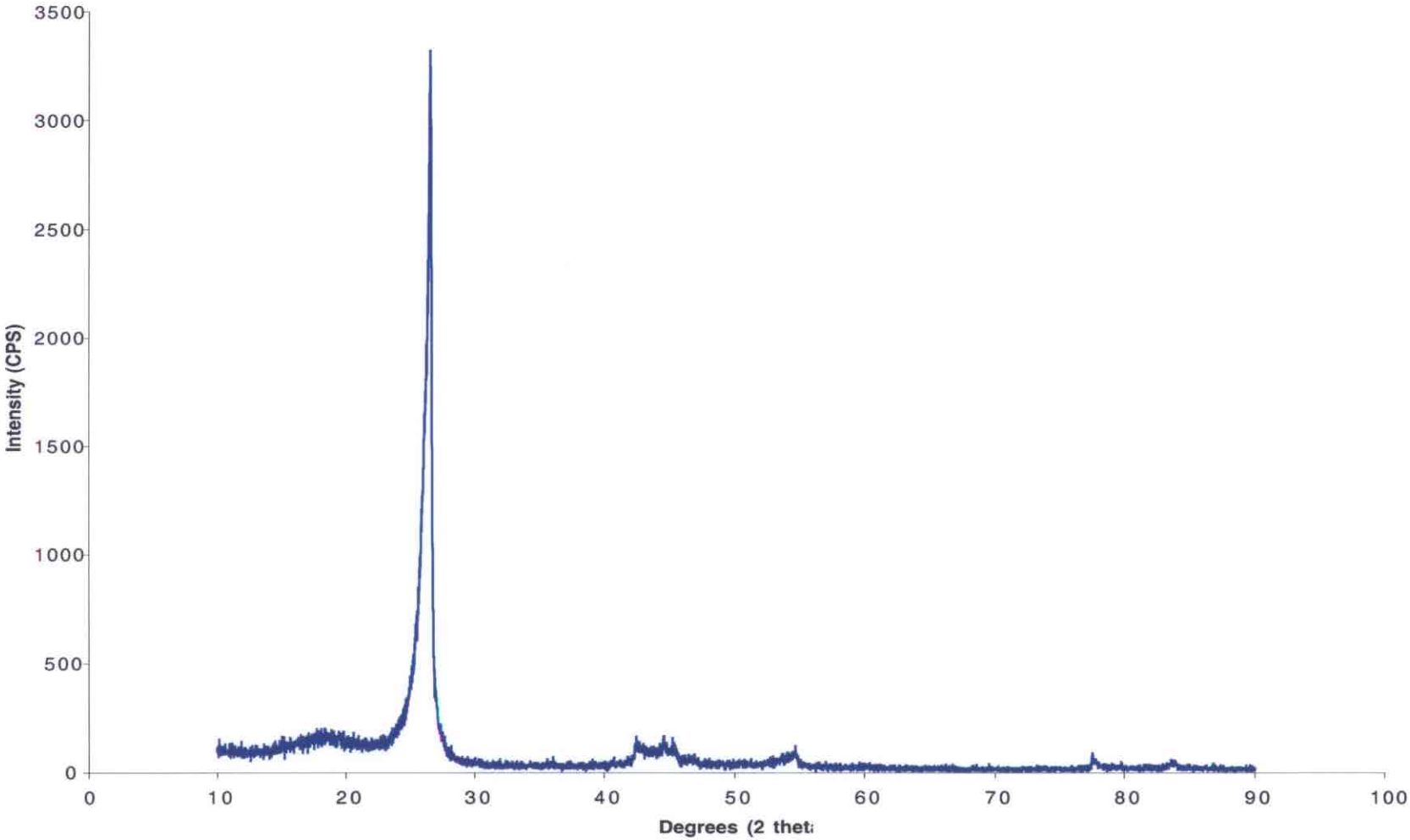

Figure 39 X-ray diffractogram of Jeddo plus iron oxide heated to 2600°C

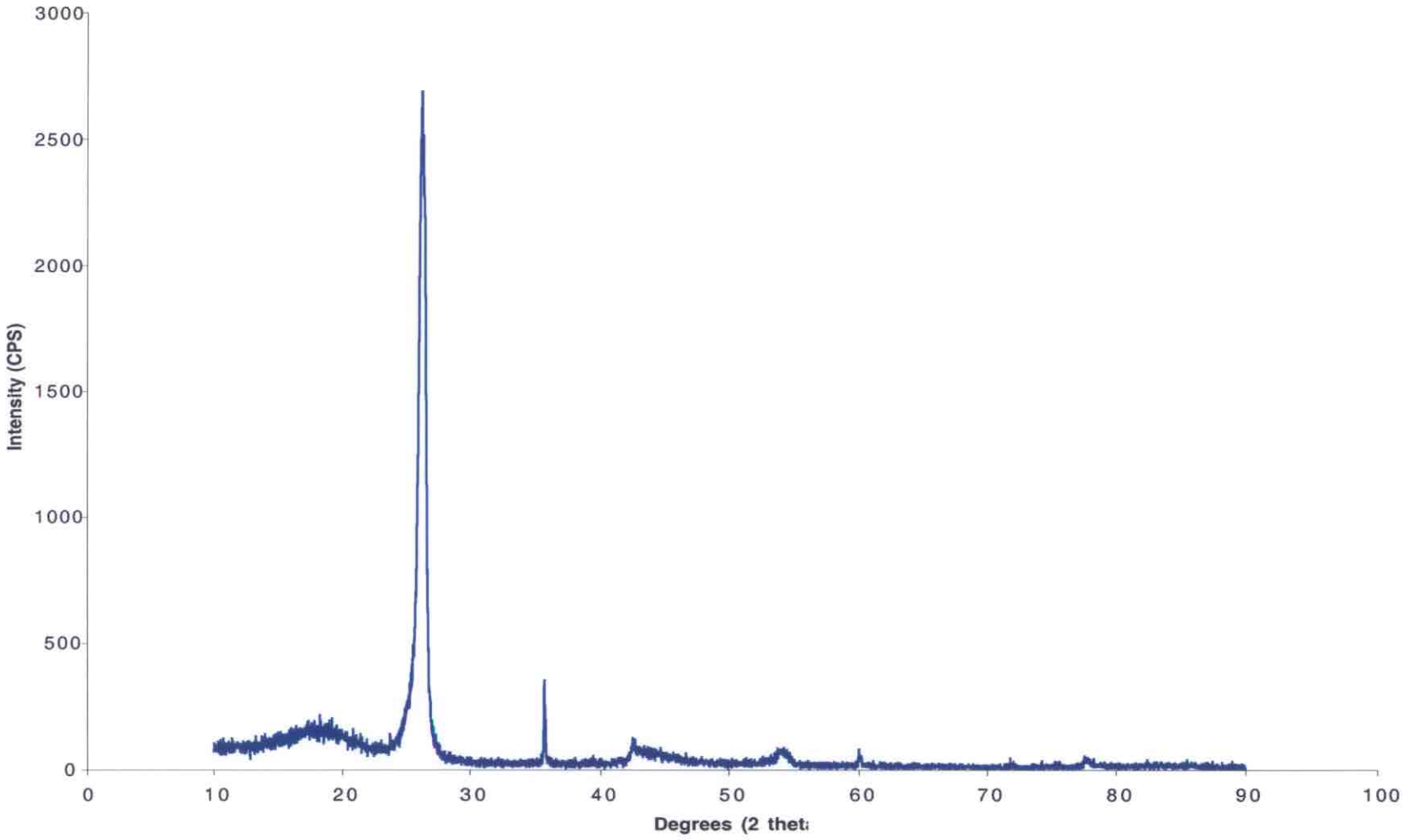

Figure 40 X-ray diffractogram of Jeddo plus quartz heated to 2600°C

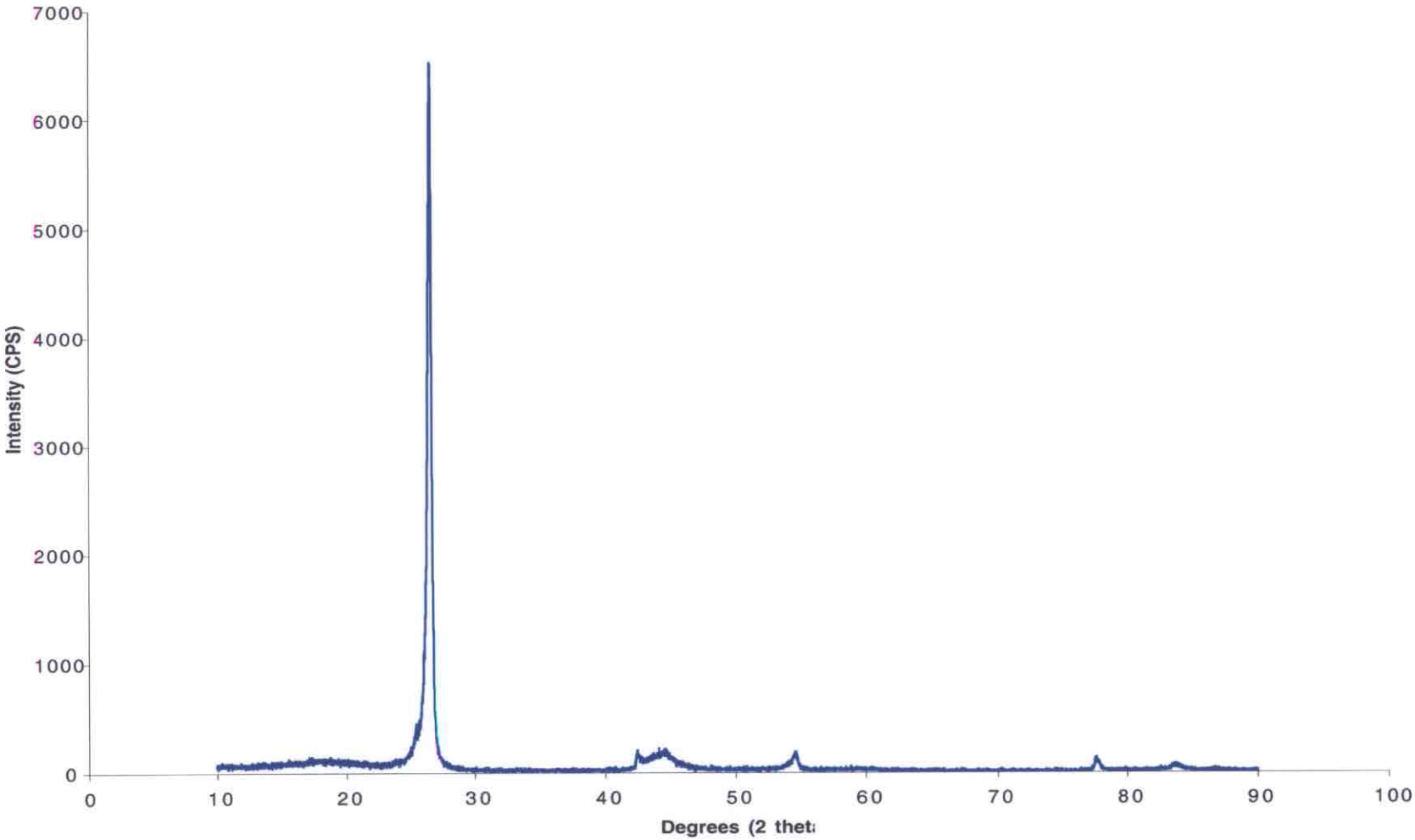

Figure 41 X-ray diffractogram of Jeddo plus calcite heated to 2600°C

could be an iron or calcium species that is not a carbide. However, analysis of Figures 39 and 41, that show the addition or iron and calcium, respectively, illustrates that no carbide peaks are present; only graphite-related peaks are seen. Enough iron and calcium had been added to the anthracite that if a carbide formed it would be detected by X-ray diffraction, but no carbide peaks were observed. This could be because no carbides actually formed, or they did form and were decomposed by the time 2600°C was achieved.

However, the addition of iron and calcium certainly have an effect on the properties of the graphite formed after heat treatment to 2600°C. Table 3 lists the d-spacings and crystallite heights for all the Jeddo plus inorganics.

Table 3 Crystallite parameters of Jeddo 2600°C after addition of "catalytic" minerals

Mineral added to Jeddo	d-spacing (Å) ±0.001	L_c (Å) ±2
Rutile	3.355	123
Quartz	3.358	135
Iron oxide	3.352	153
Calcite	3.354	248
None	3.371	123

All of the minerals had an effect on the d-spacing, and they are all roughly the same, with quartz aiding the least, but still reducing the d-spacing by 13 Å; calcite had the most dramatic affect on crystallite height.

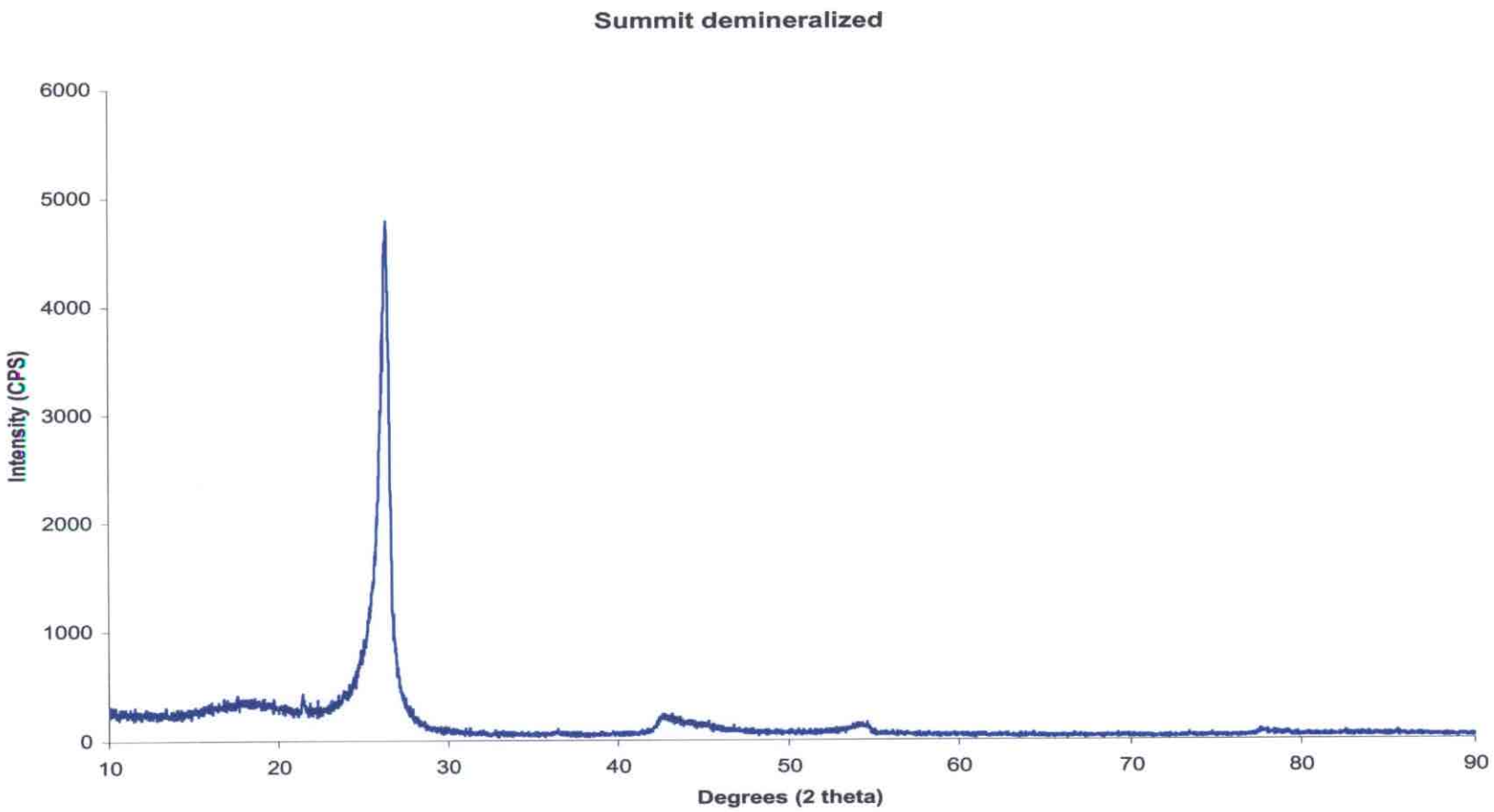

Figure 42 Demineralized Summit heated to 2600C

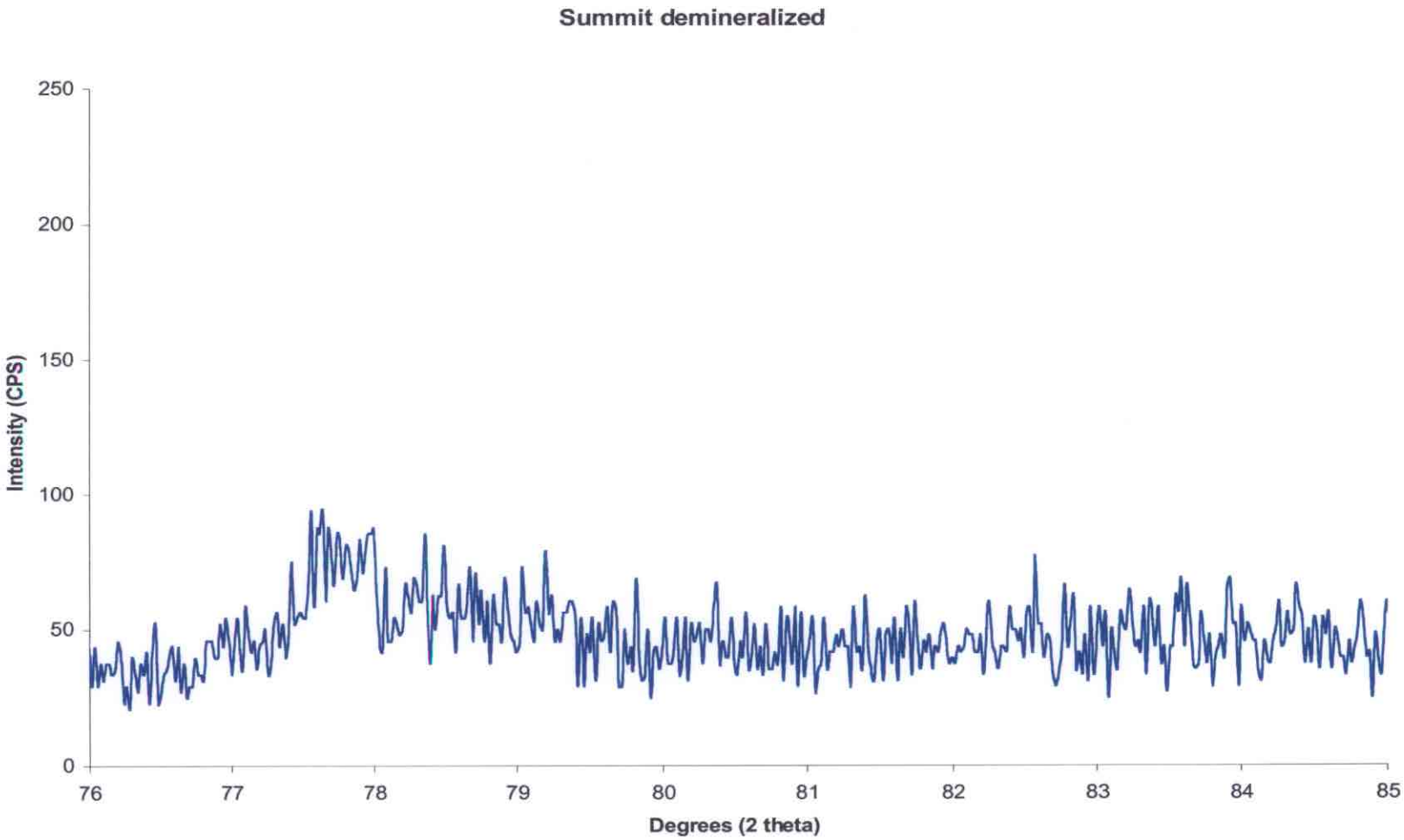

Figure 43 (112) of Demineralized Summit

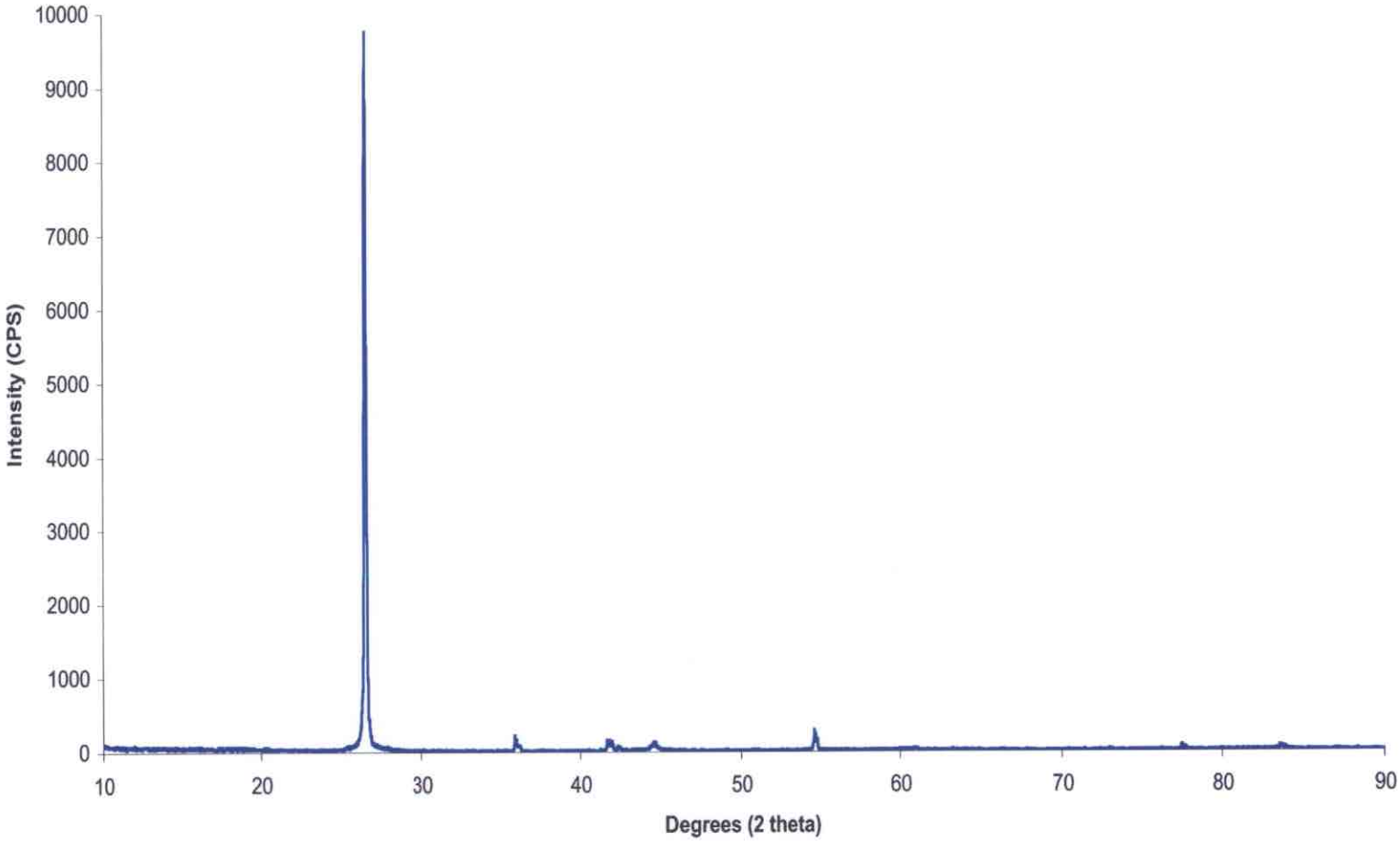

Figure 44 Demineralized Summit plus rutile, heated to 2600C

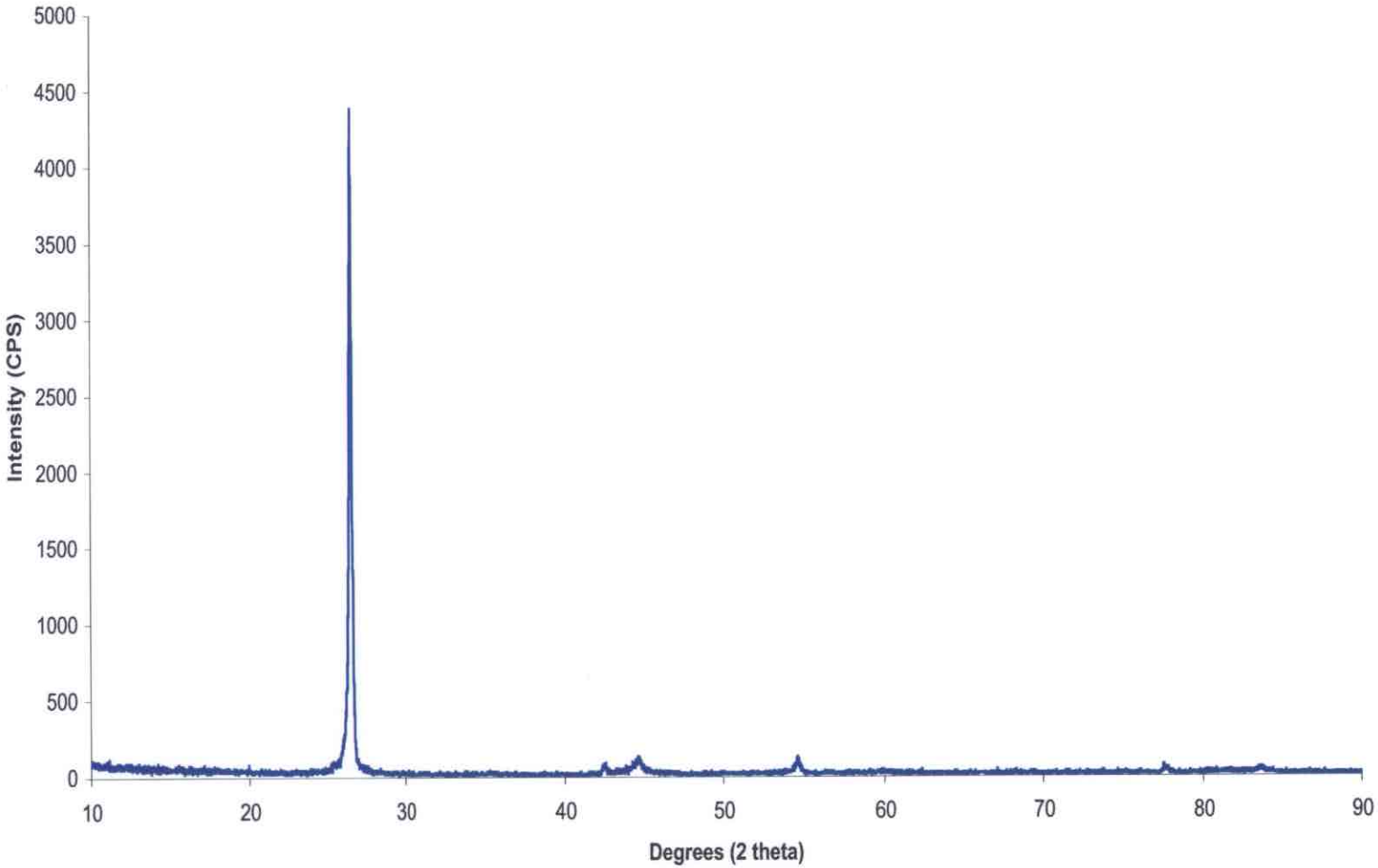

Figure 45 Demineralized Summit plus quartz, heated to 2600C

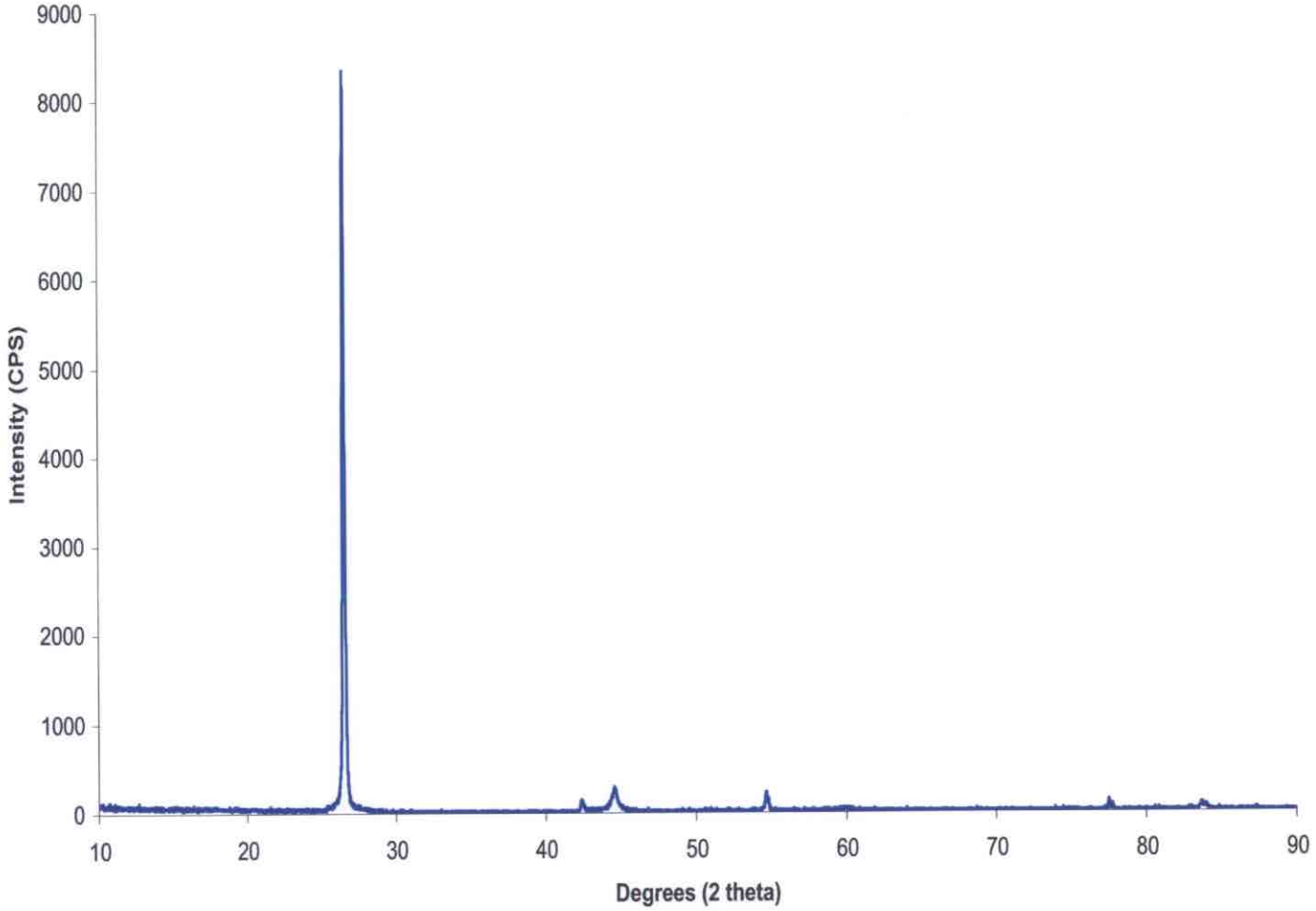

Figure 46 Demineralized Summit plus iron oxide, heated to 2600C

Figures 38 and 40 show that TiC and SiC form, respectively. The 2200°C X-ray diffraction patterns clearly show the formation of silicon carbide, so it is not surprising to see them present here. Titanium carbide, which was not seen before, is now present, suggesting that it must form at 2200°C, but be undetectable to the diffraction unit. It is also apparent that the formation of titanium carbide has an affect on the graphitization behavior of the Jeddo anthracite.

Table 3 shows that the addition of graphitization modifying minerals definitely enhances the graphitization of the least graphitizing Jeddo anthracite. This leads to the question of whether the removal of minerals will decrease the graphitizability of the Summit anthracite. To determine the answer, the Summit anthracite was demineralized, and then rutile, quartz, and iron oxide were added to the demineralized anthracite in a 3:1 ratio of anthracite:inorganic.

Figures 42 shows the X-ray diffraction pattern of the demineralized Summit anthracite heat treated to 2600°C. Upon further inspection of this pattern, it becomes apparent that the (*112*) peak is not present, and the (*110*) peak is not as well defined as in the raw heat-treated anthracites. Figure 43 is a close-up of the angle range where the (*112*) reflection should be located. This occurrence by itself shows that removal of mineral matter affects graphitization; in fact the Summit anthracite can no longer be considered a graphitizing carbon after demineralization.

Figures 44 to 46 show the diffraction patterns of the demineralized Summit anthracite plus rutile, quartz, and iron oxide. The (*112*) is visible in all the patterns, and it is obvious that the sharpness and intensity of the (*002*) peak is better than in any of the

other 2600°C heat-treated sample. Table 4 confirms that the crystallite parameters are much better than ever seen before.

Table 4 Crystallite parameters of demineralized Summit plus minerals

Inorganic Added	d-spacing (Å)	L_c (Å)
Rutile	3.352	544
Quartz	3.354	453
Iron oxide	3.349	480

Figures 44 to 46 show that the (*112*) returns to the demineralized Summit anthracite when the three inorganics listed in Table 4 are added to it. These figures and table clearly show that, at least in the case of the anthracites tested here, graphitization cannot occur without the presence of certain minerals. It also shows that minerals are not only responsible for differences in extent of graphitization, but are involved in the mechanism of graphitization itself.

In terms of a graphitization mechanism involving carbide formation and decomposition, the following is a general example of how a mineral could enhance graphitization.

Mineral melts→ Mobile liquid→ Reaction with defects, interstitials, cross-links→ Carbide forms→ Graphene layers now free to diffuse to neighboring layers→Carbide decomposes to leave a reactive carbon that adds to growing layers

A reaction sequence specific to, for example quartz, could proceed like this:

$$SiO_2 + 3C \rightarrow SiC + 2CO$$

$$SiC \rightarrow Si + \cdot C\cdot$$

The ·C· above represents a dicarbene with unfilled valences, so it would be extremely reactive to any other carbons, which would mean it would preferentially react with defects and/or cross-links.

Conclusions:

All the anthracites analyzed in this project are graphitizing carbons because they all exhibit a (*112*) peak after heat treatment to 2600°C. The Summit anthracite was the most graphitizable of the anthracite because it had the d-spacing closest to that of graphite, 3.354 Å, and the largest crystallites. Carbides formed from all the anthracites when heated to 2200°C, as evidenced by non-graphite related peaks in these samples. It was found that SiC was present in all the anthracites, and that Summit showed an additional peak that was most likely related to silicon carbide as well. These carbide peaks vanished at 2500 and 2600°C, meaning that the amount of carbides decreased, or that some type of decomposition of the carbides occurred. This decomposition would leave behind a reactive carbon capable of adding to a layer edge or removing a defect. This idea of a reactive carbon healing defects and thus aiding graphitization was supported by the reduction in d-spacing of the least graphitizing Jeddo anthracite when carbide forming elements from the inorganics rutile, quartz, iron oxide, and calcite were added. Further evidence of carbide formation and decomposition being a valuable part of the graphitization mechanism is seen in the fact that no (*112*) peak is observed if the

Summit anthracite is demineralized before being heated to 2600°C. The (*112*) re-appears if the inorganics just listed are added to the demineralized sample, i.e. the Summit anthracite is not a graphitizing carbon if the minerals associated with it are removed.

Part 2. Results of industrial graphitization of LCNN anthracite as a filler for molded graphite.

The purpose of the industrial graphitization experiment was, in essence, the completion of the scope of work endeavored in this project—to determine whether a prediction could be made as to the acceptability of an anthracite as a filler based on laboratory-scale graphitization experiments. In this research, four anthracites were selected and exposed to the same reaction conditions to determine whether differences in graphitizability would be evident. Indeed, as shown in detail in Part 1, the anthracites chosen for this research did show varied levels of graphitic development. The next step was to establish which parameters were responsible for these observed differences in graphitizability; i.e., whether they were attributable to physical, organic, or inorganic properties. Part 1 of this report showed that inorganic differences are responsible for differences in graphitizability. The next step was then to determine whether or not observations made in a laboratory could be related to industrial-scale graphitization. That is, the best graphitizing anthracite in the laboratory would be the best filler for molded graphite production provided that the acceptability of its use as a filler was dependent only on its extent of graphitization. This is not the case, because acceptability of a filler is dependent on both its extent of graphitization and propensity to form a dense, mechanically sound graphite when mixed with a binder. Although the Summit sample showed the highest degree of graphitization, it was not selected for industrial graphitization because past experience has shown high levels of ash, in this case 17.6%, leads to inadequate graphite properties and a weak filler-plus-binder compound. Because of this knowledge, the LCNN anthracite was selected for industrial research because it

was the second best in terms of graphitizability—the UAE and LCNN were the same in terms of d-spacing, but the LCNN sample produces a larger crystallite. In principle, the Summit anthracite could be an acceptable industrial filler, but only after treatment to remove its mineral impurities. Added processing of the filler, through cleaning or extended heat treatment, is undesirable in terms of the suitability of an anthracite for replacement of petroleum coke as a filler.

Carbone of America carried out the manufacture and graphitization of the anthracite and coal tar pitch molded graphite as the industrial member of this CPCPC project. Also, Carbone has created a set of standards based on physical properties of the graphites they produce that determines the grade and possible applications. This set of standards is proprietary to Carbone and are not reported here.

The LCNN anthracite was selected for industrial graphitization, to be performed at the St. Marys plant of Carbone, because it was highly graphitizable and had the lowest ash levels of any of the four anthracites. A 55-gallon drum of pea-sized anthracite was shipped first to CCE Technologies for jet milling to an average particle of 15 micron. Following the particle size reduction, the LCNN anthracite was sent to Carbone to be used as a filler in their industrial molded graphite production scheme, which uses petroleum sponge coke and coal tar pitch binders. No extrusion is performed at this facility; rather, the graphites are formed from compression or isostatic molding. It was decided to use isostatic molding through discussions with our colleagues from Carbone. A good wetting of the filler by the pitch, and subsequent absence of voids in the contact area between the coke and pitch, is essential to the mechanical stability of the graphite that will be formed following graphitization heat treatment. Anthracite has a high

microporosity, which may inhibit its wetting by coal tar pitch because the pitch would have a difficult time entering pores smaller than 20 Å. Isostatic molding applies pressure from all directions and could possibly provide the needed energy to force pitch into the micropores.

Following the decision to use isostatic molding, the ratios of pitch to anthracite were determined. It was decided to begin with 44 weight percent coal tar pitch and decrease this value in intervals of two percentage units to 38 weight percent. Forty-four was the lowest value used in the pervious work of Atria, and this ratio of coal tar pitch to anthracite seemed to produce the best graphite. Tables 5 to 7 list some of the properties recorded at Carbone for the green, baked, and graphitized carbons.

Table 5. Properties of green anthracite and coal tar pitch sample

Grade	raw material	coal tar pitch	green density	length	width	height	dry wt.	Wet wt.	Diff.
GREEN		(pph)	g/cm^3	inches	inches	inches	grams	grams	grams
P18	sponge coke	54.7	1.576	10.6	4.9	4.9	6400	2340	4060
P19	calcined coal	38	1.507	9.6	4.9	4.9	5710	1920	3790
P20	calcined coal	40	1.503	10.3	4.8	4.9	6100	2040	4060
P21	calcined coal	42	1.504	10.1	4.9	4.9	6180	2070	4110
P22	calcined coal	44	1.505	10.4	4.8	4.9	6200	2080	4120
P23	sponge coke	54.7	1.573	10.1	4.9	4.9	6260	2280	3980
P24	green coal	38	1.46	9.5	5	5	5660	1770	3890
P25	green coal	40	1.45	9.8	4.9	4.9	6000	1870	4130
P26	green coal	42	1.46	10.1	4.9	4.9	6120	1920	4200
P27	green coal	44	1.46	9.9	4.9	4.9	5900	1850	4050

Table 6. Properties of baked anthracite and coal tar pitch sample

Grade	raw material	coal tar pitch	baked density	length	width	height	dry wt	wet wt.	Diff.
BAKED		(pph)	g/cm^3	inches	inches	inches	grams	grams	grams
P18	sponge coke	54.7	1.66	9.9375	4.625	4.625	5780	2340	3440
P19	calcined coal	38	1.53	9.25	4.75	4.75	5220	1840	3380
P20	calcined coal	40	1.59	9.75	4.6875	4.6875	5580	2000	3580
P21	calcined coal	42	1.66	9.5625	4.625	4.6875	5640	2050	3590
P22	calcined coal	44	1.61	9.875	4.625	4.6875	5660	2080	3580
P23	sponge coke	54.7	1.7	9.5	4.625	4.625	5660	2260	3400
P24	green coal	38	1.56	9	4.75	4.6875	5120	1820	3300
P25	green coal	40	1.66	9.125	4.6875	4.6875	5440	1940	3500
P26	green coal	42	1.63	9.5	4.6875	4.625	5500	2020	3480
P27	green coal	44	1.62	9.25	4.6875	4.625	5320	1970	3350

Table 7. Properties of graphitized anthracite and coal tar pitch sample

Grade	raw material	coal tar pitch	baked density	length	width	height	dry wt	wet wt.	Diff.
GRAPHITE		(pph)	g/cm^3	inches	inches	inches	grams	grams	grams
P18	sponge coke	54.7	2.15	9.75	4.0625	4.0625	5680	2400	3280
P19	calcined coal	38	1.6	8.875	4.5625	4.625	4910	1880	3030
P20	calcined coal	40	1.67	9.437	4.5	4.5	5240	2040	3200
P21	calcined coal	42	1.73	9.187	4.5	4.5	5280	2080	3200
P22	calcined coal	44	1.71	9.5	4.4375	4.5	5320	2120	3200
P23	sponge coke	54.7	1.75	9.312	4.5625	4.5625	5560	2330	3230
P24	green coal	38	1.6	8.687	4.625	4.5625	4800	1790	3010
P25	green coal	40	1.71	8.812	4.5	4.5	5080	1920	3160
P26	green coal	42	1.69	9.187	4.5	4.5	5160	2000	3160
P27	green coal	44	1.67	9.000	4.5	4.5	4980	1940	3040

Tables 5 to 7 give some basic dimensions and how they changed during the heat treatment regime. Following the production of the anthracite-based graphites, P19-P22 and P24-P27, the products were tested against the standard petroleum coke graphites, P18 and P23. Figures 47-54 compare the standard properties recorded by Carbone; the c- and a- directions are also differentiated for all but median pore and ash percentage.

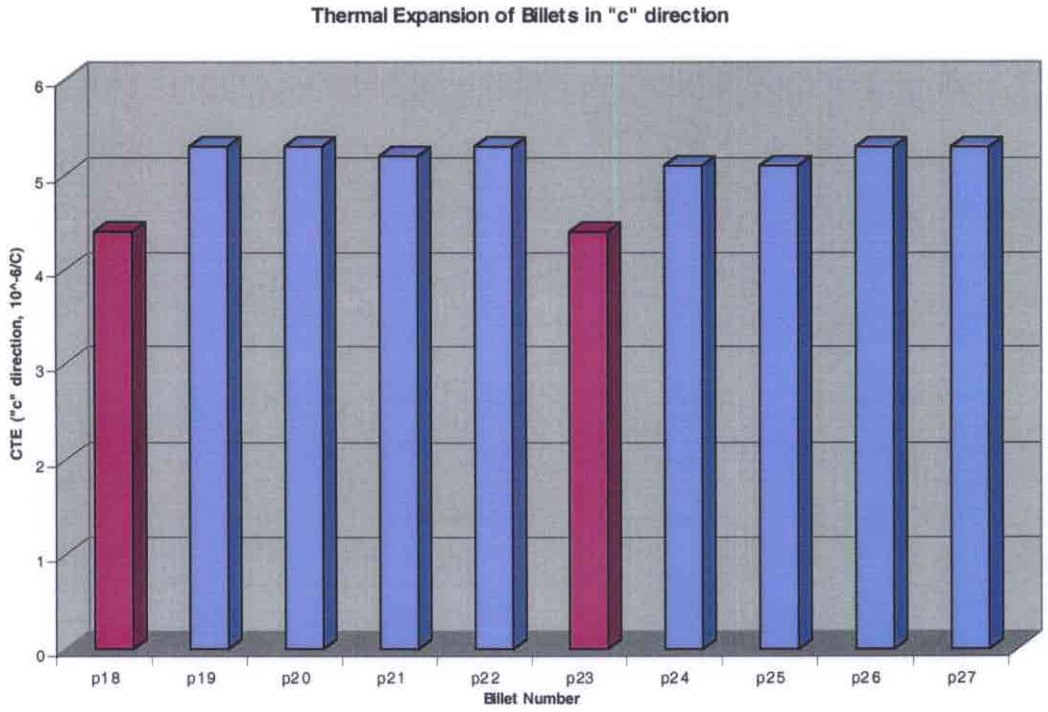

Figure 47 Thermal expansion in the c-direction

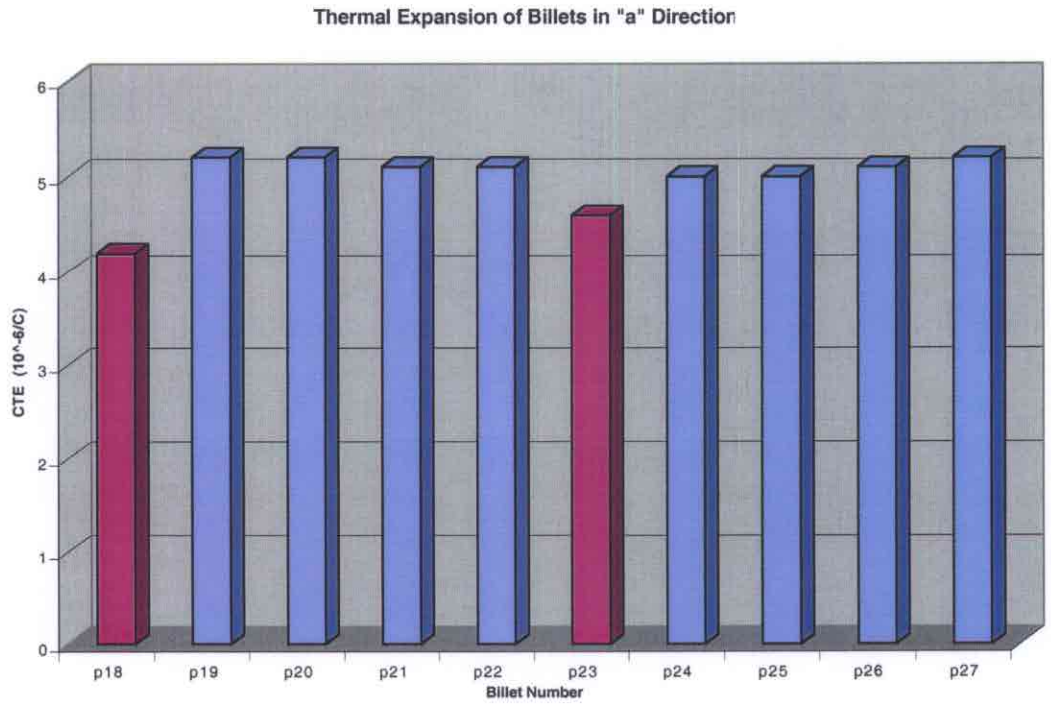

Figure 48 Thermal expansion in the a-direction

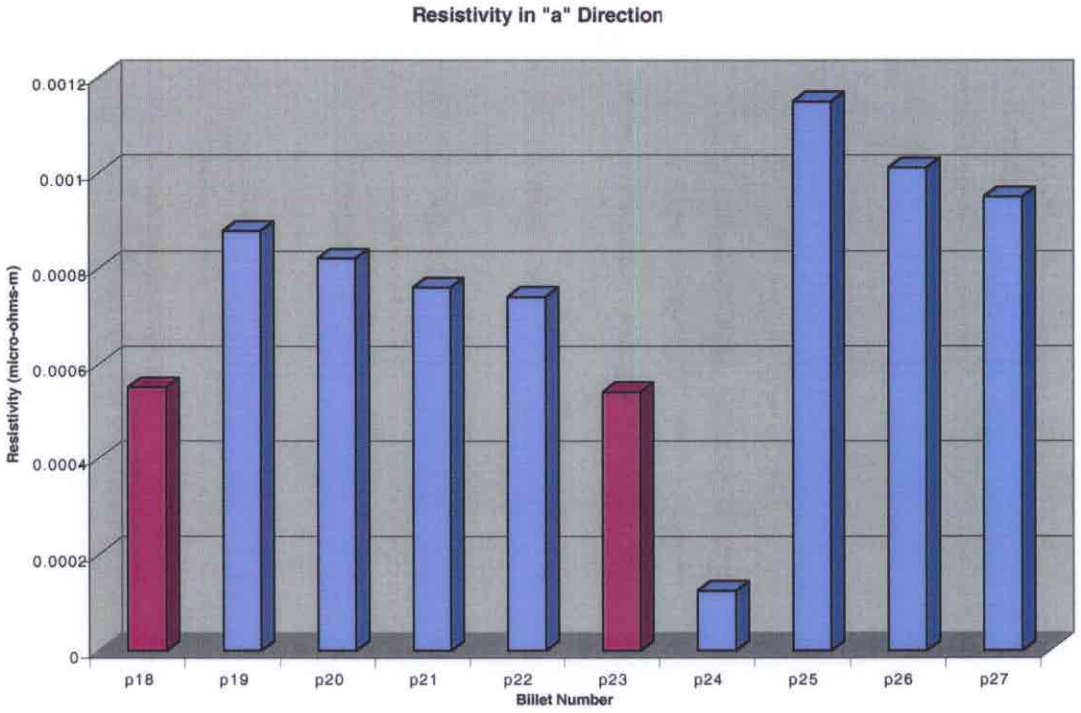

Figure 49 Resistivity in the a-direction

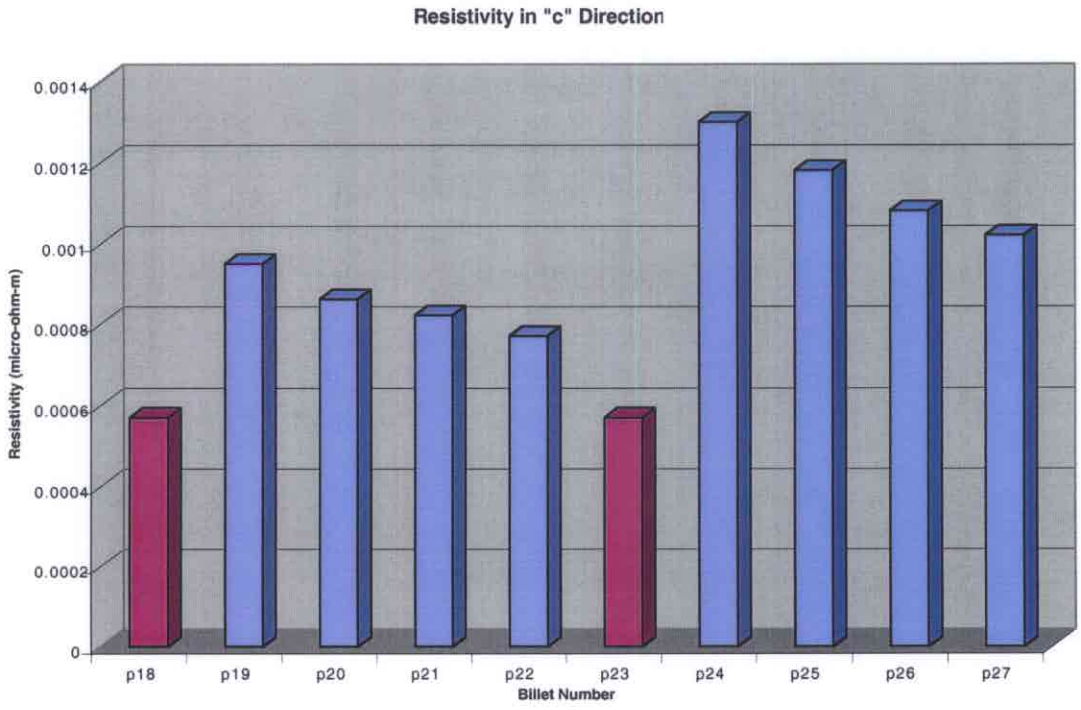

Figure 50 Resistivity in the c-direction

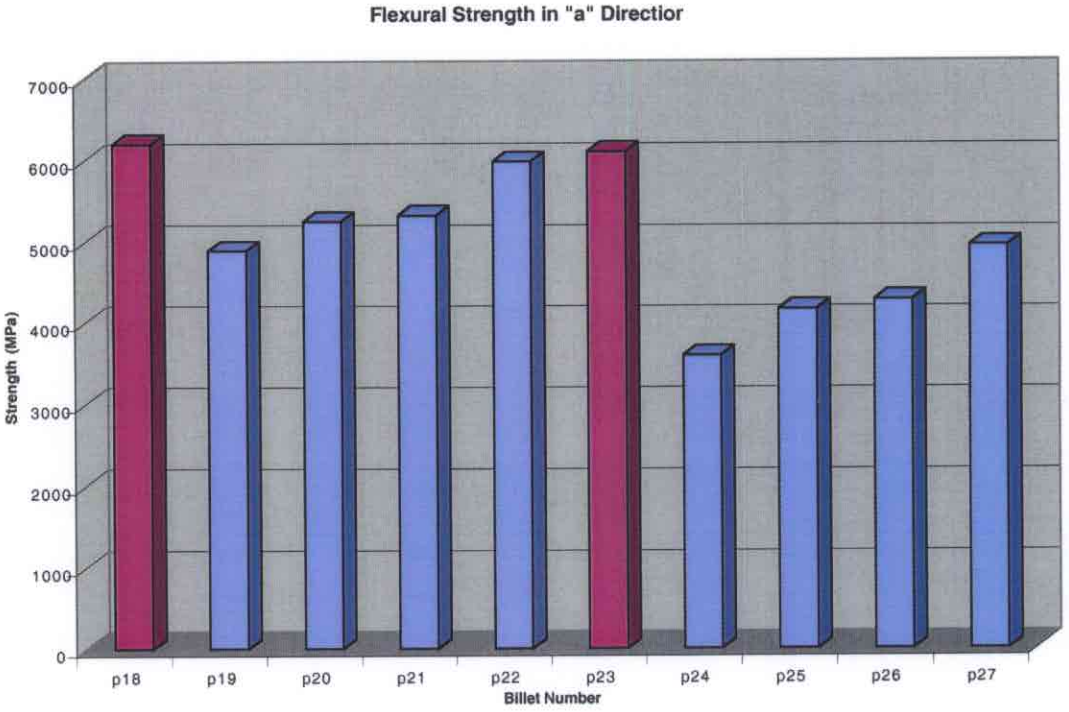

Figure 51 Flexural strength in the a-direction

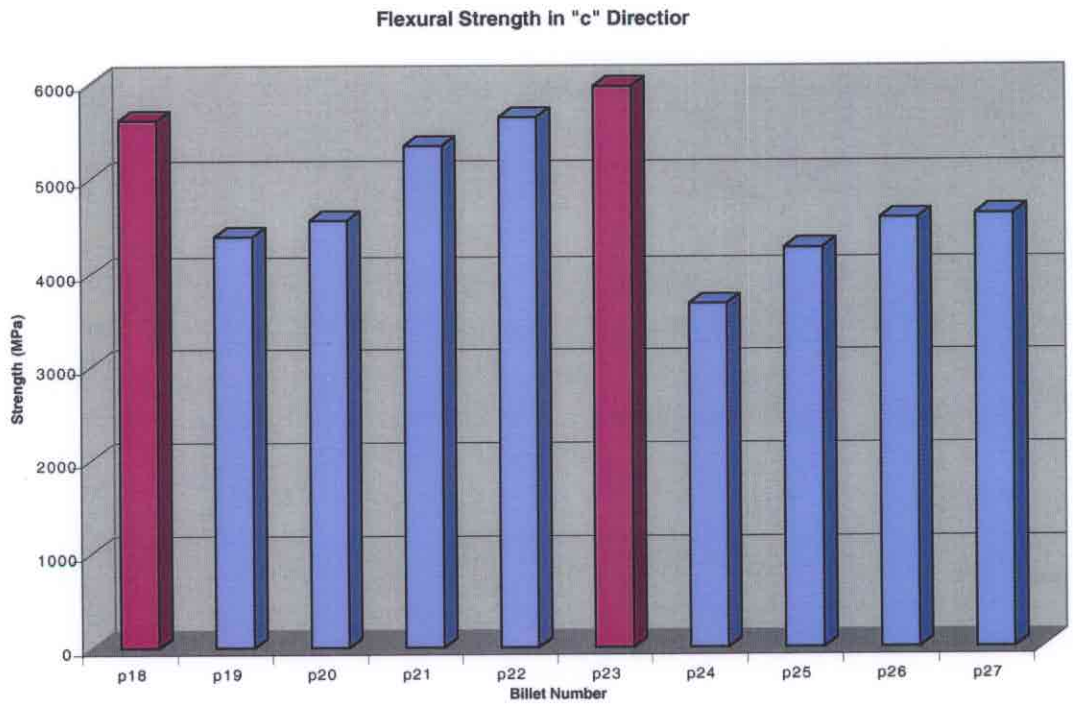

Figure 52 Flexural strength in the c-direction

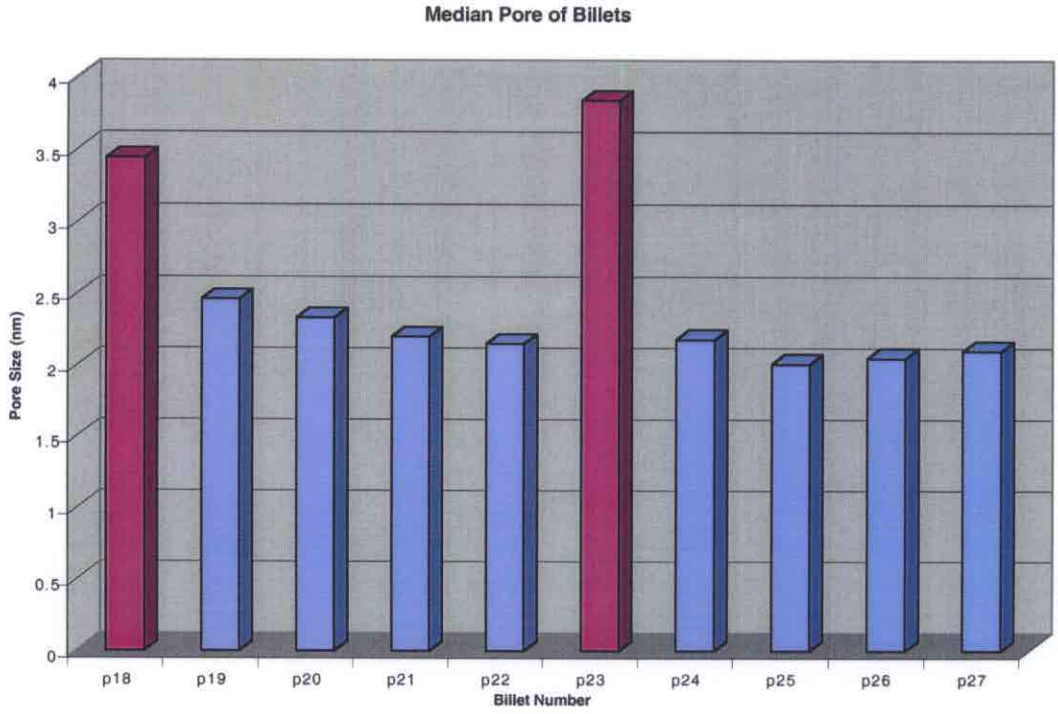

Figure 53 Median pore differences

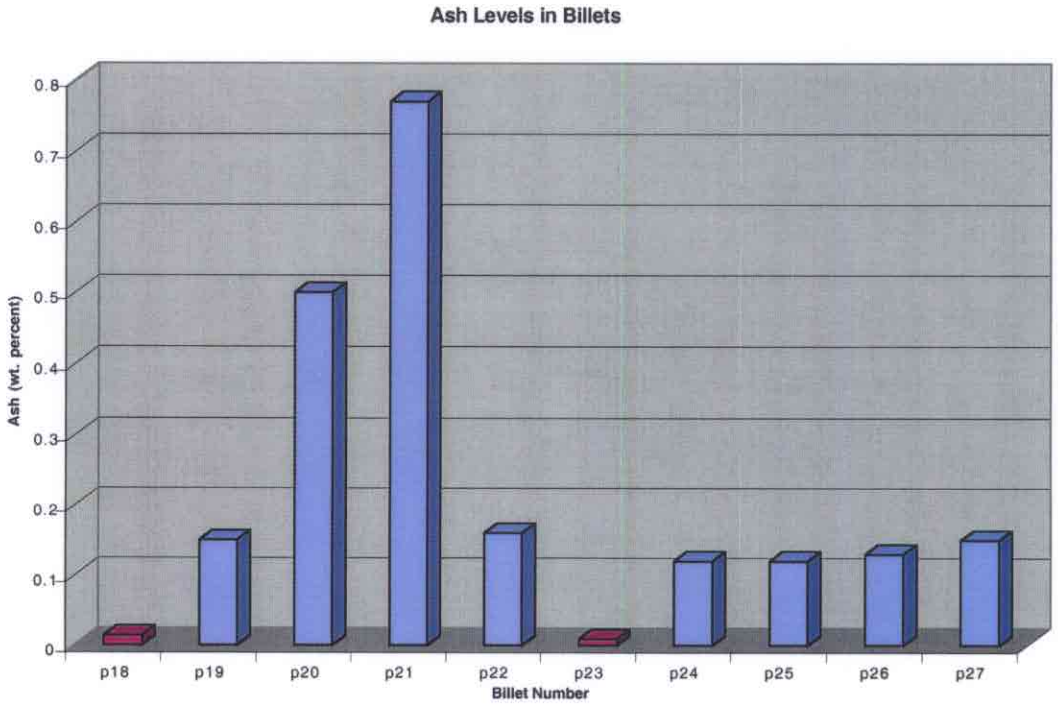

Figure 54 Ash levels

Based on the figures shown above, the anthracite-based graphites were described as "low-end" specialty graphite. The exact definition of low-end specialty graphite was not revealed. It also appears that there is very little difference in properties between the specimens made from calcined or non-calcined anthracites, which would provide another cost savings in addition to the price differential between coke and anthracite if anthracite were to be used as a filler.

Because the bulk of the research presented in this report dealt with describing the extent of graphitization of anthracite by X-ray diffraction, the anthracite-based graphites were also analyzed by X-ray diffraction. This is not a technique used by Carbone to characterize their commercial graphites, but it will help illustrate the differences between the coke- and anthracite-based graphites, and also show how an anthracite compares to a coke in terms of extent of graphitization when mixed with a binder. The d-spacing and L_c of all the samples is provided in Table 8. Table 8 shows definitively that the LCNN anthracite undergoes the same degree of graphitization as sponge coke. Thus all the criteria have been met in order to demonstrate that anthracite could replace petroleum coke as a filler for certain applications. The anthracite achieves exactly the same d-spacing and L_c of an accepted petroleum coke standard, and Figures 47 to 54 indicate it forms a sound product and has properties comparable to the coke standard. Basically, this industrial graphitization project is the culmination, or proof of concept, of this research. An anthracite that was found to be highly graphitizable in the laboratory was shown to be an adequate filler for the production of synthetic graphite.

Table A8 Crystallite parameters of "P" samples

Sample	d-spacing (Å)	L_c (Å)
P18	3.349	302
P19	3.350	177
P20	3.352	170
P21	3.349	194
P22	3.354	291
P23	3.354	291
P24	3.349	181
P25	3.359	170
P26	3.357	170
P27	3.352	167

The results of this research are so promising that scaling up to multi-ton quantities with the end goal a commercially available graphite made from anthracite would certainly be warranted.

A final confirmation of the equality of anthracite to petroleum coke as a filler for specialty graphite production is the similarity between the optical textures of the anthracite-based and coke- based graphites shown in Figure 55 to 63.

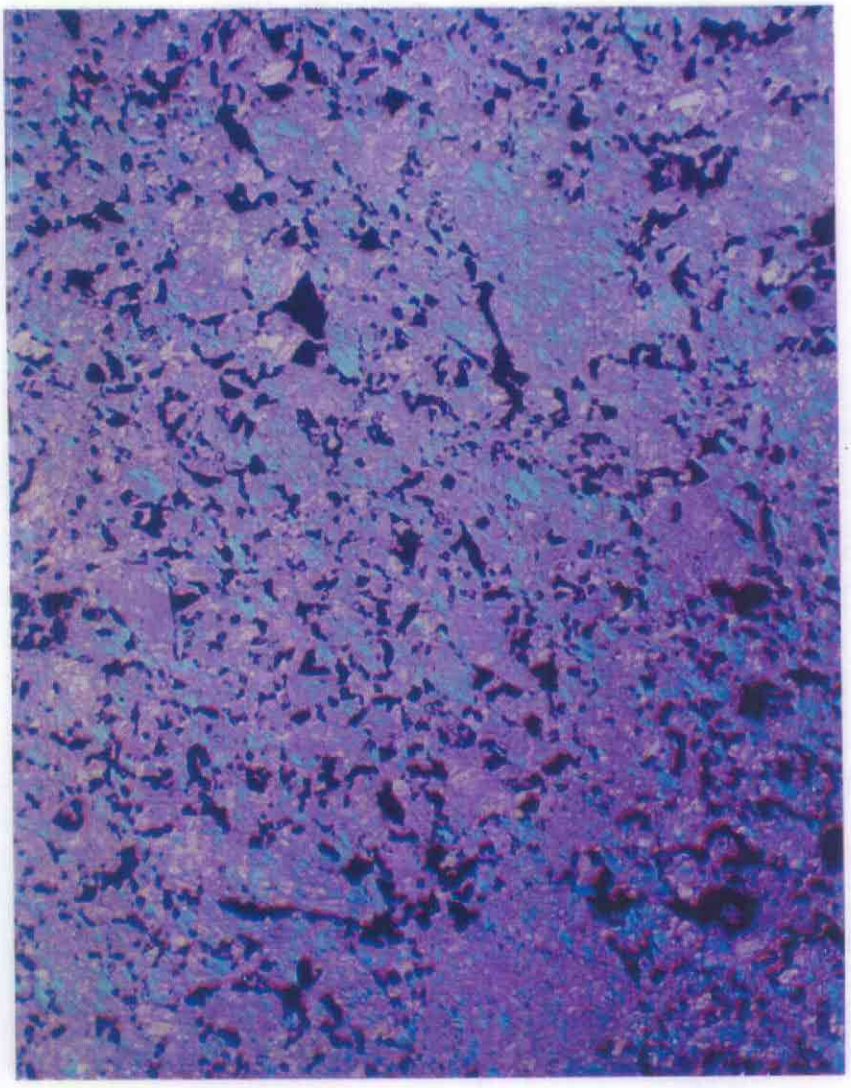

Figure 55. Optical micrograph of p18, 100X magnification

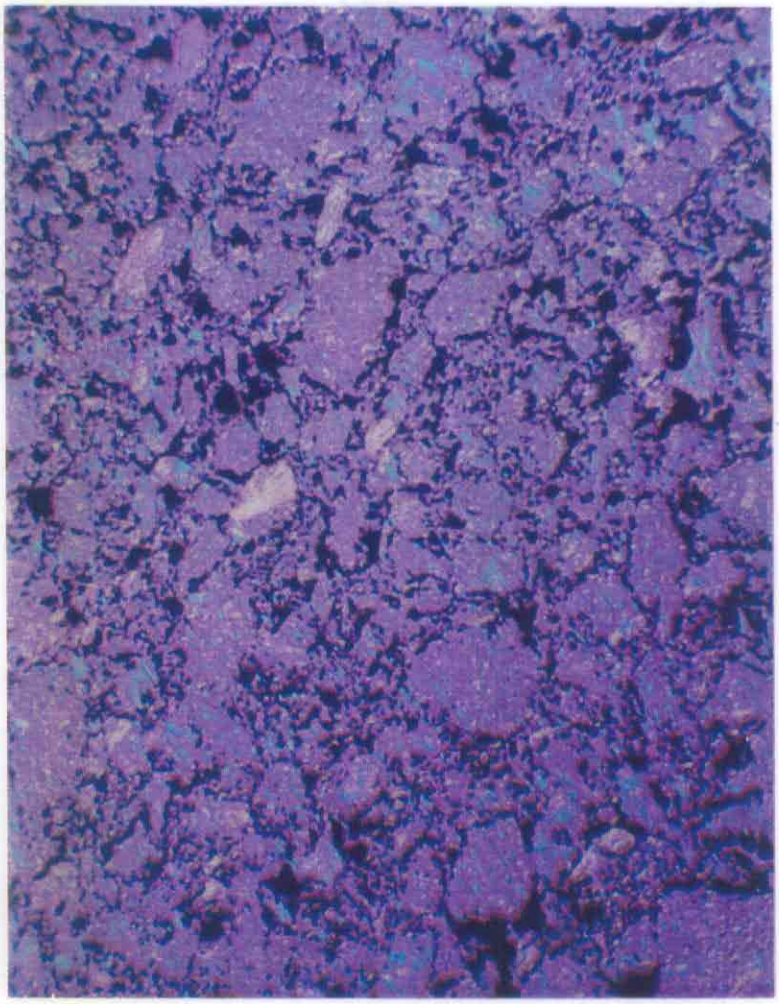

Figure 56. Optical micrograph of p19, 100X magnification

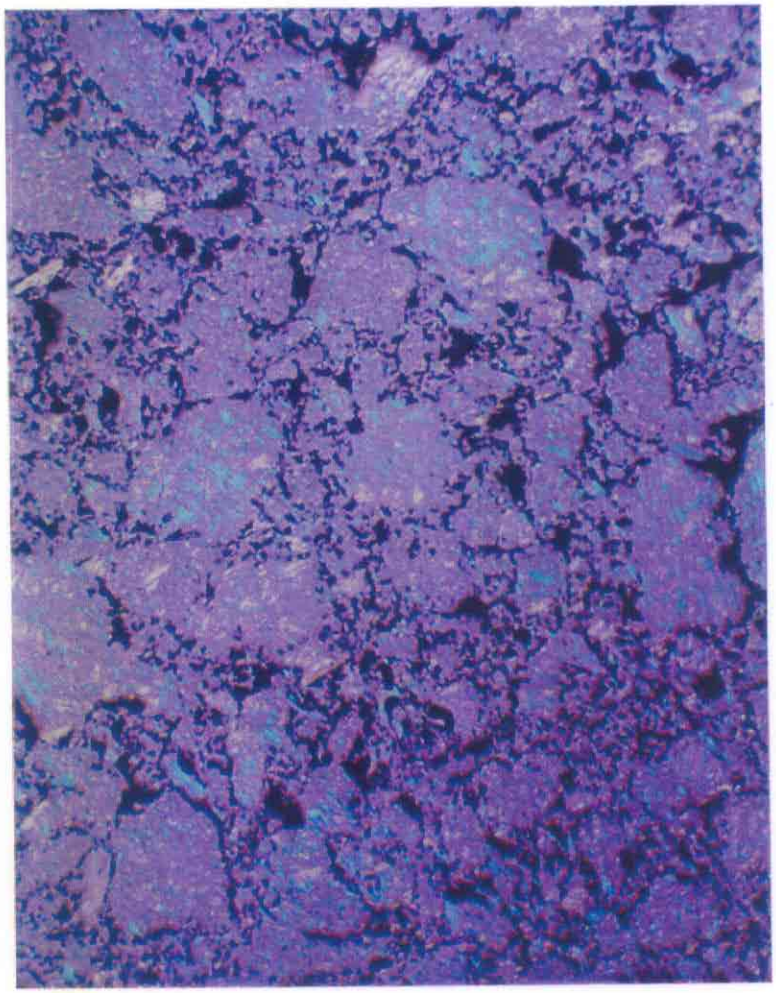

Figure 57. Optical micrograph of p20, 100X magnification

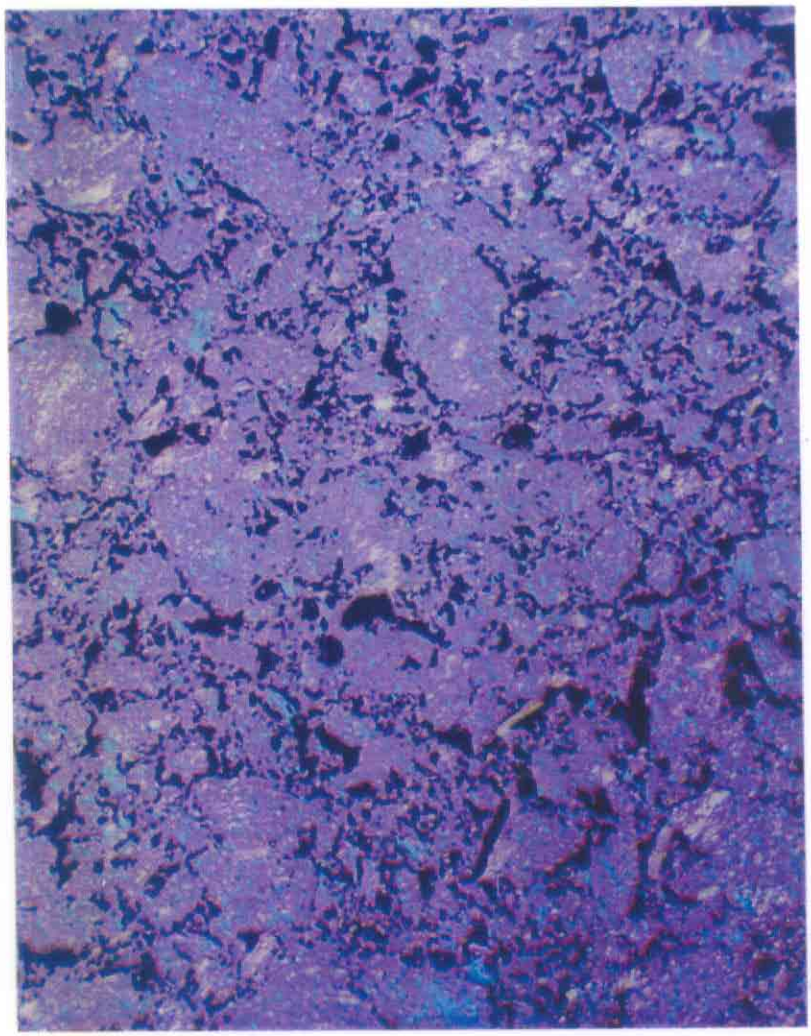

Figure 58. Optical micrograph of p21, 100X magnification

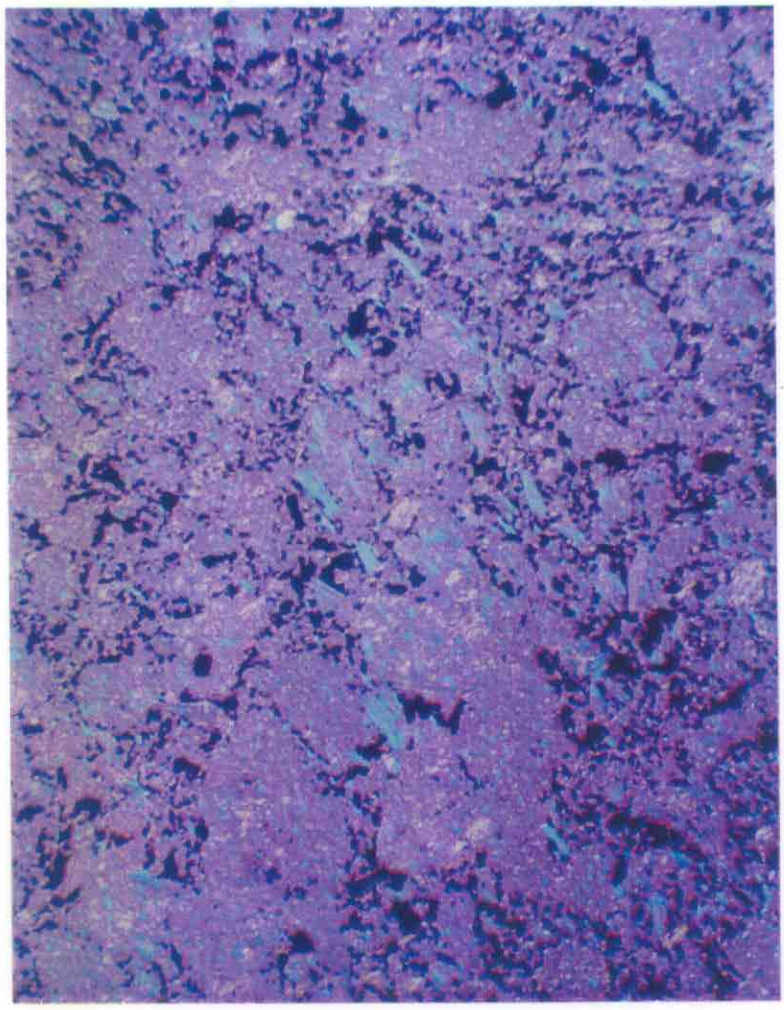

Figure 59. Optical micrograph of p22, 100X magnification

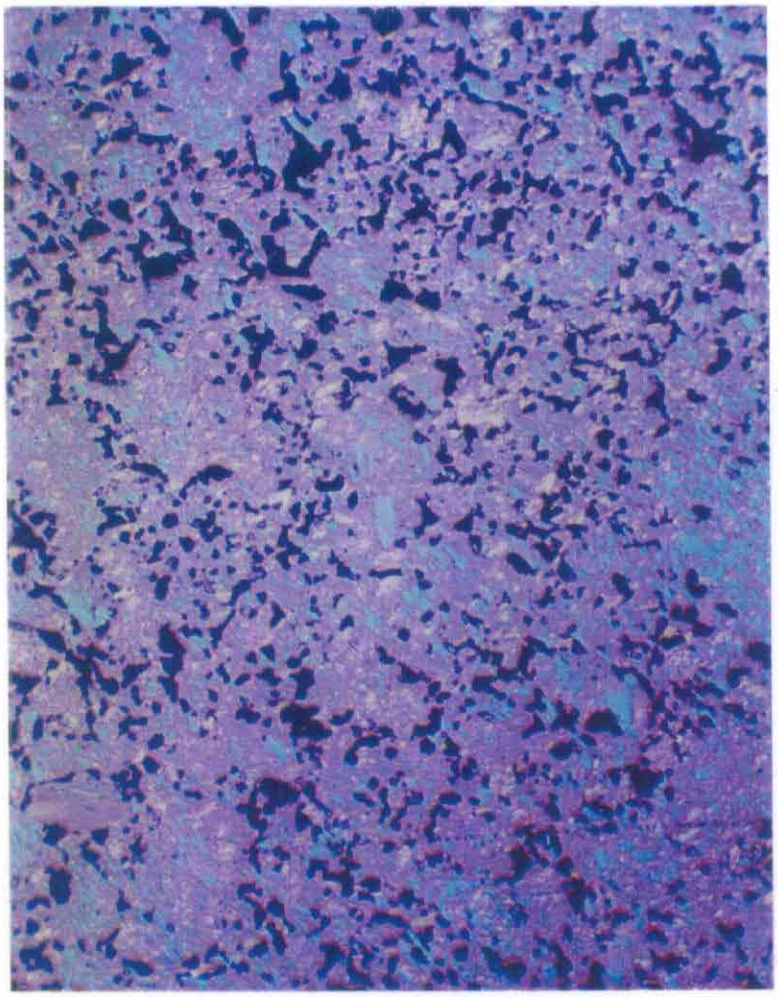

Figure 60. Optical micrograph of p23, 100X magnification

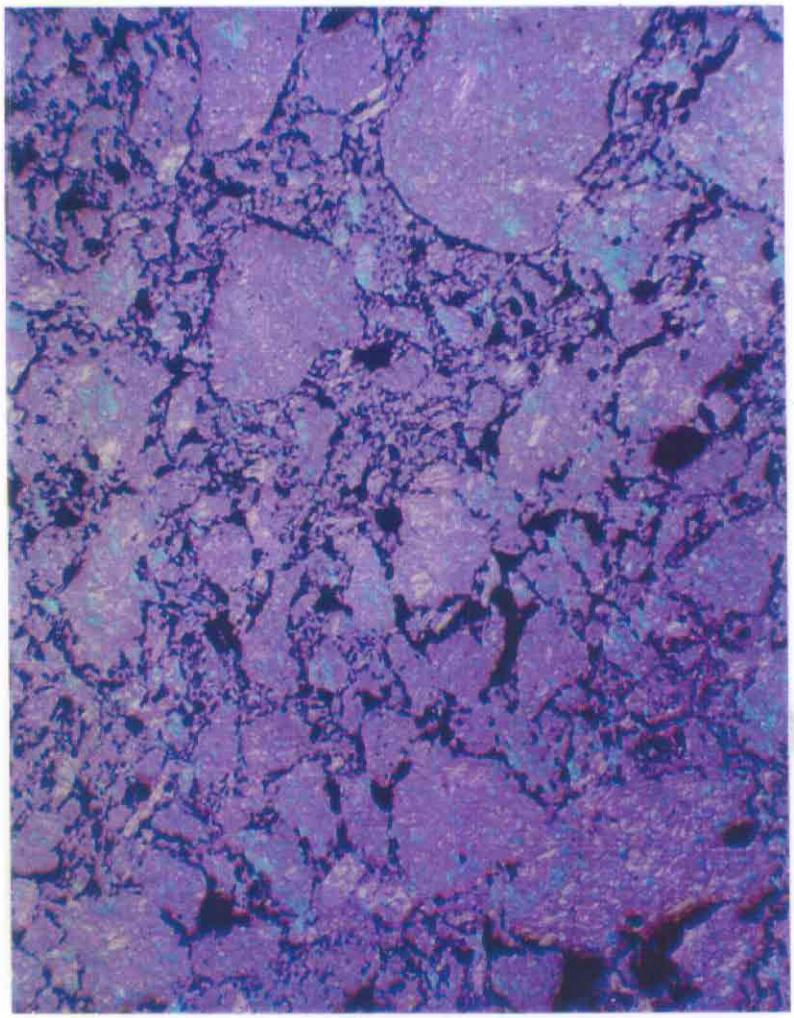

Figure 61. Optical micrograph of p24, 100X magnification

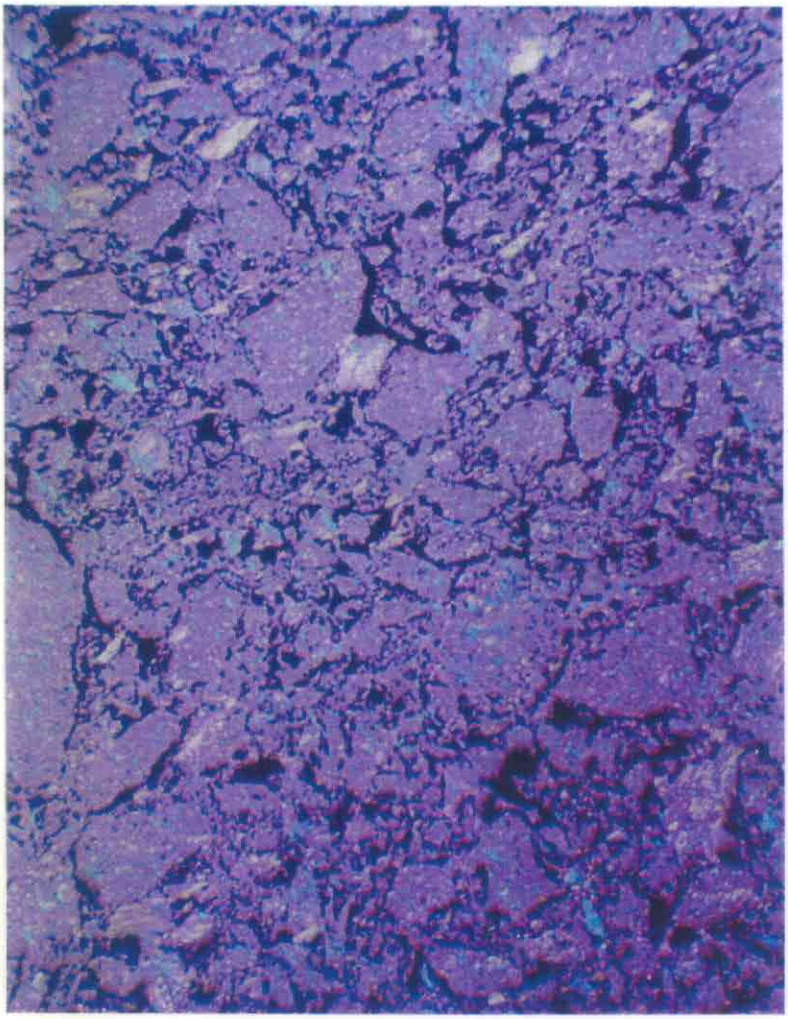

Figure 62. Optical micrograph of p25, 100X magnification

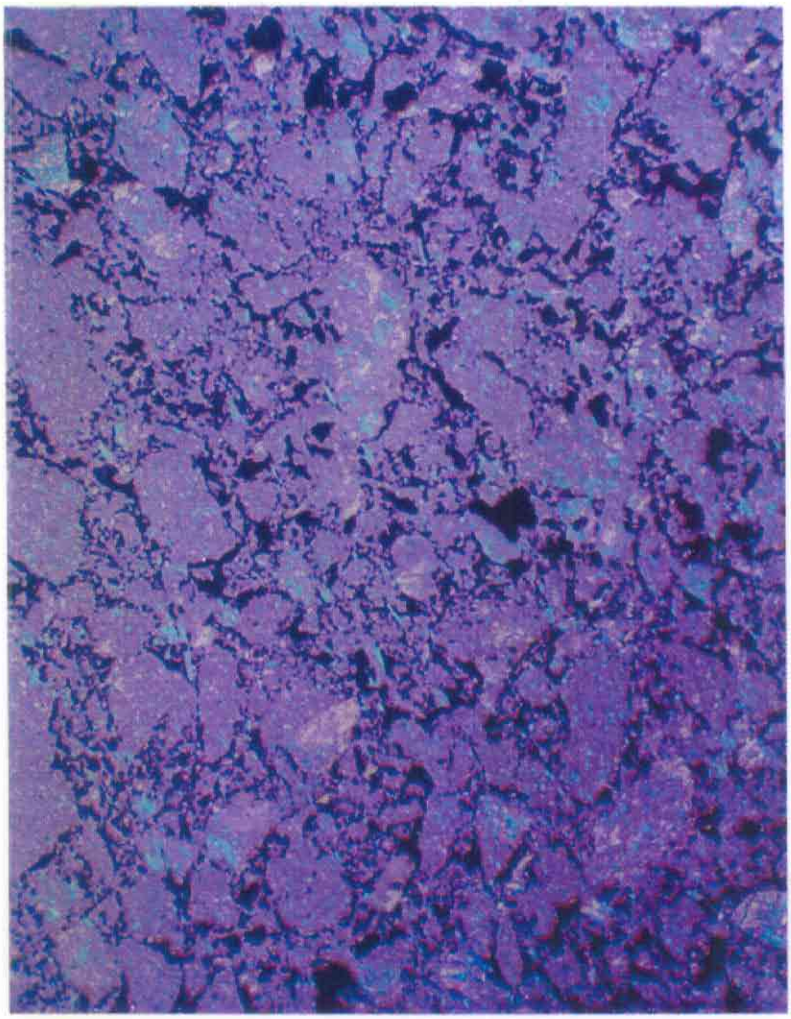

Figure 63. Optical micrograph of p26, 100X magnification

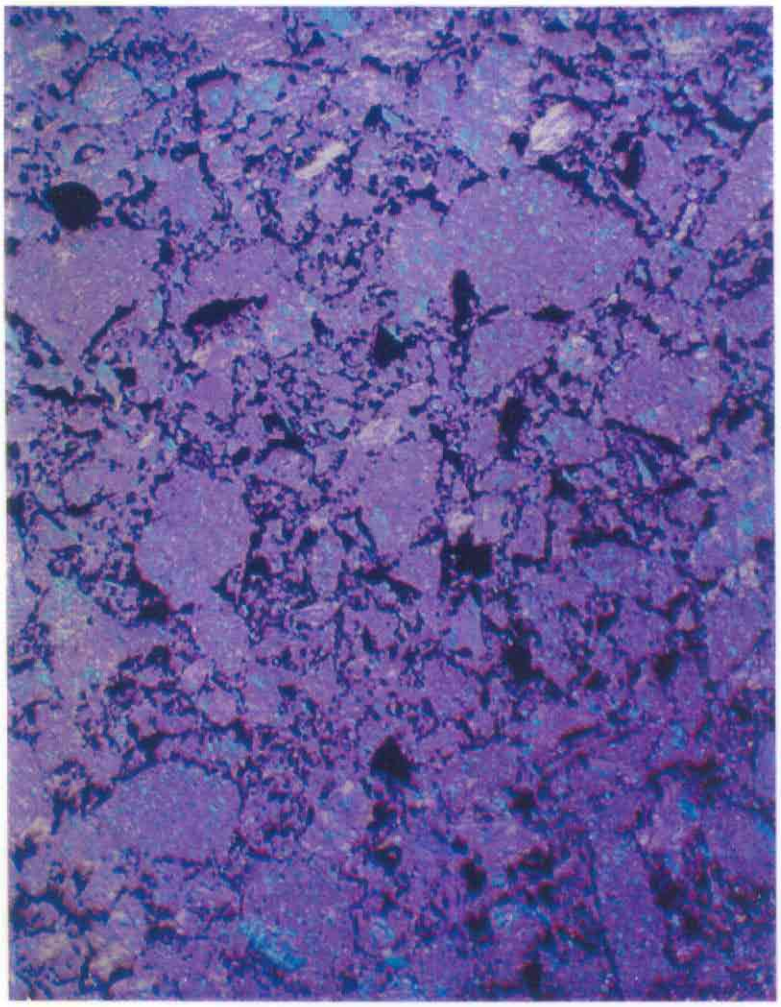

Figure 64. Optical micrograph of p27, 100X magnification

References

1. Franklin, R.E., *Crystallite growth in the graphitizing and non-graphitizing carbons.* Proceedings of the Royal Society of London, Series A, 1951. **209** : p. 196-218.

2. Oberlin, A. and G. Terriere, *Graphitization Studies Of Anthracites By High Resolution Electron Microscopy.* Carbon, 1975. **13** : p. 367-376.

3. Oberlin, A., *Carbonization and Graphitization.* Carbon, 1984. **22** (6): p. 521-541.

4. Maire, J. and J. Mering, *Graphitization of Soft Carbons*, in *The Chemistry and Physics of Carbon*, P.L. Walker Jr., Editor. 1970, Marcel Dekker, Inc.: New York. p. 125-190

5. Atria, J., Masters thesis, *Novel Approach to the Production of Graphite from Anthracite*, in *Materials Science and Engineering.* 1995, Pennsylvania State University University Park. p. 78-109

6. Zeng, S., F. Rusinko, and H. Schobert, *Producing High-quality carbon and/or Graphite Materials from Anthracite by Catalytic Graphitization*, . 1996, Pennsylvania State University: PEDA 9303-4019 university Park. p. 114.

7. Blanche, C., D. Dumas, and J. Rouzaud, *The microtexture of anthracites: a key to understand their graphitizability.* Coal Science, 1995: p. 43-47.

8. Oberlin, A. and J.P. Rouchy, *Transformation des carbones non graphitables par traitement thermique en presence de fer.* Carbon, 1971. 9 : p. 39-46.

9. Guinier, A., *X-ray Crystallographic Technology*. 1952, London: Hilger and Watts Ltd.

10. Fischbach, D.B., *The Kinetics and Mechanisms of Graphitization*, in *The Chemistry and Physics of Carbon*, P.L. Walker Jr., Editor. 1971, Marcel Dekker, Inc.: New York. p. 1-106.

11. Fitzer, E. and Kegel, *Reaktionen von kohlenstoffgesattigter vanadiumcarbideschmelze mit ungeordnetem kohlenstoff.* Carbon, 1968. **6** : p. 433-446.

12. Weisweiler, W., N. Subramanian, and B. Terwiesch, *Catalytic Influence of Metal Melts on the Graphitization of Monolithic Glasslike Carbon.* Carbon, 1971. 9 : p. 755-761.

13. White, J.L. and J.M. Pontelandolfo, *Graphite-Carbide Materials Prepared by Hot-Working with a Dispersed Liquid-Carbide Phase.* Carbon, 1966. **4** : p. 305-314.

14. Noda, T., Y. Sumiyoshi, and N. Ito, *Growth of Single Crystals of Graphite from a Carbon-Iron Melt.* Carbon, 1968. 6 : p. 813-816.

15. Baraniecki, C., P.H. Pinchbeck, and F.B. Pickering, *Some Aspects of Graphitization Induced by Iron and Ferro-Silicon Additions.* Carbon, 1969. 7 : p. 213-224.

16. Yokokawa, C., K. Hosokawa, and Y. Takegami, *Low Temperature Catalytic Graphitization of Hard Carbon.* Carbon, 1966. 4 : p. 459-465.

List of Acronyms and Abbreviations

BSU	Basic structural units
CCE	(name of company)
CCSEM	Computer controlled scanning electron microscopy
CPCPC	Consortium for Premium Carbon Products from Coal
FWHM	Full width at half maximum
(*hkl*)	Miller crystallographic indices
HRTEM	High-resolution transmission electron microscopy
HTT	Heat-treatment temperature
LCNN	Lehigh Coal and Navigation (anthracite)
SAD	Selected area diffraction
SCINTAG	(manufacturer of X-ray diffraction equipment)
TEM	Transmission electron microscopy
UAE	United Arab Emirates (anthracite)